AD-A101 529 AN IF (INTERMEDIATE FREQUENCY) CLUTTER SIGNAL GENERATOR 1/2
FOR THE DREO EW (..(U) DEFENCE RESEARCH ESTABLISHMENT
OTTAWA (ONTARIO) G A WARDLE DEC 86 DREO-956

UNCLASSIFIED F/G 17/4.3 NL

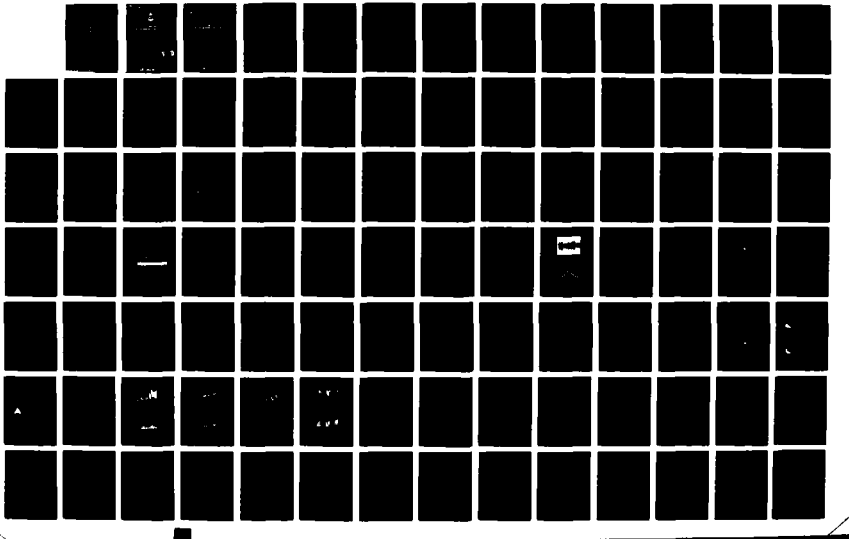

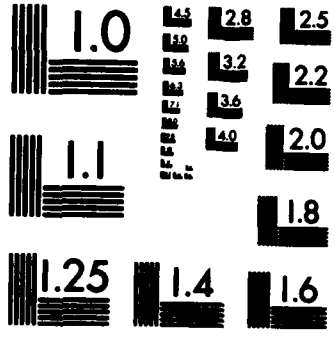

MICROCOPY RESOLUTION TEST CHART
NATIONAL BUREAU OF STANDARDS-1963-A

National Defence / Défense nationale

AN IF CLUTTER SIGNAL GENERATOR FOR THE DREO EW ENGAGEMENT SIMULATION FACILITY

by

Geoffrey A. Wardle

DEFENCE RESEARCH ESTABLISHMENT OTTAWA
REPORT NO. 956

Canada

December 1986
Ottawa

National Defence / Défense nationale

AN IF CLUTTER SIGNAL GENERATOR FOR THE DREO EW ENGAGEMENT SIMULATION FACILITY

by

Geoffrey A. Wardle
Radar Countermeasures Section
Electronic Warfare Division

DEFENCE RESEARCH ESTABLISHMENT OTTAWA
REPORT NO. 956

PCN
041LD12

December 1986
Ottawa

ACKNOWLEDGEMENTS

The author expresses his gratitude to both Prof. B. Syrett of Carleton University and Dr. W. K. McRitchie of DREO. Their encouragement, suggestions and criticisms were of great value. Also, the suggestions of Mr. J. Nielsen regarding the hardware design are gratefully acknowledged, as is his implementation of the 0/180° SPDT circuit.

ABSTRACT

This report describes the implementation of an intermediate frequency (IF) radar clutter generator. The generator provides signals for the monopulse tracking radar which forms part of the Electronic Warfare Engagement Simulation Facility at the Defence Research Establishment Ottawa. Land clutter signals with log-normal, Weibull and exponential spatial amplitude distributions are produced, as well as exponential sea clutter signals. Fluctuating clutter from wind blown scatterers is modelled using narrowband amplitude modulation. Clutter induced angle tracking errors are also represented. The report describes the major clutter mechanisms relevant to noncoherent radars in low grazing angle scenarios. The hardware and equations used in modelling are described, and the report presents envelope detected waveform plots and histograms. This work has applications in accurate modelling of radar performance in low-altitude engagements.

SOMMAIRE

Le présent rapport décrit l'implantation d'un générateur de clutter radar en fréquences intermédiaires (FI). Le générateur produit des signaux destinés au radar de poursuite monopulsé qui fait partie intégrante de l'installation de simulation des engagements de guerre électronique du Centre de recherches pour la défense Ottawa. Le générateur produit des signaux de clutter de terre selon une distributin normale logarithmique une distribution de Weibull et une distribution d'amplitude spatiale exponentielle, ainsi que des signaux de clutter de mer exponentiels. Le clutter variable dû aux diffuseurs transportés par le vent est modélisé par modulation d'amplitude en bande étroite. Les erreurs angulaires de poursuite sont aussi représentées. Le rapport décrit les principaux processus de clutter des radars non cohérents selon des scénarios de faibles angles d'incidence. Le texte décrit le matériel et les equations de modélisation et contient les histogrammes et graphiques des formes d'ondes détectées par enveloppe. Le résultats de ces travaux peuvent être appliqués à la modélisation fidèle de la performance radar dans le cadre d'engagements faible altitude.

TABLE OF CONTENTS

TABLE OF CONTENTS (cont.)

LIST OF TABLES

LIST OF FIGURES

LIST OF FIGURES (cont.)

LIST OF FIGURES (cont.)

LIST OF IMPORTANT SYMBOLS

A - element of surface area

A_c - physical area of clutter resolution cell

A_r - receive antenna effective aperture area

C - conversion factor relating P_{del} to P_r

c - the speed of light, equal to 3.0×10^8 m/s

DIFF - difference between $\sigma^o_{min,ss}$ and $\sigma^o_{max,ss}$

f_{clut} - RF clutter signal used in TRS receiver experiment

f_d - doppler frequency

f_{dpv} - doppler shift due to platform velocity

f_{dss} - doppler shift due to sea-state

f_t - transmit frequency

f_{tgt} - RF target signal used in TRS receiver experiment

G_t - transmit antenna gain

$G\Delta_{el}(\theta')$ - approximating function for Δ_{el} relative to Σ versus normalized clutter off-axis angle

$G(\theta_n)$ - antenna gain expressed as a function of off-axis angle

h - antenna height

P_{del} - power delivered by clutter generator to TRS receiver

P_r - received power

P_t - peak transmitted power

P_w, P_e - received power for (respectively) Weibull and exponential models

P_{wmed}, P_{emed} - median received power for (respectively) Weibull and exponential models

P_{wn}, P_{en} - normalized received power for (respectively) Weibull and exponential models

$R, R_{min}, / R_{max}$ - general case, minimum, and maximum range, respectively.

R_e - effective earth radius. R_e=8500km, which is 4/3 the real value.

t - time

V - platform velocity

v - detector output voltage

v_{med} - median detector output voltage

v_n - normalized detector output voltage

W_α - eight bit control word for the antenna gain D/A

W_Σ - eight bit control word for the Σ D/A

α - Weibull parameter

Δ - monopulse difference signal (general case)

Δ_{az}, Δ_{el} - monopulse azimuth and elevation difference signal, respectively

λ - radar transmit wavelength

θ' - clutter off-axis angle normalized to $(\theta_{bel}/6.0)$, the ratio of the simulation elevation beamwidth to the TRS's elevation beamwidth.

θ_{baz} - antenna azimuth beamwidth

θ_{bel} - antenna elevation beamwidth

θ_d - depression angle

θ_{el} - antenna elevation look angle

θ_n - clutter off-axis elevation angle

ψ - grazing angle, defined as the angle between the local horizontal at the reflecting surface and the radar beam direction

σ - target radar cross-section

σ^o - radar differential cross-section of a clutter resolution cell

$\overline{\sigma^o}$ - average value of σ^o

$\sigma^o_{max,ss}$ - maximum published value of σ^o for a given sea-state

σ^o_{med} - median value of σ^o

$\sigma^o_{min,ss}$ - minimum published value of σ^o for a given sea-state

Σ - monopulse sum signal

τ - pulsewidth

GLOSSARY

A/D	analog-to-digital converter
AM	amplitude modulation
BPF	band-pass filter
CFAR	constant false alarm rate
CW	continuous wave
D/A	digital-to-analog converter
ECCM	electronic counter-countermeasure
ECM	electronic countermeasure
EWESF	Electronic Warfare Engagement Simulation Facility
FIR	finite impulse response
IF	intermediate frequency
LNA	low noise amplifier
LO	local oscillator
MTI	moving target indicator
pdf	probability density function
PRF	pulse repetition frequency
PRI	pulse repetition interval
RAM	random access memory
RF	radio frequency
ROM	read only memory
SPDT	single pole double throw
STC	sensitivity time control
TRS	Threat Radar Simulator
TTL	transistor transistor logic
TWT	travelling wave tube
VCXO	voltage controlled crystal oscillator

1.0 INTRODUCTION

1.1 DREO EW Engagement Simulation Facility

One of the primary objectives of the Radar Countermeasures Section of DREO's Electronic Warfare Division is to investigate new electronic countermeasure (ECM) techniques. Also of interest is the effectiveness assessment of current ECM equipment and techniques. To aid in meeting these objectives a hardware EW Engagement Simulation Facility (EWESF) has been developed with which radar engagement scenarios can be realistically modelled in real time. The EWESF consists of a Threat Radar Simulator (TRS), microwave anechoic chamber, and target/jammer generation equipment, as shown in Fig. 1. Target and chaff returns plus jamming waveforms are generated under the control of the ECM Simulator computer. A timing pulse from the radar indicates zero range. Delay circuitry is used to generate the low level return pulses at the correct range. If appropriate, actual jamming hardware can be incorporated into the loop. Signals are radiated at RF through the anechoic chamber via three arrays of dipole antennas to the TRS at the other end of the chamber. By monitoring the performance of the radar simulator, the effectiveness of the ECM can be assessed.

The TRS is a complete tracking radar receiver which tracks target echoes in azimuth, elevation and range. A high power transmitter is not required--instead the low power return signals plus the local oscillator are derived from a common synthesizer using a phase locked loop arrangement. Rather than replicating individual threat radars with dedicated hardware, the distinguishing characteristics of a number of threat systems can be incorporated. This is facilitated by modular design and use of digital, programmable circuitry. The TRS can be configured to model a wide range of terminal threat systems such as active missile seekers, and fire control radars for air interceptors, surface-to-air missiles, and anti-aircraft artillery.

Fig. 2 is a block diagram of the TRS. The radar simulator employs a three channel monopulse antenna and positioner. The three channels are multiplexed onto two downconversion channels, detected, and processed to produce a sum signal (Σ) for range tracking and display and difference signals (Δ_{az} and Δ_{el}) for angle tracking. Monopulse antennae typically have four horn feeds which result in four squinted beams [1]. Radiation arriving along the axis of symmetry of the antenna produces equal amplitudes in the beams, while off-axis radiation causes an imbalance. From imbalances in horn pairs, azimuth and elevation difference signals are derived. The sum of the signals in the four horns is the Σ signal. The sum signal can be digitized and processed using MTI (moving target indicator) and CFAR (constant false alarm rate) techniques. The digital output can be range tracked and also converted to an analog signal for display.

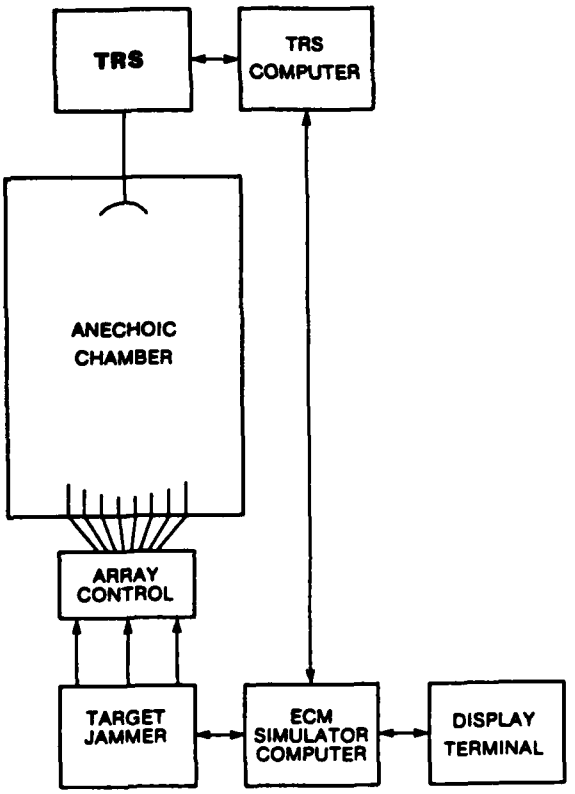

FIGURE 1: THE DREO ELECTRONIC WARFARE ENGAGEMENT SIMULATION FACILITY

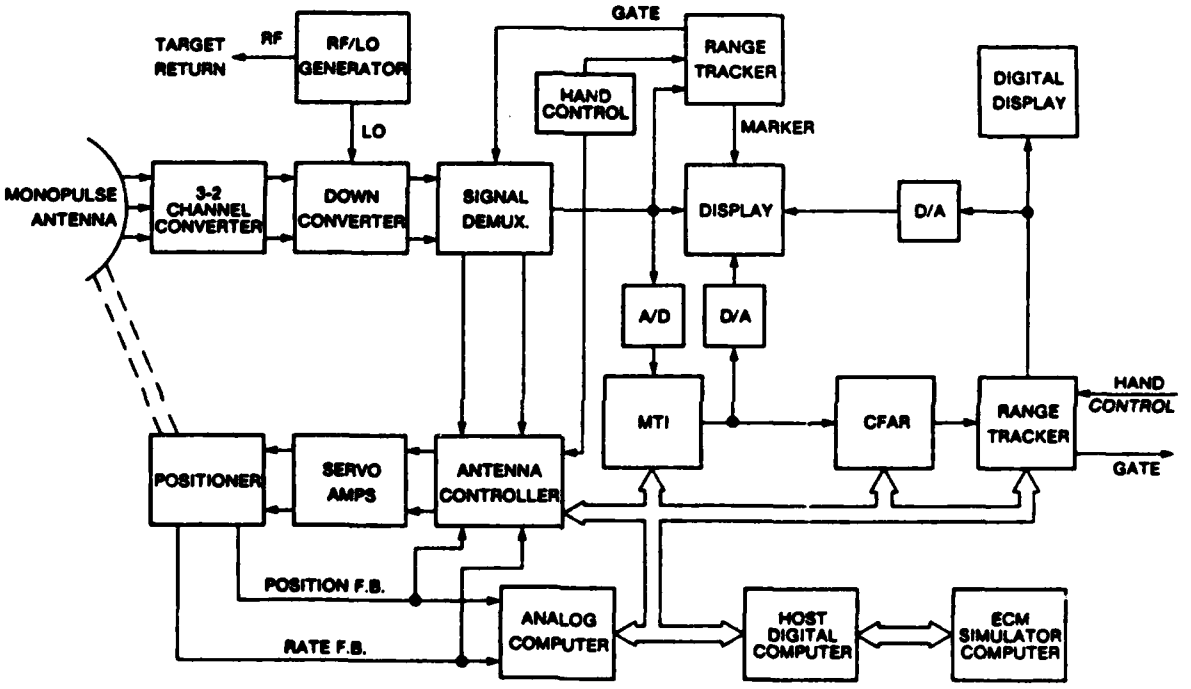

FIGURE 2: THREAT RADAR SIMULATOR BLOCK DIAGRAM

1.2 Need For a Clutter Simulation

Typically, fire control radars must be capable of detecting and tracking targets while receiving unwanted reflections (clutter) from the surrounding land or sea surface. To cope with clutter, a variety of processing schemes have been developed. These include adaptive thresholding, coherent and noncoherent moving target indication (MTI), and pulse doppler processing. While each of these techniques is highly effective, radar performance is still degraded by clutter, particularly when low elevation angle targets are present. At low angles clutter returns are often much greater than the target return, causing a severely degraded probability of detection. If the target is detected and track is initiated, the range gate can transfer lockon to the clutter. Also, clutter existing in the range gate can cause an angle error signal that can interfere with target angle tracking. Any radar engagement simulation that realistically models radar performance at low angles must therefore include clutter.

Additional motivation for this work stemmed from the inclusion in the TRS of noncoherent MTI. This processing scheme uses a finite impulse response (FIR) filter to cancel out non-fluctuating returns. Because a moving target has a doppler shift, a beat frequency develops in the radar receiver when its echo is received coincidentally with non-doppler shifted clutter. Hence the target fluctuates and is passed through the filter, whereas the clutter is cancelled. Because this scheme relies on clutter as a reference signal, it will actually cancel moving target returns when clutter is not also received. In order to make use of the TRS's MTI capability, a clutter simulation was therefore required.

A third motivating factor for a clutter simulation was the desirability of gaining insight into how clutter affects the numerous processes of a monopulse radar. These processes include the derivation of angle error signals from the RF signals incident on the monopulse antenna, the computation of a detection threshold, range tracking, and auto acquisition or re-acquisition. This insight allows one a greater appreciation of the problems of a radar designer, the typical solutions or "fixes", and the penalties incurred by these fixes when the radar operates in an environment different than that for which the fix was intended. This insight is invaluable in radar electronic countermeasure (ECM) research, where exact signal processing arrangements of hostile radars are generally unknown. Accurate simulation of these radars depends heavily on the application of the same radar principles that were applied in the design of the hostile radar.

The project goal is to design and implement a clutter signal generator for use in the EWESF. Rather than radiate RF clutter signals in the anechoic chamber, a simpler yet more versatile option--the injection of signals into

the TRS receiver at IF--is discussed. The measurements that validated this approach are described. Principal clutter mechanisms are identified. These mechanisms are relationships between environmental or radar parameters (ie. windspeed or polarization) and clutter characteristics, (ie. amplitude probability density function or spectral width). The effect of these characteristics on various configurations of the TRS is assessed, and those essential for a clutter simulation are identified. Specifications for the generator are stipulated. The final hardware design is documented, as is its rationale. Models for land, sea, and generic clutter are described in detail. Finally, plots of envelope detected output waveforms are presented, as are amplitude histograms.

1.3 RF Transmission Versus IF Injection

Initially, dedication of one of the anechoic chamber dipole arrays to the generation of clutter echoes appeared to be the obvious approach to implementing clutter. An advantage to this RF transmission approach was that it would have allowed target and clutter signals to combine in the monopulse antenna, allowing observation of the effect of clutter on angle tracking performance. There were, however, some disadvantages.

One disadvantage was the difficulty in modelling clutter's elevation angle of arrival variation with range. The EWESF feed structure applies a common signal to all dipole elements in an array. Individual elements can be turned on or off under computer control but only at a maximum rate of 30 Hz. High speed switching of the array dipole elements would have been required to replicate a range (time) dependence of elevation angle of arrival. This would have required additional computing capacity and software. Even if high speed switching had been feasible, the angle of arrival could only have been represented crudely. Dipole separation in each of the arrays is 1.1°.

A further disadvantage of RF transmission was the narrow azimuth sector over which clutter could be made available. Fig. 3 indicates the angular coverage of the three overlapping dipole arrays installed in the anechoic chamber. While these angular ranges are considered sufficient for target generation, they are inadequate for the simulation of clutter seen by typical radars scanning over large azimuth sectors. It was desired that clutter be made available over the entire 86° azimuth search sector of the TRS antenna.

To transmit clutter returns at RF, one array would have to be dedicated to this purpose, preferably the 8x8 or 16x16. The dedication of either to clutter generation would have severely limited the EWESF's ability to model multiple target scenarios.

Because of the problems associated with RF transmission, the feasibility of injecting IF clutter signals into the TRS receiver was investigated. The approach is illustrated in Fig. 4, which shows the TRS receiver with power combiners inserted to couple in two clutter signals, one for each receiver

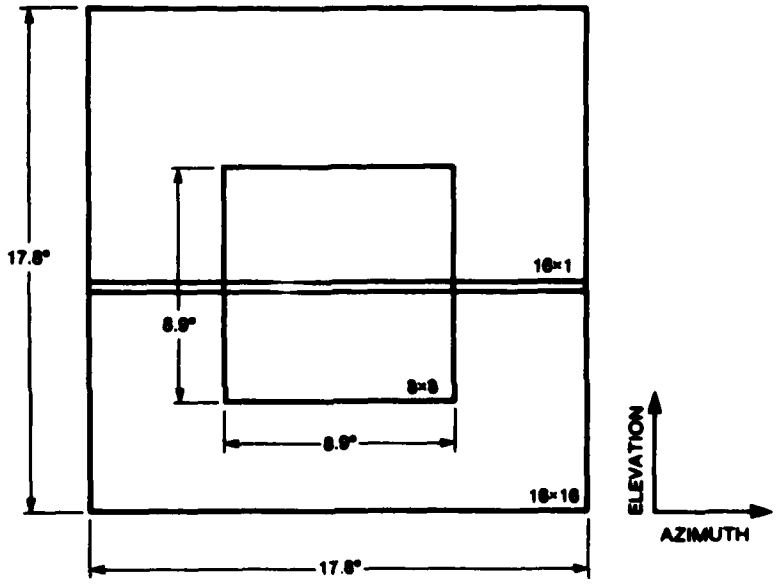

FIGURE 3: ANECHOIC CHAMBER ANTENNA ARRAY DIMENSIONS (AS VIEWED FROM RADAR)

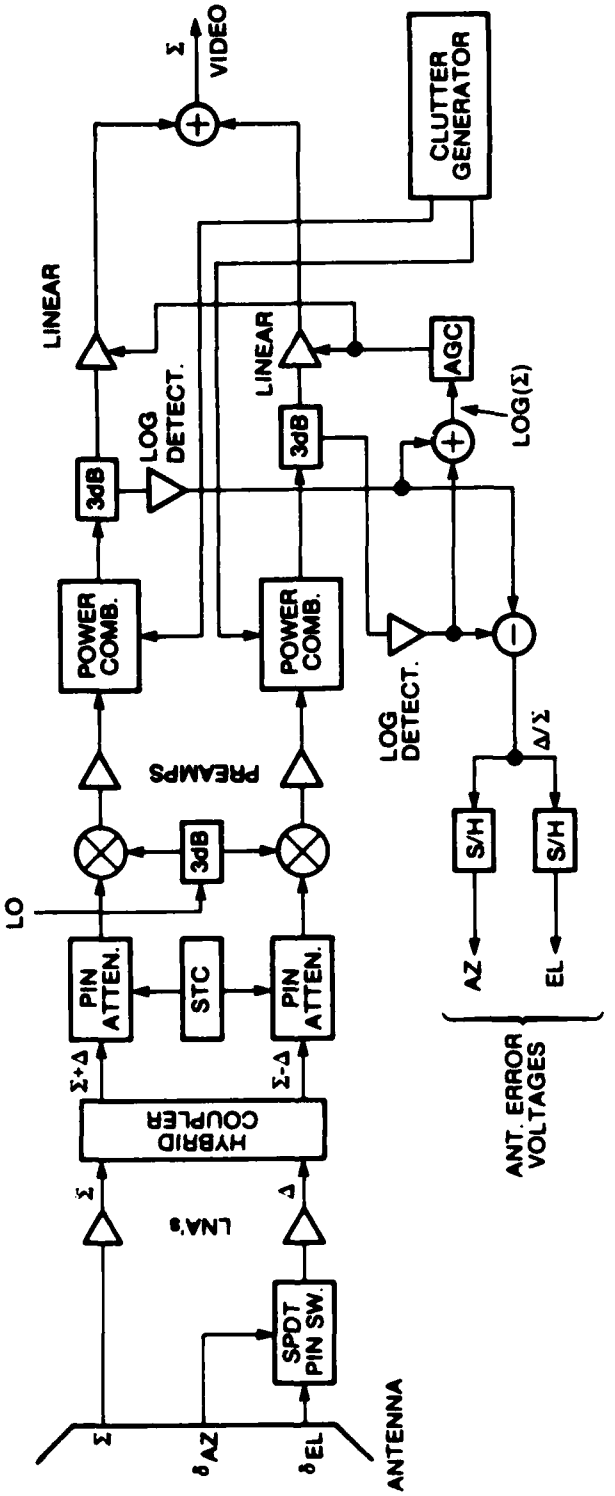

FIGURE 4: TRS RECEIVER DIAGRAM
Note the power combiners inserted to couple in the clutter signals.

channel. Two obvious advantages were that an array would not be required and that the clutter simulation could be made to extend over the full 86° azimuth search sector. An apparent disadvantage was that the effect of the clutter on the monopulse angle tracking process would not be represented. However, it was felt that this could be overcome by developing hardware that produced an amplitude imbalance between the two IF clutter signals proportional to the Δ_{el} component that real clutter would induce into the receiver. The remaining objection was that any effects occurring in the single pole double throw (SPDT) PIN switch, low noise amplifiers (LNAs), hybrid coupler, mixers and preamplifiers that precede the IF section would not be represented. Measurements were then carried out to ensure that these effects were negligible.

The SPDT PIN switch, low noise amplifiers and hybrid coupler were not expected to cause any measurable effects provided LNA saturation did not occur. An experiment was designed to identify possible mixer and preamplifier effects. Receiver outputs were measured for two conditions: 1) two simultaneous RF inputs (target and clutter) applied to the PIN attenuator, and 2) one RF input to the PIN attenuator and one IF input to the power combiner at the preamp output. All signals were continuous wave. Comparisons revealed no differences in receiver outputs over the range of signal power and doppler frequencies likely to be encountered. (IF and video output spectra were examined.) The exception was that two continuous wave equal power RF inputs f_{clut} and f_{tgt} separated by a simulated doppler frequency f_d of a few kHz or tens of kHz caused spurious components at $f_{clut}+nf_d$ and $f_{tgt}-nf_d$. The spurs were visible only when input power levels were within 5 dB of the maximum allowable level, which is defined here as the level causing the preamp to operate at its 1 dB compression point. As the spurs were 50 dB less than the desired signals, they were regarded as inconsequential. The spurs were likely third order intermodulation products, as they did not exist when only one RF input was present.

The measurements indicated that the receiver would produce comparable outputs whether the clutter signal was delivered by the antenna at RF or injected at IF. Development of an IF clutter generator was therefore feasible.

2.0 CLUTTER

2.1 Radar Cross Section of Distributed Targets

Two targets separated by less than the 3 dB antenna beamwidth in angle or by less than a pulsewidth in range cannot be resolved by a noncoherent radar such as the TRS. In typical clutter models for noncoherent radars the environment is modelled using a grid (in polar coordinates) of resolution

cells with these dimensions. Objects small relative to the size of a resolution cell can be defined as point targets and objects large relative to a cell can be defined as distributed targets, as in [2]. The land or sea surface surrounding the radar can be regarded as one massive distributed target whose echo can be modelled on a cell by cell basis.

While a point target reflects a pulse back to the radar as illustrated in Fig. 5a), an extended target reflects power in such a way that individual pulses are not generally visible. In Fig. 5b) the signal at t=T is a summation of power reflected from the portion of the distributed target lying between R_{MIN} and R_{MAX} and antenna beamwidth limits. This resolution cell causes a power density at the radar antenna in a similar manner to a point target, and can therefore be assigned a radar cross section. Skolnik [3] defines the radar cross section of a target as "the (fictional) area intercepting that amount of power which, when scattered equally in all directions, produces an echo at the radar equal to that from the target; or in other terms,

$$\sigma = \frac{\text{power reflected toward source/unit solid angle}}{\text{incident power density}/4\pi}$$

$$= \lim_{R \to \infty} 4\pi R^2 \left| \frac{E_r}{E_i} \right|^2 \quad (1)$$

where R=distance between radar and target, E_r=reflected field strength at radar, and E_i=strength of incident field at the target. Once a value of σ has been assigned received signal power P_r can be computed using the radar range equation:

$$P_r = \frac{P_t G_t \sigma A_r}{(4\pi R^2)^2} \quad (2)$$

where P_t watts are transmitted from an antenna of gain G_t and effective aperture area A_r.

As indicated above, the resolution cell's reflectivity determines its cross section. If the land or sea reflectivity is assumed constant in the cell vicinity, Σ becomes directly proportional to cell area, which is determined by the radar's pulsewidth and antenna beamwidth. In [4], σ^o is defined as the differential scattering cross section, and is a coefficient independent of these parameters. Use of σ^o implies that clutter return is contributed to by a large number of scattering elements whose phases are

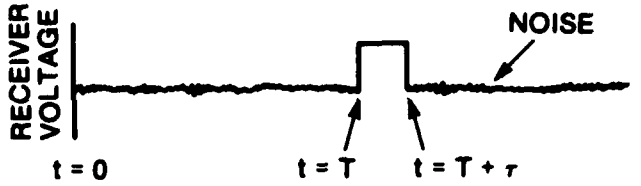

FIGURE 5a): REFLECTION FROM A POINT TARGET

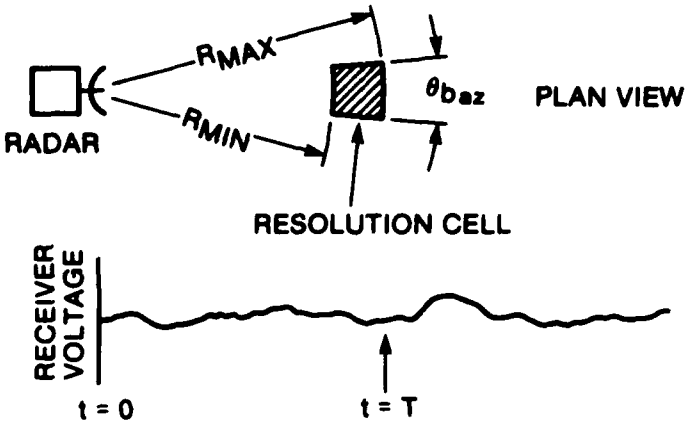

FIGURE 5b): REFLECTIONS FROM A DISTRIBUTED TARGET
Here: $R_{MIN}=(c/2)(T-\tau)$ and $R_{MAX}=(c/2)T$.
$c=3.0 \times 10^8$ m/s, T and τ are in seconds and R_{MIN} and R_{MAX} are in metres. θ_{baz} is antenna azimuth beamwidth.

independent. If a region illuminated at a given instant by a radar contains n scattering elements the radar equation can be written as:

$$P_r = \sum_i^n \frac{P_{ti}G_{ti}A_{ri}\sigma_i}{(4\pi R_i^2)^2}$$

$$= \sum_i^n \frac{P_{ti}G_{ti}A_{ri}(\sigma_i/\Delta A_i)\Delta A_i}{(4\pi R_i^2)^2} \qquad (3)$$

where ΔA_i is an element of surface area and where P_{ti}, G_{ti}, A_{ri} are radar parameters appropriate for an element at the location of ΔA_i and σ_i is the radar cross-section of the ith scatterer. The quantity $(\sigma_i/\Delta A_i)$ is the incremental scattering cross-section for element i. The average value of this quantity can be represented by σ^o. Average power is given by:

$$\bar{P}_r = \sum_i^n \frac{P_{ti}G_{ti}A_{ri}\sigma^o\Delta A_i}{(4\pi R_i^2)^2} \qquad (4)$$

In the limit we can write:

$$\bar{P}_r = \frac{1}{(4\pi)^2}\int_{\text{illuminated area}} \frac{P_r G_t A_r \sigma^o dA}{R^4} \qquad (5)$$

which is a valid relationship if the illuminated area is large enough to contain many independent scatterers [3].*

The term grazing angle is commonly used to denote the angle between the local horizontal at the reflecting surface and the radar beam direction [5, p.30]. The low grazing angle case encountered by a surface based radar or sea-skimming missile seeker was of primary interest to the author. In this case the area of the illuminated resolution cell increases with range. This effect is illustrated in Fig. 6b), where the far resolution cell has

---

*Over small illuminated areas, such as those of dimensions comparable to individual scatterers, the concept of an average value of $(\sigma_i/\Delta A_i)$ is meaningless.

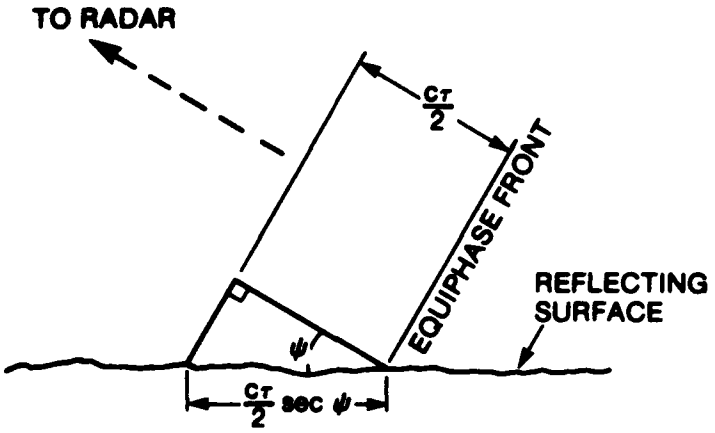

FIGURE 6a): SIDE VIEW OF LOW GRAZING ANGLE GEOMETRY
τ is pulsewidth, ψ is grazing angle.

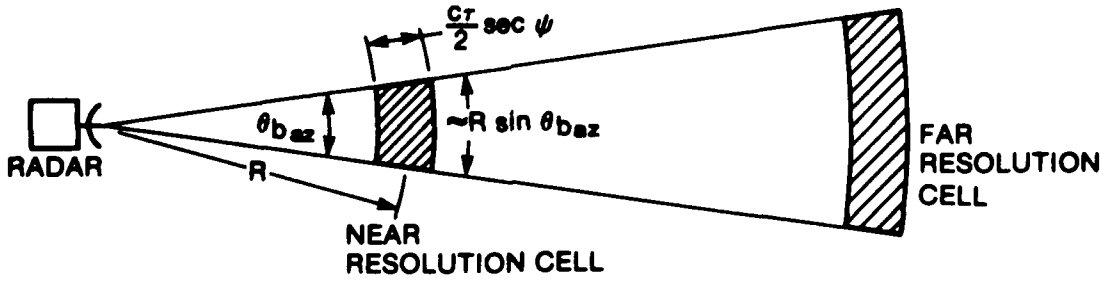

FIGURE 6b): PLAN VIEW OF LOW GRAZING ANGLE GEOMETRY
R is range to centre of cell, θ_{baz} is radar antenna azimuth beamwidth.

approximately double the area of the near resolution cell. From the figure, the area of each cell is $(c\tau/2 \sec\psi)(R \sin\theta_{baz})$, where τ is the pulsewidth, ψ is the grazing angle, R is the range to the centre of the cell, and θ_{baz} is the radar antenna azimuth beamwidth. This increase in illuminated area with range results in the following radar range equation [3]:

$$P_r = \frac{P_t G_t^2 \lambda^2 \sin\theta_{baz} (c\tau/2) \sec\psi \, \sigma^\circ}{(4\pi)^3 R^3} \qquad (6)$$

This relationship is valid to the radar horizon for land clutter, and to the range at which the critical angle occurs [4] for sea clutter. (Beyond the critical angle clutter power decreases much more quickly than R^{-3}, as discussed in section 2.3.)

Because of its noiselike properties, clutter lends itself to description using statistical terminology. Clutter can be regarded as an RF signal described by a sequence of instantaneous power P_r values. To characterize it the sequence can be viewed as having been generated by a random process. Clutter can then be characterized by a probability density function (pdf) with mean and standard deviation. Real clutter can be recorded and then analysed to determine what random process would produce a signal with similar characteristics. Equation (6) indicates P_r has a σ° dependency. Because it is independent of radar parameters, clutter models in the literature generally refer to the distribution of σ° [6]. In this report $\bar{\sigma}^\circ$ will denote the distribution mean and σ° will denote a specific value corresponding to a given resolution cell.

A Gaussian random process can be used to model physical phenomena in which the observed random variable at a particular instant of time is the result of a large number of individual random events [7]. The mathematical justification for this is the central limit theorem. The electromagnetic field produced at the antenna by the clutter return in a particular resolution cell is the vector sum of independent scatterers. If the scatterers are each of equal magnitude but of phase randomly distributed over 0 to 2π, both in phase and quadrature components of the composite signal will have Gaussian distributions. The voltage of such a signal has a Rayleigh shaped distribution and it's power is exponentially distributed [2]. Hence to specify for modelling purposes the return power corresponding to the resolution cell, if no information about the cell (such as the number or size of scatterers) is known a priori, a random process governed by an exponential distribution can be used to generate σ°. Knowing the area of the cell equation (6) will provide a value of received power P_r. If we define the clutter power in a discrete manner with one value for each cell, this procedure can be repeated for all cells to produce a simulated clutter power envelope. The envelope will have an exponential spatial amplitude distribution.

2.2 Land Clutter Generation Requirements

The Rayleigh (exponential power) land clutter model has been employed widely in MTI analyses, and it is applicable for grazing angles above 5 degrees [8]. However, for lower grazing angles encountered by ground based radars the Weibull [9,10,11] and the log-normal [9,5] distributions have been used. The three distributions are shown in Fig. 7. The log-normal distribution has the longest tail and is therefore the most severe of the three, ie. it most greatly limits the radar's ability to detect and track targets. The deviation from Rayleigh statistics has been attributed to shadowing and the presence of occasional strong reflectors [2]. Both these factors become increasingly important as the transmit pulsewidth is narrowed and terrain features are resolved. Because clutter was required for radar pulsewidths ranging from 0.2 to 2.25 μs, the clutter generator had to be capable of producing all three clutter types.

The land surrounding a typical ground-based radar is composed of patches of different terrain types, such as forested areas separated by farmland. Within a patch, σ° varies from cell to cell in a manner determined by a particular distribution.* Different patches may be described by different distributions, or, as in the model described in chapter 4, by a common distribution with an individual mean and standard deviation for each patch. Clutter returns from terrain of varied composition may be described as nonhomogeneous. Homogeneous clutter returns are returns from the same terrain type, such as trees or grass, and have a unique $\bar{\sigma}^\circ$ and standard deviation. These should not be confused with spatially uniform clutter returns, which have zero standard deviation [12].

Ground clutter commonly has gaps where little or no signal is present. This is caused by shadowing due to prominent terrain features such as hills or man-made structures. Shadowing results in groups of resolution cells with little or no incident energy. These consequently reflect negligible energy back to the radar. An ability to represent shadowed areas was required for the clutter generator.

An important property of ground clutter is that it's spatial characteristics are dependent on the radar's pulsewidth. This is evident in Fig. 8, where individual patches and shadowed areas become resolved as the width decreases. In a fire control radar the pulsewidth is commonly narrowed as the system changes from the search to the track mode, in order to increase range resolution. The increased resolution aids in accurate weapons delivery and also reduces target masking by clutter. A capability of separate clutter waveforms for search and track modes was a generator requirement. An ability to produce finely structured waveforms with narrow peaks and troughs was also required, particularly for narrow pulsewidth cases. A survey of available memory and D/A devices revealed that a 0.2 μs waveform update period was a realistic design goal.

---

*Where patches are extremely small (only a few cells) it may be unclear what the appropriate distribution is. However, the terrain comprised of these patches can be assigned a single pdf.

LOG-NORMAL
(St. deviation of σ° = 5 dB)

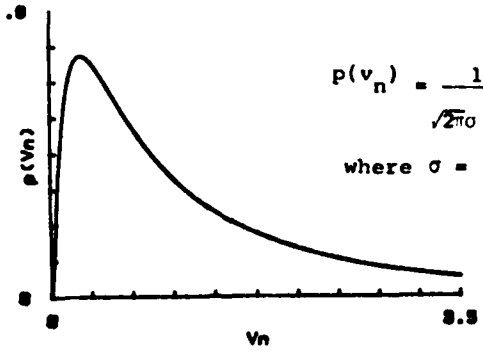

$$p(v_n) = \frac{1}{\sqrt{2\pi}\sigma\, v} \exp\left[\frac{-1}{2\sigma^2}\left(\ln\frac{v}{v_{med}}\right)^2\right] \quad (7)$$

where σ = standard deviation of $\ln\sigma^\circ$

WEIBULL
(α = 2.5)

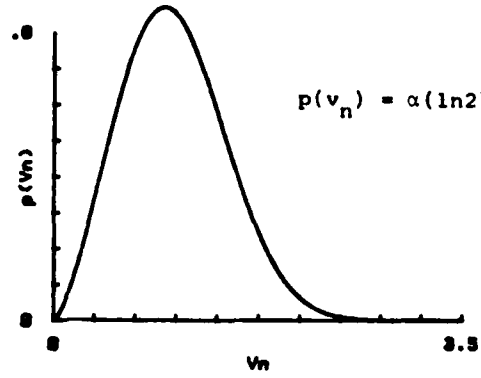

$$p(v_n) = \alpha(\ln 2)\left(\frac{v}{v_{med}}\right)^{\alpha-1} \exp\left[-\ln 2\left(\frac{v}{v_{med}}\right)^{\alpha}\right] \quad (8)$$

EXPONENTIAL
(α = 1.0)

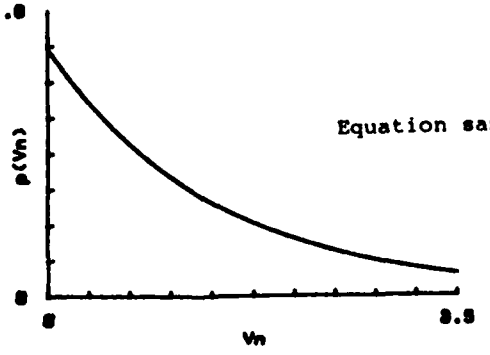

Equation same as Weibull

FIGURE 7: COMMON DISTRIBUTIONS USED IN CLUTTER MODELLING
v_n is normalized detector output voltage=v/v_{med}, where v_{med} is the median voltage, defined here as 1 V. A square law detector is assumed, where $v=kP_r$.

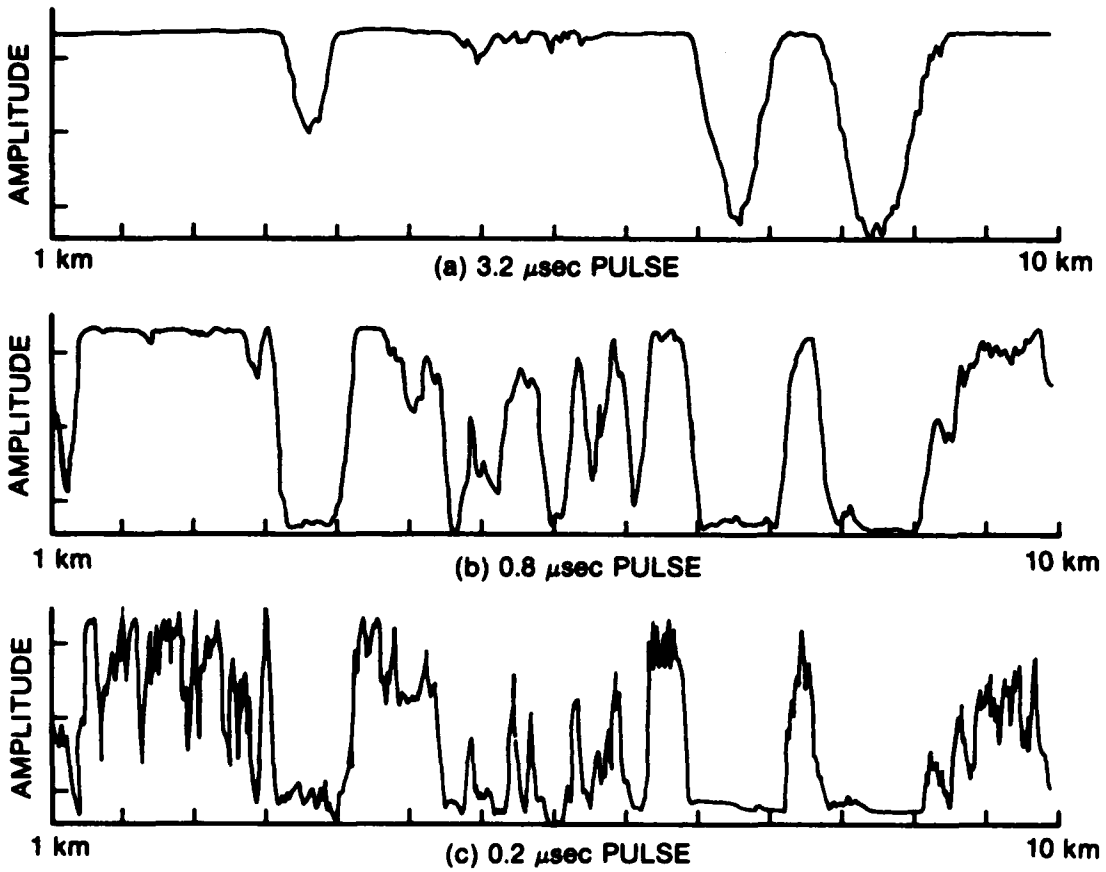

FIGURE 8: LAND CLUTTER VARIATION WITH PULSEWIDTH
Reproduced from [5].

Above discussions have dealt with the spatial amplitude characteristics of the clutter signal. When clutter contains wind-blown scatterers such as trees, the composite return from a resolution cell will fluctuate due to the vector addition of reflected signals, some of which are doppler shifted. This fluctuation limits MTI clutter cancellation. For a given target location and known value of $\bar{\sigma}^\circ$ clutter fluctuation directly affects the local false alarm rate and probability of detection [13]. Ground clutter is generally assumed to have a Gaussian shaped doppler spectrum, with a standard deviation of a few Hz or tens of Hz. For windspeeds of 2 to 50 knots [5] presents values of spectrum standard deviation ranging from 0.01 to 0.6 m/s. Assuming a Gaussian spectrum, the standard deviation will equal 0.42 times the 3 dB spectral width in velocity units. Using this and the standard doppler equation with transmit frequency f_t = 9.0 GHz* gives values of spectral width ranging from 1.4 to 87 Hz. An amplitude modulator with variable bandwidth and a spectral shape approximating Gaussian became a further requirement of the clutter generator.

A typical ground based radar scans a large volume of space, and can vary its antenna position between a few degrees below horizontal (maximum clutter) and straight up (minimum clutter). A way of attenuating the clutter waveforms as a function of the TRS antenna look angle was a further requirement of the generator. A 45 dB dynamic range was considered adequate for this function.

Second-time around clutter echoes are echoes from reflecting surfaces beyond the maximum unambiguous range of the radar. The radar antenna height determines the range to the radar horizon. Clutter echoes from beyond this range will not occur. If the pulse repetition frequency (PRF) is high enough that the maximum unambiguous range is less than the clutter horizon's range, second-time around clutter will be received. For example, assume a range to the radar horizon of 30 km, and a maximum unambiguous range of 15 km (corresponding to a PRF of 10 kHz). Returns from reflecting surfaces from 15 to 30 km will be superimposed on those from 0 to 15 km. For staggered PRF MTI radars these echoes are decorrelated and hence do not completely cancel in the FIR filter. The resultant clutter residue limits radar performance somewhat, but because of sensitivity time control (STC) and the greater range its effect is considered minimal. Hence a capability of generating second-time around clutter echoes was not included in the clutter generator.

2.3 Sea Clutter Generation Requirements

Even more so than terrain clutter, sea clutter characteristics are heavily dependent on a large number of surface and radar parameters. Sea clutter authors discuss at great length the effect of frequency, polarization,

---

*This value, while somewhat arbitrary, was chosen because the TRS operates at X-band.

look angle, pulsewidth, antenna beamwidth, frequency agility, presence of whitecaps, wave velocity, water particle velocity, average wave height and windspeed on sea clutter characteristics. Fortunately the latter five parameters can be represented (albeit crudely) by a single parameter called sea-state, defined by Nathanson as "...a single number that grossly summarizes the degree of agitation of the sea and the characteristics of its surface. The relationship between wave height and wind velocity or sea state is not clearly defined;..."[5,p 231]. But accurate modelling of sea echo over even a small range of parameter values is a formidable problem. The single most important requirement of the clutter generator was that it be software programmable so that more detailed models than those developed by the author could be implemented later as the need arose. However, a reasonably detailed study of published data did allow a good first order model to be developed.

There is general agreement in the literature that sea clutter at medium grazing angles (above 10 degrees) for relatively low resolution radars obeys the central limit theorem and has Rayleigh distributed amplitude statistics [5,14]. Nathanson [5] indicates this applies at low grazing angles in the 6 to 9 GHz range to radars with pulsewidths greater than 0.25 μs and beamwidths greater than or equal to 1°. Hence the Rayleigh voltage/exponential power model was used in the sea clutter model described in chapter 4, where the radar modelled has relatively low resolution. At low grazing angles, if resolution is increased the amplitude distribution changes, and the clutter as seen on an A-scope takes on a "spiky" appearance [14]. This is a combination of two factors: 1) at low grazing angles there is a higher probability that a given wave crest will be shadowed by other crests, hence a lower density of reflecting waves in the resolution cell [15], and 2) for higher resolution radars the wave structure may begin to be resolved [4]. This spikiness can be equated to a lengthened tail of the amplitude distribution. The deviation from the Rayleigh distribution also increases with sea-state. An explanation for this is that the average distance between wave crests is longer, causing a lower density of reflectors in a given resolution cell [15].

The distribution is also dependent on whether the radar transmits horizontally or vertically polarized energy. Horizontally polarized clutter is spikier than that of vertical polarization for two cases: 1) the pulsewidth is short enough that individual waves are resolved, and 2) the pulsewidth is large enough that more than one wave is included [4]. For case 2), the spikiness has been attributed in [4] to an interference effect from the energy reflected from the individual, unresolved scatterers.

Much effort has been expended attempting to determine the exact distribution for a specific sea-state and set of radar parameters. Among the models proposed are the log-normal, Weibull, contaminated-normal, log-Weibull and K-distributions [14]. It was considered desirable that the generator be capable of any of these distributions.

Skolnik [4] and Nathanson [5] both indicate a non-linear increase in $\bar{\sigma}^{\circ}$ with grazing angle. The total variation of $\bar{\sigma}^{\circ}$ with grazing angle can be more than 30 dB at X-band. $\bar{\sigma}^{\circ}$ also increases with sea-state, as can be seen in the tabulated data in [5]. Inclusion of the $\bar{\sigma}^{\circ}$ dependency on grazing angle and sea-state was considered essential for the clutter generator. $\bar{\sigma}^{\circ}$ is higher for vertical than for horizontal polarization [16], but the author was unable to find a generally agreed relationship between the two cases over the wide range of surface and radar parameter values. Also, the spatial extent of the large echoes has been observed to be smaller for horizontal than for vertical polarization [16]. To limit the scope of the project only horizontally polarized radar clutter was modelled, ie. the sea clutter model was based on published data pertaining to horizontally polarized radars only. Other polarizations may be included at a later date.

Three scattering regions have been identified in the literature. At large grazing angles (near vertical incidence) the echo is large, apparently due to facet-like surfaces oriented perpendicular to the radar. This is referred to as the quasi-specular region [3]. As these returns exist only at extremely close ranges they are not included in the chapter 4 model. At low grazing angles (those below the "critical angle"[4]) $\bar{\sigma}^{\circ}$ decreases quickly versus decreasing ψ. This is called the interference region since direct and scattered signals are out of phase producing destructive interference. As this region is not well defined in graphically presented X-band data in [3] it has also not been included in the sea clutter model. The remaining angular region, the plateau or diffuse region, has as principle scatterers those components of the sea that have dimensions comparable to transmit wavelength λ. The model has been based on published data corresponding to this region.

Sea clutter has a spectrum that results from the distribution of radial velocities of the scatterers [5], plus constructive and destructive interference from the scatterers [17]. This spectrum is commonly assumed to be Gaussian shaped*. The return from a given resolution cell decorrelates with time. 10 ms is given in [18] and [4] as a decorrelation time for low resolution radar. For a 1 kHz PRF radar returns would be correlated from pulse-to-pulse but would decorrelate over 10 pulses. (For high resolution radars the decorrelation time is much greater than 10 ms [18]). The existence of this effect dictated that a decorrelating amplitude modulator with variable characteristics be included in the clutter generator design. Nathanson [5] reports an almost linear dependence of the 3 dB spectral bandwidth on

---

*Asymmetrical spectra have been observed when white caps are present. This asymmetry appears to increase with increasing surface roughness [19]. Because an amplitude modulation scheme was used, all spectra produced by the clutter generator are symmetrical. This limitation is considered minor.

sea-state. For sea-states of 1 to 5 he presents experimental values ranging from 0.1 to 2.9 m/s, which would at f_t = 9.0 GHz translate to 6 to 176 Hz. Generation of an AM spectrum with a variable bandwidth became a further design goal.

Note that relatively slow fluctuations in clutter due to 1) variations in the amplitude or slope of individual ocean waves passing through the illuminated area, and 2) long-term modifications to the sea [17] were not included as generator capabilities. As these fluctuations occur over a large number of radar pulse repetition intervals (PRIs) their effect is considered secondary.

Clutter can be pulse-to-pulse decorrelated through the use of pulse-to-pulse frequency agility. A change in transmit frequency of the inverse of the pulsewidth is sufficient to cause successive returns from a given cell to be independent [14], while having no effect on point targets. This is because the return from a distributed target is the vector addition of returns from independent scatterers with random phases.* Hence the amplitude of a single cell return will fluctuate in a noise like manner. Integration over a number of successive PRIs can then raise the signal-to-clutter ratio [20]. Frequency agility is a common radar technique not only because of its ability to improve detection capability in sea clutter, but as an electronic counter-countermeasure (ECCM), and as a technique used to reduce glint. (Glint is wander of the apparent target angular position about its phase centre.) For these reasons it was desired that the clutter generator be capable of generating signals that were independent from PRI-to-PRI.

Sea clutter as viewed from a moving platform (such as a sea skimming missile) will have a mean doppler frequency f_d that is, for low grazing angles, approximately equal to $2V/\lambda$, where V is platform velocity and λ is transmit wavelength. Even for stationary platforms, a non-zero mean doppler will exist. [5] reports this shift for horizontal polarization as being dependent upon both wind speed and wave height. For vertical polarization the shift is primarily dependent on wave height. The mean doppler of horizontally polarized clutter is reported as being two to four times that of vertically polarized clutter. A further generator requirement was that a mean doppler

---

*High resolution radars resolve the wave structure and hence see individual scatterers. Presumably this is why the technique is reported as ineffective for high resolution radars in [20] and for a 0.1 μs pulsewidth radar in [18].

shift proportional to sea-state and platform velocity could be given to the signals. Note that the mean doppler is also dependent on the azimuth look angle, being maximum when the radar looks upwind and being reduced by a cosine factor [7] for other look angles. This cosine variation was omitted from the generator to limit its complexity.

As the radar scans in azimuth, it illuminates different sectors of the sea surface. In [15] returns from adjacent sectors separated by two or more sea-wavelengths are considered independent. The 5.36° azimuth beamwidth used in the chapter 4 model defines sectors that would normally encompass several sea wavelengths. Hence adjacent resolution cells are considered independent. This assumption may not be valid for close ranges combined with sea-state 5, where sea wavelengths can be as much as 260 ft. [5].

There are likely to be a number of additional sea clutter trends reported in the literature that were not allowed for in the clutter generator design. Generally a trend will be observed by an author but no mathematical description will be proposed. In any event limited time and resources dictated excluding these. One is likely to be the deviation from Rayleigh statistics that increases with increasing sea state. This is due to the average distance between wavecrests increasing, causing a lowered density of reflectors in a given resolution cell [15]. Another is that $\bar{\sigma}°$ is larger in the upwind or downwind direction than crosswind [16].

Note that as discussed in section 2.2, second time around clutter echoes are not generated.

3.0 CLUTTER SIGNAL GENERATION

3.1 Hardware Overview

In the previous chapter the requirements for a clutter generation system were identified. This chapter describes the actual implementation of the generation system. Sufficient detail is presented to allow an appreciation of the design, its key features, and the measurements performed during the design process. Additional material of a more detailed nature can be found in Appendix A.

The hardware consists of an IF component arrangement to perform amplitude modulation, plus a controller. The overall system is described here, followed by a detailed description of the IF components and a two part description of the controller. Detailed information on the memory based circuitry of the controller appears in Appendix A.

As shown in Fig. 9, the clutter signal originates from a 60 MHz voltage controlled crystal oscillator (VCXO). This is controlled by the stabilizer circuit, which is capable of phase locking the VCXO to the 60 MHz signal used in generating the target RF signals. Once phase locking has been accomplished a doppler offset can be requested by the host computer and

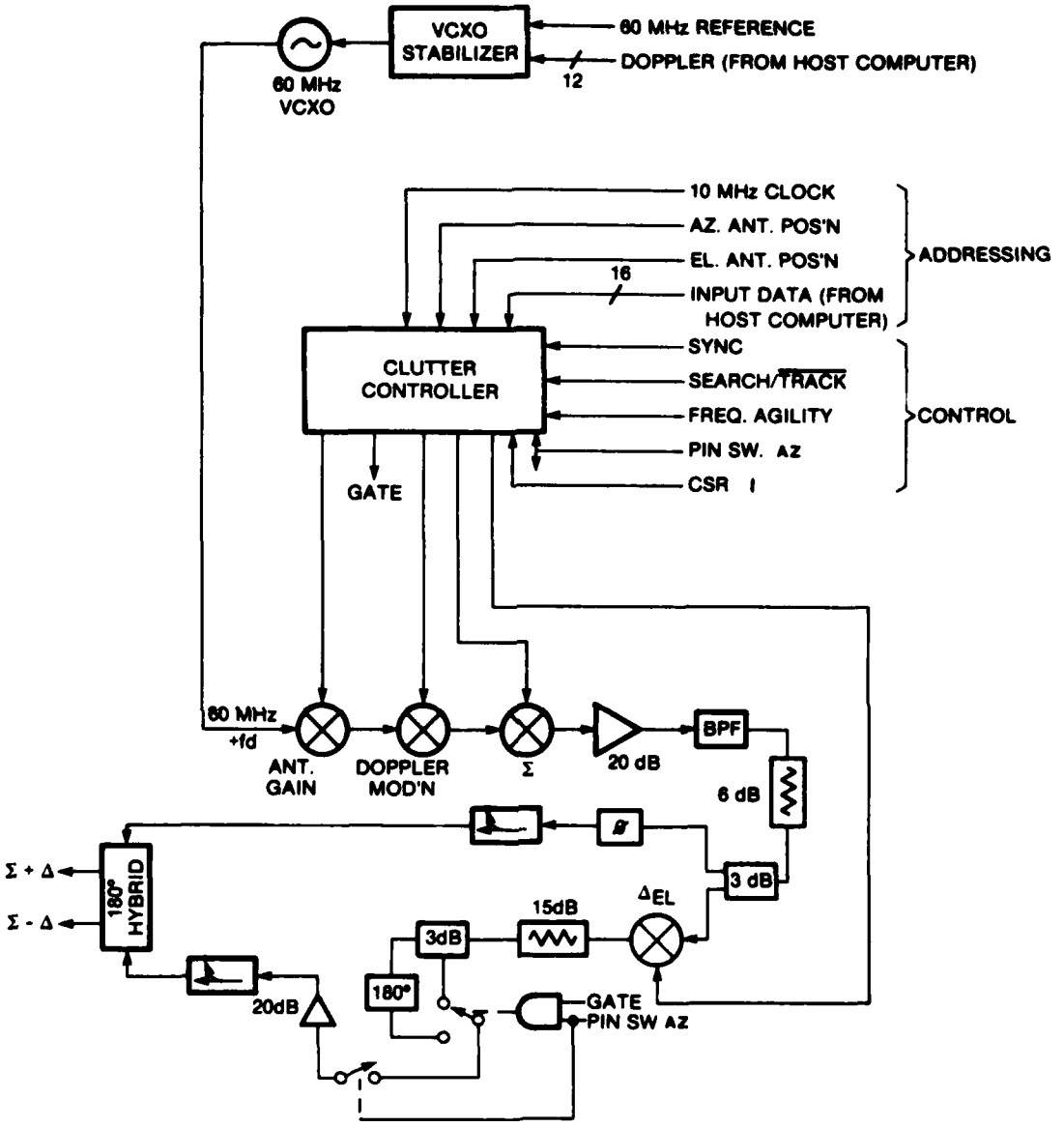

FIGURE 9: CLUTTER SIGNAL GENERATION SYSTEM

achieved by offsetting the VCXO tuning voltage. The ability to accurately control the target-to-clutter difference frequency is necessary for scenarios involving the TRS's MTI processor.

Four attenuators are used to modulate the 60 MHz signal. The attenuator control currents are produced by the clutter controller based on data loaded into its 100 k bytes of RAM before the beginning of an engagement scenario. Memory addresses are generated using counters and digitized elevation and azimuth antenna position voltages. The addressing process is controlled by the decoding of various TTL lines from the TRS and host computer.

The antenna gain attenuator reduces the clutter signal levels when the reflecting surface is not illuminated by the main antenna lobe. The generator was designed primarily for the low grazing angle clutter that is seen by radars with antenna heights in the 5 to 50 m range. Because the reflecting surface typically subtends a small range of depression angles, a detailed representation of antenna gain versus range (time) is not required. The clutter's range extent is subdivided and a depression angle is calculated for each interval. This angle is used to compute the antenna gain, and hence the appropriate attenuator setting, for the interval. The antenna gain has a 54 dB dynamic range. Control is via a memory chip addressed by a range counter and a digitized version of the radar's elevation look angle voltage.

After scaling for antenna gain the signal is modulated with a variable bandwidth pseudo-random noise waveform. This replicates clutter fluctuation due to wind-blown scatterers such as trees or ocean waves, and can be disabled via a front panel switch for non-fluctuating clutter. The Σ attenuator then sets the signal amplitude according to the software based model of $\sigma°$. Signal amplitude is redefined each 200 ns, allowing the fine structure of narrow pulsewidth clutter to be replicated. This attenuator has a 56 dB dynamic range.

After amplification and filtering to remove harmonics of 60 MHz, the signal is split into two channels. The arrangement following the power splitter was designed to replicate the process occurring in the TRS receiver, where Σ and Δ components are added and subtracted in a hybrid coupler to produce $\Sigma+\Delta$ and $\Sigma-\Delta$ [21]. The upper channel (as shown) carries the clutter component. Because in search mode, the TRS does not produce Δ, the lower channel is effectively disconnected causing identical hybrid outputs. In track mode, the lower channel produces a signal proportional to Δ_{el}, the elevation difference component. This component is combined with Σ in the 180° hybrid to produce $\Sigma + \Delta_{el}$ and $\Sigma - \Delta_{el}$ signals. The phase of Δ_{el} is determined by a diode/transformer/amplifier arrangement represented in Fig. 9 as a single pole double throw (SPDT) switch. Control of this equivalent switch and the Δ_{el} attenuator is provided by a memory chip addressed by range and elevation angle. Δ_{el} is in phase with Σ for scatterers above boresight, and 180° out of phase with Σ for those below boresight, as in the TRS. A manual phase adjuster in the upper channel was used to obtain correct phasing at the hybrid inputs.

The Δ_{az} component that clutter would induce in a monopulse receiver has not been represented. It is felt that this component would be minimal for radars on the ground, on ships, and on non-spinning missiles, where clutter power in the left and right pairs of antenna horns would be approximately equal. Because Δ in the TRS alternates between Δ_{az} and Δ_{el} on successive PRIs, during every other PRI the Δ_{el} attenuator is set to maximum attenuation and the biases are removed from the SPDT diodes. This gives a combined loss of approximately 100 dB in the lower channel, so that Δ_{az} is effectively zero.

3.2 IF Components

Individual IF components are identified in Fig. 10. The Minicircuits ZMAS-3 and ZEM-2 were selected for use as attenuators. While the ZMAS-3 is marketed as an electronic attenuator, the ZEM-2 is a mixer. The schematic diagrams for both devices are identical except for port labels. Mixers can be used as attenuators by applying a control current to the IF port and the input signal to the RF port, with the output appearing at the LO port [22]. Applying a current to the IF port partially forward biases two of the four mixer diodes, causing a controllable amount of applied power to arrive at the LO port. The schematic and an equivalent circuit for the ZEM-2 when operated in this fashion appear in Fig. 11. For the Σ attenuator a 20 ns response time was desired, so that the signal level could be redefined every 200 ns with a 10% transition time. A 60 dB dynamic range was also a goal. Because a PIN diode attenuator with these specifications was unavailable* the ZEM-2 was chosen for use as the Σ attenuator. It was also convenient to use a ZEM-2 for the doppler modulation attenuator.

The antenna gain and Δ_{el} attenuators did not require a fast response time but did require the ability to operate with input power levels above +1 dBm. The ZEM-2s were unsuitable as their attenuation range was reduced at power levels above this. Hence ZMAS-3s were chosen for the remaining attenuators. Specifications for both devices are found in table 1.

---

*A Lorch DA601NL digital attenuator was evaluated, but was expensive ($3000 U.S.) and exhibited spike shaped switching transients. Other commercial attenuators did not meet the combined speed, range and price requirements.

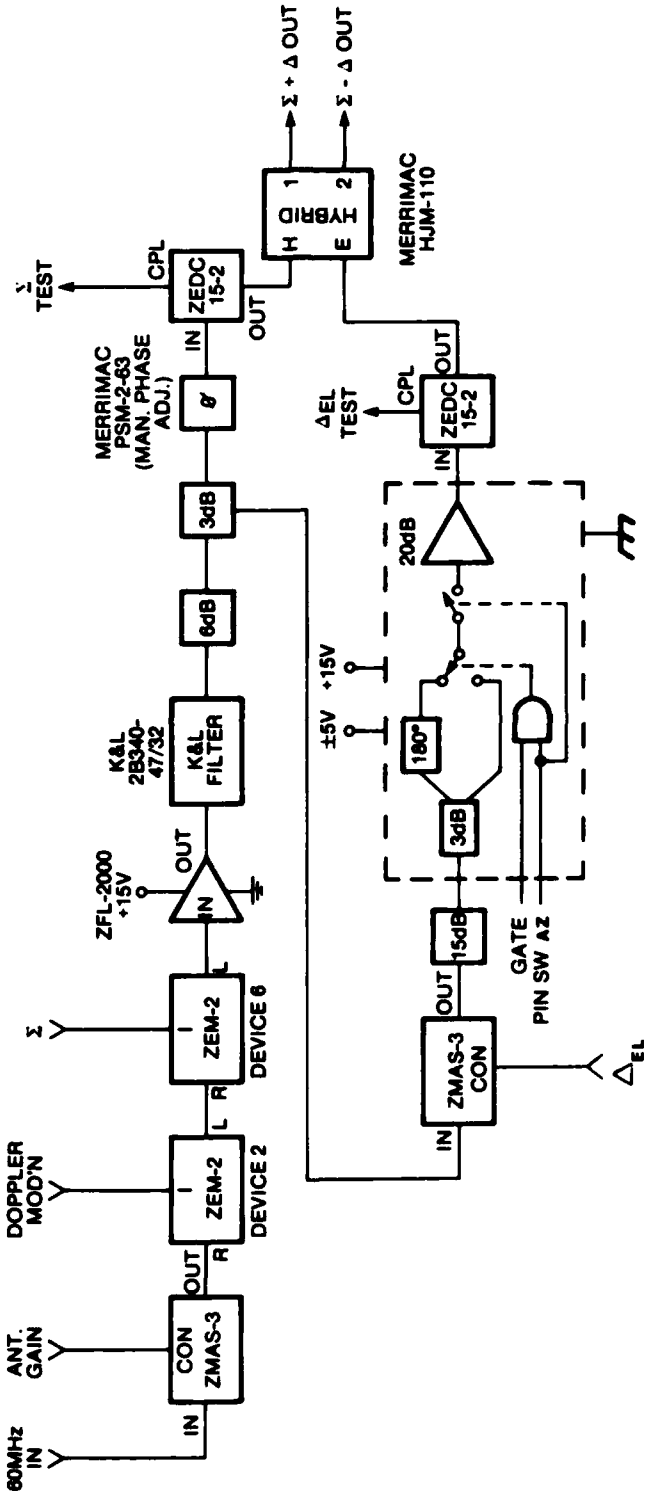

FIGURE 10: IF COMPONENTS

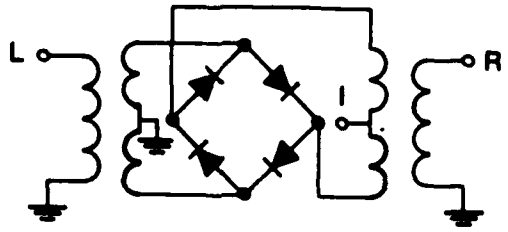

FIGURE 11a): ZEM-2 SCHEMATIC DIAGRAM
From Minicircuits catalogue.

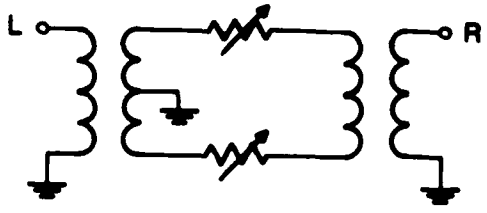

FIGURE 11b): EQUIVALENT CIRCUIT WHEN USED AS AN ATTENUATOR

TABLE 1: Attenuator Specifications

Specification:	ZMAS-3	ZEM-2
Dynamic Range (Measured)	54 dB	56 dB
Max. Input Power	+30 dBm	+17 dBm
Control Freq. Range	DC-50 kHz	DC-1000 MHz at IF port
Input Freq. Range	1-200 MHz	10-1000 MHz at RF port
Cost (1-4 items)	$66.95 U.S.	$59.95 U.S.

One problem common to both attenuators was nonlinearity of the attenuation versus control current transfer function. The nonlinearity is illustrated in Figs. 12 and 13. These measurements were taken using the clutter controller D/A circuits, which produce current varying linearly with input control word. The non-linearities, though severe, were compensated for in the controlling software. The non-linearities also created severe harmonics, but these were removed by a K & L tubular bandpass filter having a 47 MHz centre frequency and a 32 MHz 3 dB bandwidth. The filtered output is shown in Fig. 14.

Because the 1 dB compression point of the TRS preamplifiers is 0 dBm, this defined the desired maximum output level of the clutter generator. The +7 dBm VCXO output level became -5 dBm after passing through the three cascaded attenuators (Fig. 10) even with minimum attenuation settings. A Minicircuits ZFL-2000 20 dB amplifier provided the needed boost in power levels.

As was mentioned previously, the two channel arrangement in Fig. 10 replicates the process occurring in the TRS receiver. Analysis of measurements in [21] revealed Δ_{el} in the TRS receiver could be expressed as a function of Σ and elevation look angle. Hence by splitting the clutter Σ signal and modulating one channel with the same function, a Δ_{el} clutter component could be produced. Measurements were carried out on the TRS to determine what the function was. A CW 9.0 GHz source was connected to the 16x16 antenna array through a TWT amplifier and variable attenuator. The antenna's azimuth drive gear was locked at 0° so that the antenna could be moved in elevation only. The most direct approach would have been to measure Σ and Δ_{el} at the hybrid coupler inputs (see Fig. 4). However, due to the careful phasing of these signals and the difficulty of accessing antenna mounted circuitry, this was not done. Instead an HP 436A power meter and HP 8481A power sensor were connected to the hybrid coupler outputs once a spectrum analyzer confirmed that a clean 9.0 GHz signal was present.

Two sets of measurements were made. For set #1, the centre two dipoles in the top 16 x 16 array row were switched on. The antenna was then moved

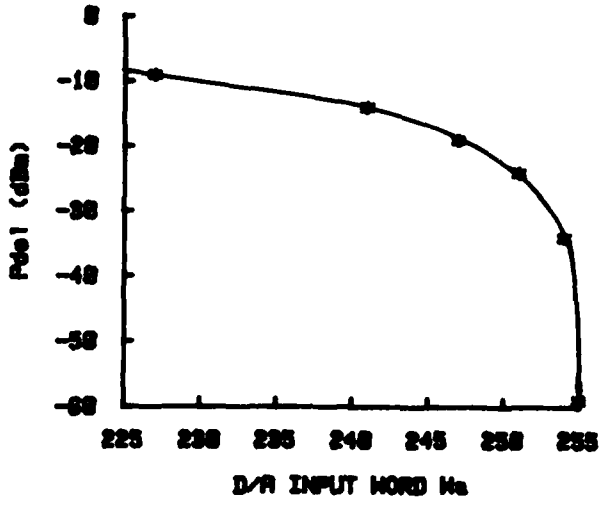

FIGURE 12: ZMAS-3 ATTENUATION MEASUREMENTS
Not shown is $(P_{del},Wa)=(-4,0)$.

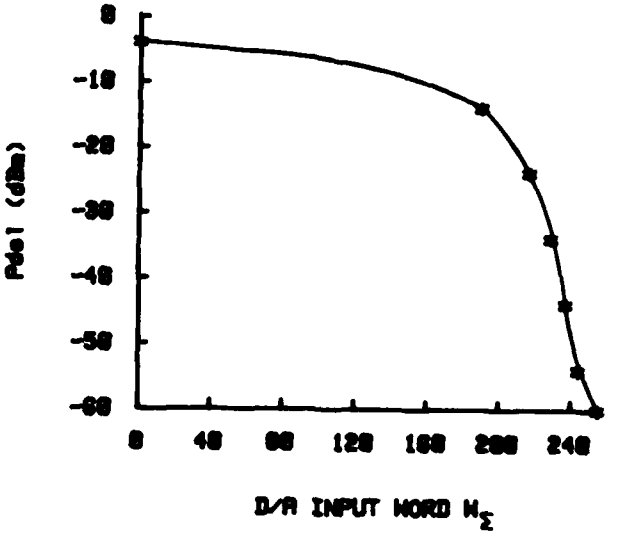

FIGURE 13: ZEM-2 ATTENUATION MEASUREMENTS

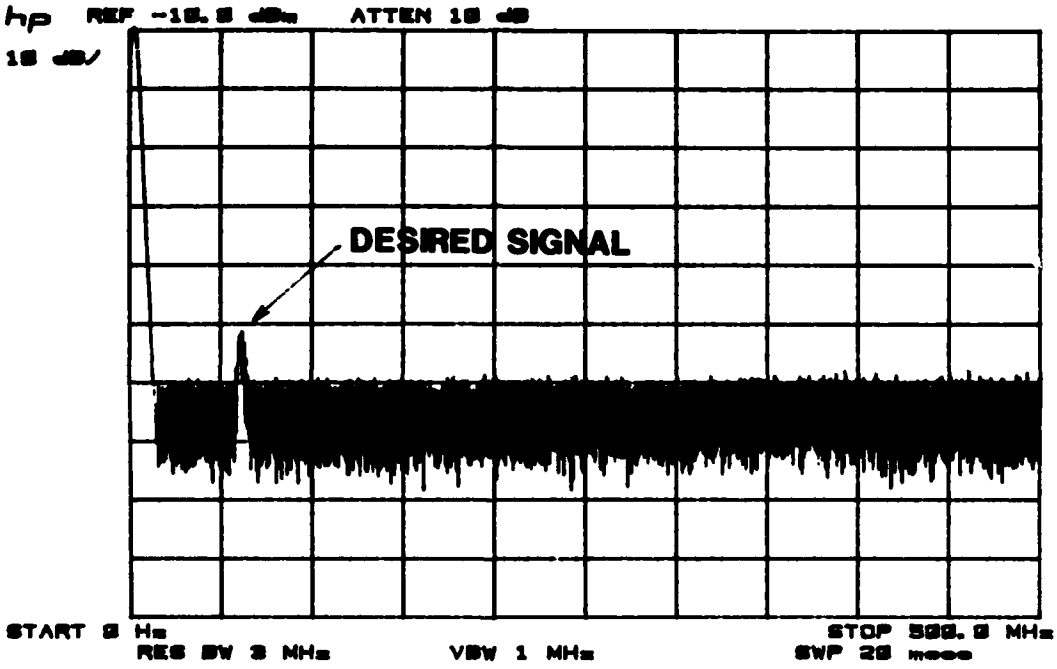

FIGURE 14: CLEAN SPECTRUM PRODUCED BY ZEM-2
CASCADED WITH K & L TUBULAR FILTER

from boresight to pointing angles below the "target" dipoles. Antenna movement was done manually using its vernier as the position indicator. At each pointing angle, the amplitude of the $\Sigma+\Delta$ channel was measured for: a) PIN switch off so $\Sigma+\Delta = \Sigma$, and b) PIN switch on so $\Sigma+\Delta = \Sigma+\Delta_{el}$. The procedure was repeated for set #2 except that the centre two dipoles in the bottom 16 x 16 array row were used and the $\Sigma-\Delta$ channel was measured. The antenna was moved from boresight to pointing angles above the "target". $\Sigma+\Delta_{el}$ was stronger than Σ for targets above boresight, and $\Sigma-\Delta_{el}$ was stronger than Σ for targets below boresight, confirming the expected phase relationships documented in [21].

A simple program was written to compute the level of the Δ_{el} hybrid input relative to the Σ input, assuming that perfect addition and subtraction of the signal vectors had taken place in the hybrid coupler. The plot of the converted measurement data appearing in Fig. 15 has the expected monopulse difference curve shape.

An approximating equation:

$$G\Delta_{el}(\theta') = \begin{cases} 15.5\sqrt{\sin(|\theta'|\pi/8)}-11 & \text{for } -4^\circ \le \theta' \le 4^\circ \\ 15.5\sin(\pi/2+(\theta'-4)\pi/32)-11 & \text{for } 4^\circ < \theta' \le 12^\circ \\ -15.5\sin(-\pi/2+(4+\theta')\pi/32)-11 & \text{for } -4^\circ > \theta' \ge -12^\circ \end{cases} \qquad (9)$$

which also appears in Fig. 15 provides a good characterization of the TRS receiver angle tracking function. Here $\theta' = \theta_n 6.0/\theta_{bel}$, which scales the curve's horizontal axis for radars with elevation beamwidths different than the TRS's 6.0°. θ_n is the off axis angle of the clutter. The required Δ_{el} attenuation (in dB) is defined by:

$$\begin{aligned} \text{ELATTN} &= |G\Delta_{el}(\theta')-5| && \text{for } -12 \le \theta' \le 12^\circ \\ &= 54 \text{ dB} && \text{elsewhere} \end{aligned} \qquad (10)$$

The memory chip for this attenuator is addressed by a range counter plus elevation look angle in a similar manner to the antenna gain memory chip.

As indicated in the Fig. 15 plot, Δ_{el} exceeds Σ by as much as 4.5 dB. For this reason the lower channel in Fig. 10 has a gain of approximately this amount relative to the upper channel.

Because the ZMAS-3 has an insertion phase of 152° at 60 MHz (as measured on a network analyzer) an additional phase shift was required in the upper channel to ensure correct vector addition and subtraction. To calibrate the manually adjustable phase shifter, a program was run on the host computer which set the Δ_{el} attenuator so that equal signal levels existed at the

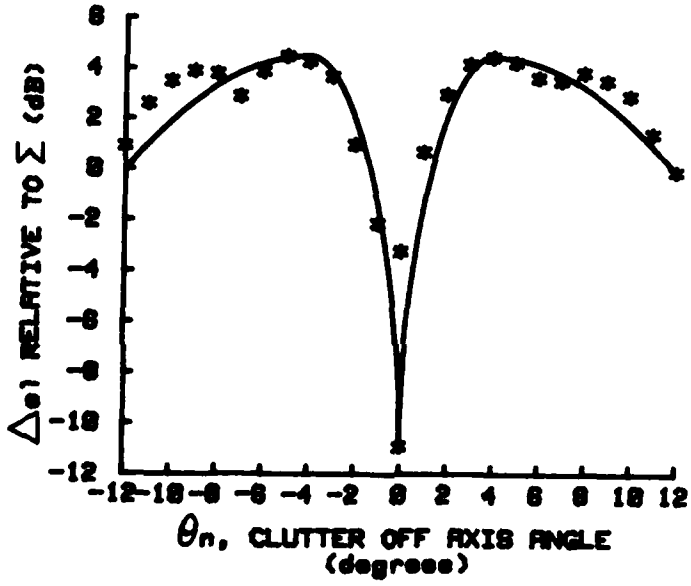

FIGURE 15: APG-502 MONOPULSE ANTENNA MEASUREMENTS WITH APPROXIMATING FUNCTION
The approximating equation uses θ_{bel}=6.0°.

hybrid inputs. The phase shifter was adjusted until minimum signal existed at the $\Sigma + \Delta$ output with 180° channel phase selected. After completion of the phasing the $\Sigma+\Delta$ channel exhibited levels of -27 dBm and +7 dBm for 180 and 0° channel phases, respectively. (The inverse of these results was observed on the $\Sigma-\Delta$ channel.) Network analyzer measurements showed that the ZMAS-3's insertion phase does not vary with control current, so proper phases exist at all signal levels.

3.3 Clutter Controller

3.3.1 Antenna Gain, Σ and Δ_{el} Modulation

The antenna gain, Σ, and Δ_{el} attenuator control currents are produced by D/A converters driven by control words read from memory. These control words are generated by software that is run before a scenario begins on the host PDP 11/44 computer. The algorithms used in generating these words are described in chapter 4.

The memory sections that are addressed by spatial coordinates appear in Fig. 16. All sections shown have 1024 of locations in range, which at 200 ns (30m) per location allows clutter to be simulated out to 30 km, if desired. The Σsearch memory covers the entire 86° azimuth search range of the radar antenna. The Σtrack memory covers a sector slightly greater than that of the 16x16 array. (The radar is not expected to enter the track mode outside the 16 x 16 array angular limits.) The antenna gain and Δ_{el} memories have equal dimensions and cover a 20° range of elevation look angles. At look angles above 20° both attenuators are set for maximum attenuation.

Not shown in Fig. 16 are the Σfa/search and Σfa/track memories used for frequency agility clutter. Like the other Σ memories these have 1024 of locations in the range dimension, but the 1 k byte rows are addressed sequentially using the frequency agility counter, which is clocked every PRI. As each row contains values that are statistically independent, the effect is to produce pulse-to-pulse uncorrelated clutter. Eight rows exist for search and eight for track modes. Hence the values repeat after eight PRI.

In addition to the 100 k bytes of RAM, an 8 k ROM chip addressed by range (1024 locations) and azimuth look angle (8 locations) has been included. The ROM can be programmed to produce a simplified clutter waveform for use in testing and maintenance. The ROM values control only the Σ attenuator, so the antenna gain and Δ_{el} mechanisms are not represented in the ROM mode.

3.3.2 Doppler Modulation

Resolution cells containing windblown trees or ocean waves reflect clutter signals that fluctuate in amplitude from PRI to PRI, as was discussed in chapter 2. In order to represent this effect the doppler

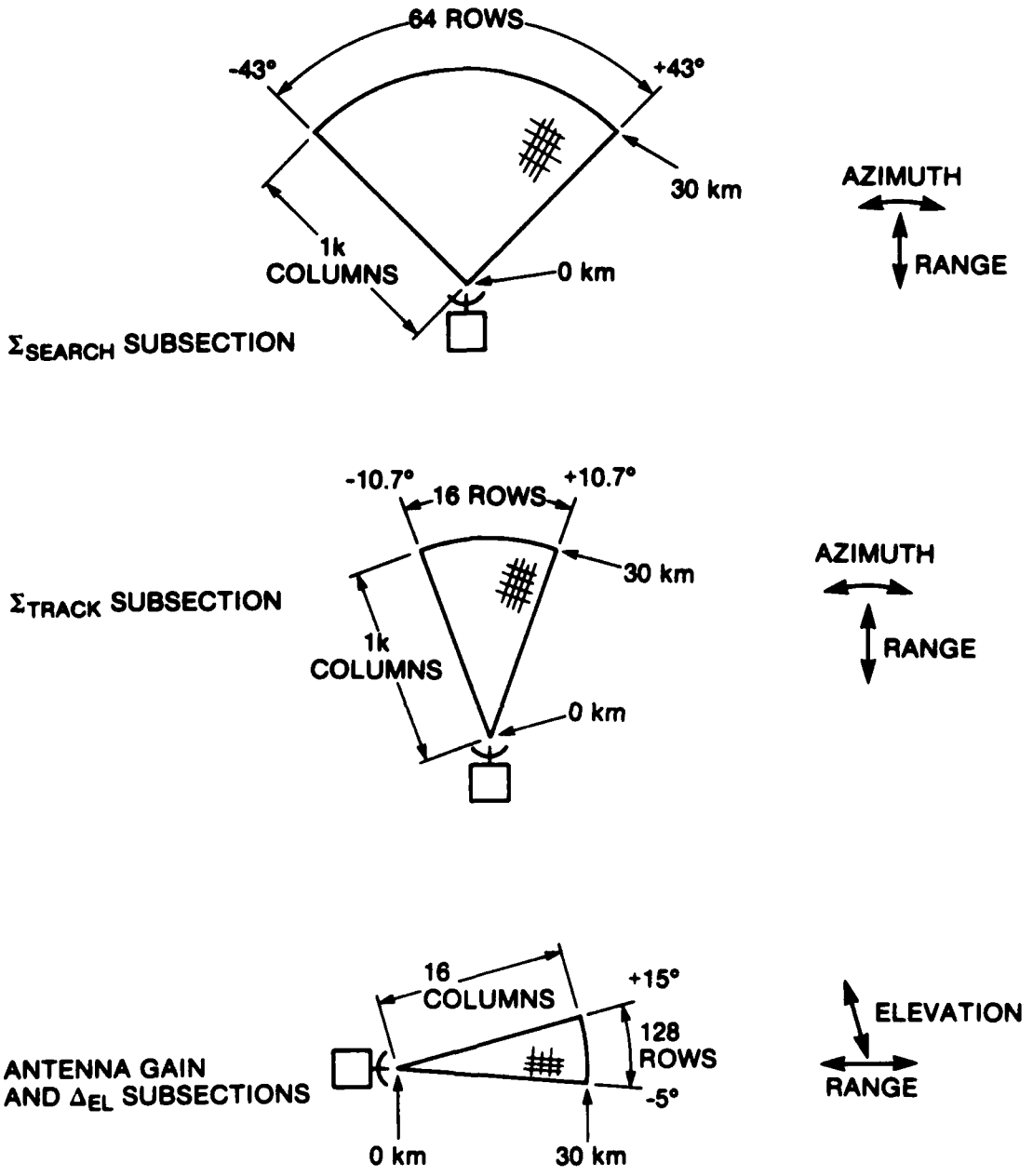

FIGURE 16: MEMORY SUBSECTIONS ADDRESSED BY RADAR COORDINATES

modulation attenuator was included. This attenuator is driven by a pseudo-random noise waveform that is passed through a variable filter and amplifier. The amplitude, DC offset, and spectral width of the control waveform are all front panel controllable. Additionally, the attenuator can be disabled for non-fluctuating clutter via a front panel switch. Disabling the attenuator sets the control current to a steady value.

In chapter 2, values of 3 dB spectral width ranging from 1.4 to 87 Hz for land clutter and 6 to 176 Hz for sea clutter were discussed. To produce an amplitude modulated signal with these spectral widths, low pass filtering of a noise modulation signal with relatively constant energy over the DC to 200 Hz region is carried out.

To implement a spectrum which has an exact Gaussian shape an extremely high order filter is required. However, a good representation can be realized by a workable order number filter. The approach taken here is to cascade biquadratic and Butterworth filter stages. The biquadratic filter has a low-pass notch frequency response, and the notch can be tuned to produce various spectral widths. Use of a switched capacitor version allows pole and zero locations to be moved by varying the frequency of an applied clock signal [23]. The Butterworth filter's low-pass response provides additional attenuation at frequencies above the notch. It also compensates for the switched capacitor filter's high gain at multiples of the clock frequency, and it attenuates any clock feedthrough.

The hardware that generates the control waveform for the doppler attenuator appears in Fig. 17. Two 8 bit serial shift registers are cleared on power up by a one-shot and then clocked at 2 kHz. Feedback gates produce an exclusive-NOR feedback function. Four bits from each shift register are summed together, with each bit weighted differently. The two sets of 4 bits are then subtracted at the op amp. This arrangement produces a pseudo random noise waveform which is applied to the MF10 switched capacitor filter. The MF10 is clocked by a voltage controlled oscillator whose control voltage is determined by a front panel switch setting. Settings produce 2,4,6,8 and 10 kHz clocks which result in MF10 cutoff frequencies of 20,40,60,80 and 100 Hz. Further filtering is performed by a Cermetek CH1290 active filter chip. It is used here in the low pass configuration with a cutoff frequency of 100 Hz. The filter output is summed with an adjustable DC offset using one of the CH1290's on chip op amps. Both offset and summer gain are front panel adjustable, allowing the user to vary the percentage of amplitude modulation. For non-fluctuating clutter, -15V is added to the summer via a FET switch. This causes the summing op amp to saturate, producing a steady control current for the doppler modulation attenuator.

Time and frequency domain measurements of the doppler modulation circuitry appear in Figs. 18a) and 18b). A fluctuating envelope such as that produced by wind-blown scatterers can be seen in Fig. 18a). The corresponding spectrum in Fig. 18b) has a shape that is approximately Gaussian.

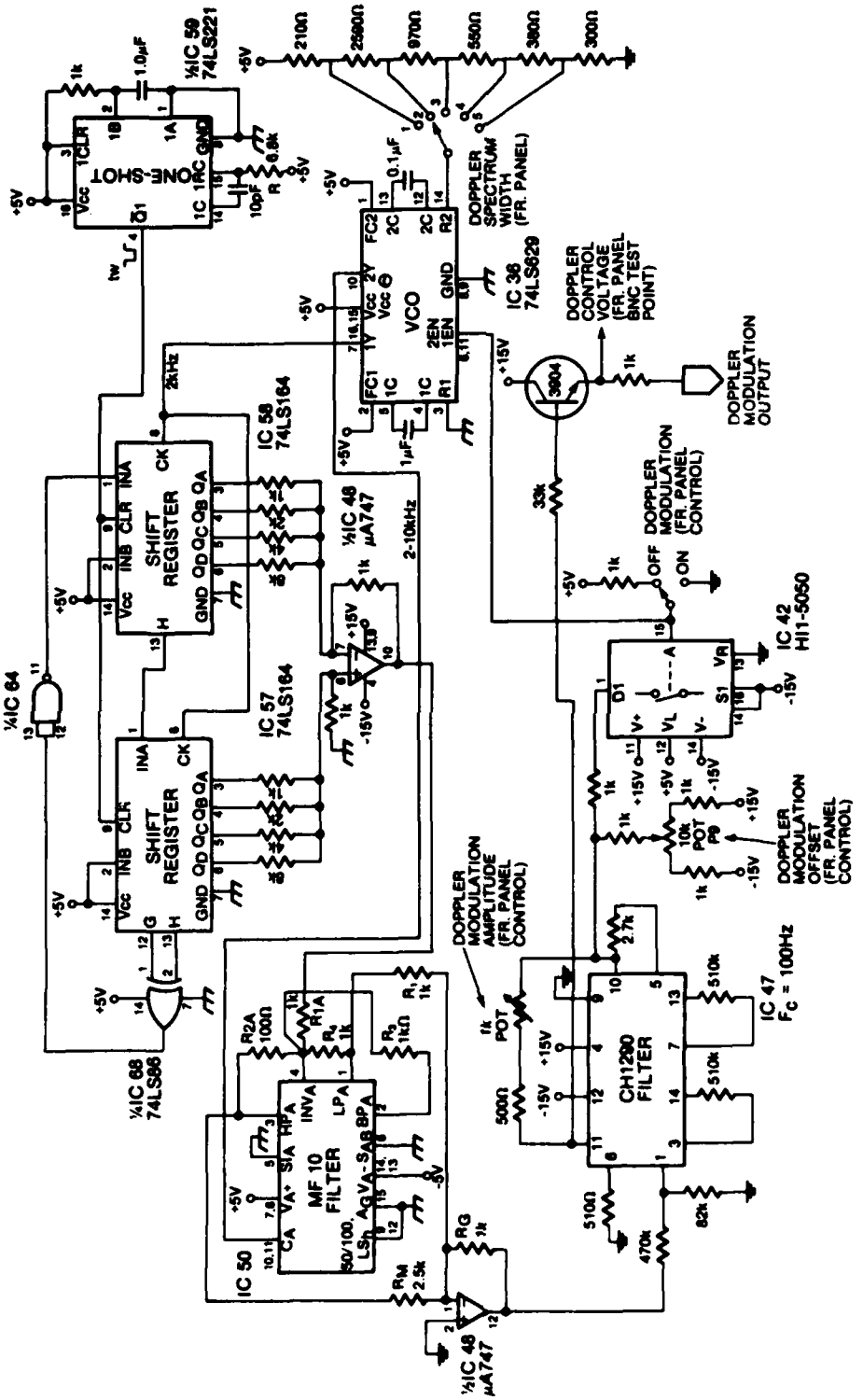

FIGURE 17: DOPPLER MODULATION ATTENUATOR CONTROL CIRCUITRY
For fluctuating clutter from wind-blown scatterers.

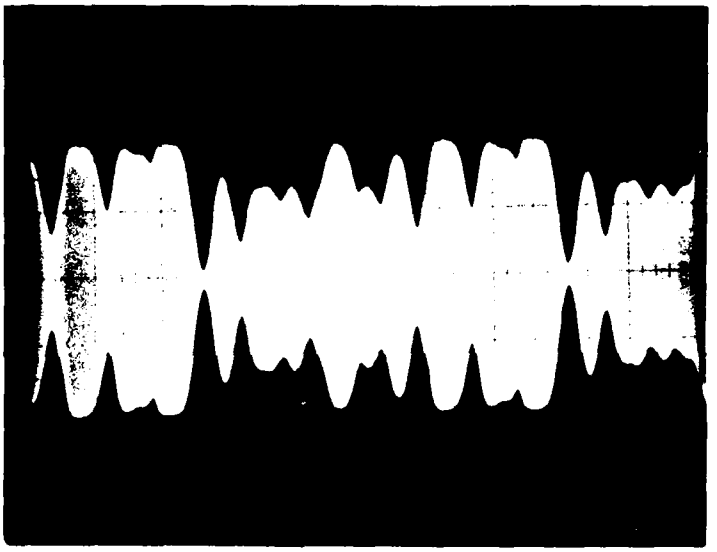

FIGURE 18a): DOPPLER MODULATION (TIME DOMAIN)
A steady 60 MHz signal was applied to the doppler modulation attenuator, which was set for a 200 Hz bandwidth. Vertical scale is 0.2 V/division; horizontal is 20 ms/division.

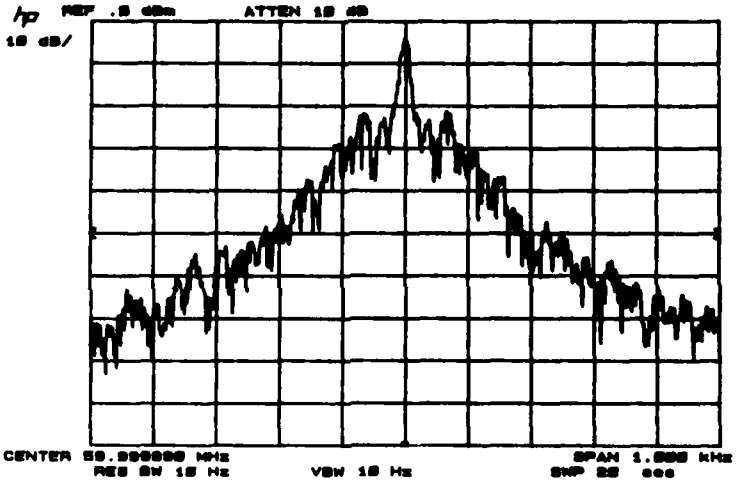

FIGURE 18b): DOPPLER MODULATION (FREQUENCY DOMAIN)
Spectrum is of the signal appearing in Fig. 18a)

4.0 CLUTTER MODELS

4.1 Introduction

The previous chapter described the hardware comprising the clutter generation system. The characteristics of the generated clutter signals are largely determined by the control words loaded into the controller's memory. These control words are generated and downloaded by software that runs on the host PDP 11/44 computer. Algorithms used by the software are described in this chapter. Derivations are included where appropriate.

All software was written using the host computer's Fortran-77, with the exception of two routines used to load the clutter data onto the DR11c interface, which were written in MACRO. Instead of storing clutter values on the system disk, each value is downloaded to the clutter generator immediately after it is generated. By not storing the data use of large portions of host computer memory is prevented. Model parameters can easily be checked by viewing the source file before execution. Also, new clutter waveforms can be quickly generated through the modification and execution of a single program. This proved to be a major advantage during the debugging stages of both the software and hardware. Generation and downloading of clutter data takes approximately 1.5 minutes for Weibull and exponential models and 4 minutes for the log-normal models.

Five separate clutter models will now be described: "detailed" land clutter, three varieties of generic land clutter, and sea clutter.

4.2 Detailed Land Clutter Model

The detailed land clutter model is not site specific. Instead the model contains a mix of farmland, forest, grassland and hills that might typically be illuminated by a radar operating in central Europe. While the model is considered sufficiently detailed to replicate the effect of typical land clutter on the TRS subsystems, secondary clutter mechanisms such as the dependence of σ° on transmit frequency, polarization, grazing angle, moisture content of vegetation, and time of year have not been included.

In the model, σ° is log-normally distributed. This is consistent with the majority of the clutter literature pertaining to low grazing angle scenarios [12]. From [3], the pdf for σ° is:

$$p(\sigma^\circ) = \frac{1}{\sqrt{2\pi}\sigma\sigma^\circ} \exp\left[-\frac{1}{2\sigma^2}\left(\ln\frac{\sigma^\circ}{\sigma^\circ_{med}}\right)^2\right] \quad \sigma^\circ > 0 \tag{11}$$

where σ° is the differential radar cross section, σ°_{med} is the median value of σ°, and σ is the standard deviation of $\ln\sigma^\circ$. Received power P_r is proportional to σ°, and if a square law detector characteristic is

assumed (output voltage $v=kP_r$ with $k=1$) the pdf of the detector output can be written as:

$$p(v) = \frac{1}{\sqrt{2\pi}\sigma v} \exp\left[-\frac{1}{2\sigma^2}\left(\ln \frac{v}{v_{med}}\right)^2 \right] \tag{12}$$

where v_{med} is the median value of v and σ remains the standard deviation of $\ln\sigma^\circ$. (This equation is plotted in Fig. 7.) The log-normality means that σ°, when expressed in dB, has a normal (Gaussian) distribution:

$$p(\sigma^\circ) = \frac{1}{\sqrt{2\pi}(\text{st. dev.})} \exp\left[-\left(\frac{\sigma^\circ - \bar{\sigma}^\circ}{(\text{st. dev})} \right)^2 \right] \tag{13}$$

where all parameters are expressed in dB. To generate a random number with a Gaussian distribution, the technique used is to add 12 independent, uniformly distributed random numbers:

$$g = \sum_{k=1}^{12} u_k - 6 \tag{14}$$

where u_k is uniformly distributed between 0 and 1 [2]. This produces a distribution with zero mean and unity variance. g is then multiplied by the standard deviation in dB and σ°_{med} (dB) is added, scaling and shifting the distribution so that it is no longer "standardized" [24]. For the highest standard deviation used in the model (10 dB for farmland) σ° values have a 120 dB range. As the Σ attenuator has a dynamic range of approximately 60 dB, the tails of the distribution are not fully represented. However, 60 dB represents a deviation of three standard deviations on either side of the mean, so 99.74% of the random values are correctly represented for the worst case clutter. Values falling outside the 60 dB range are set equal to the closest limit in software.

The values for u_k are generated using the Fortran-77 pseudo-random number generator available on the host PDP 11/44 computer. An initial value or "seed" must be specified--hence use of the same seed each time clutter is generated allows complete reproducibility of results.

The log-normal pdf was used for all regions. As shown in Fig. 19 and table 2 the terrain has arbitrarily been divided into regions of different terrain types.

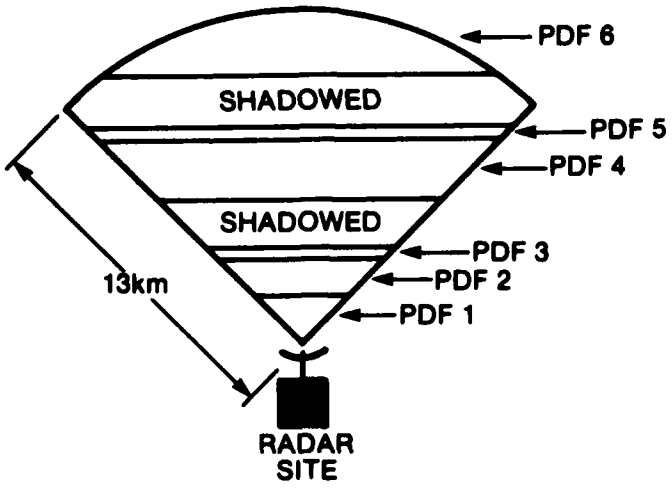

FIGURE 19: RADAR SEARCH SECTOR SHOWING TERRAIN TYPE DEFINITIONS.

TABLE 2: Parameters Defining Terrain Regions

PDF	TERRAIN	$\bar{\sigma}$ °	st. deviation of σ°
1	farmland	-33	10.0
2	forest	-27	7.5
3	grassland	-35	2.5
4	farmland	-33	10.0
5	grassland	-35	2.5
6	forest	-27	7.5

Different regions were assigned different means and standard deviations based on published data. Data in [8] indicates standard deviations of 7.5 dB for woods and 10 dB for farmland are appropriate for $\psi = 1°$, at X band. [12] suggests a standard deviation of 2.5 dB is appropriate for homogeneous clutter such as grass. [25] reports values of $\bar{\sigma}°$ = -27 and -33 dB for wooded hills and farmland, respectively, again for ψ= 1° at X band. [26] proposes a $\bar{\sigma}°$ of -35 dB for grass at X band.

The radar parameters used in both the detailed and generic land clutter models are found in table 3.

TABLE 3: Ground Based Radar Parameters

PARAMETER	VALUE
search pulsewidth	0.6 μs
track pulsewidth	0.2 μs
elevation beamwidth θ_{bel}	1.0°
azimuth beamwidth θ_{baz}	1.34°
antenna height h above mean terrain level	10.0m
antenna gain G_A	40 dB
transmitter peak power P_t	200kW
transmitter wavelength λ	.033m

Pulsewidths and the antenna azimuth beamwidth were chosen for computational convenience. All parameters are typical for noncoherent monopulse tracking radars, but no specific radar was modelled.

Shadowed areas are implemented by setting the Σ attenuator control word to 255 for all memory addresses corresponding to the shadowed region. 255 sets the Σ attenuator to maximum attenuation. As shown in Fig. 19, shadowed areas exist in two separate regions running across the radar viewing sector. This simulates the effect long ranges of hills would have on the clutter. Note that most clutter models will include some shadowed cells as well as some that are highly reflective, depending on the shape of the distribution function. But large shadowed regions and other major terrain features can only be implemented by explicitly declaring them in the model.

The relationship:

$$R_{max} = (2R_e h)^{0.5} \tag{15}$$

was used to determine the maximum range of the clutter. This formula represents the earth as a smooth sphere with an effective radius equal to 4/3 the actual value. Hence R_e = 8500 km. R_e accounts for clutter that is received from beyond the geometric horizon because of the curved propagation path. Beyond R_{max}, which was 13,038 m in the model, the Σ attenuator was set for maximum attenuation.

Because of the small grazing angles involved, ψ is assumed zero and the physical area of each resolution cell is approximated by:

$$A_c = (\tau c/2)R\sin\theta_{baz} \tag{16}$$

where R is range. Note that the physical area of each range cell is proportional to R. Hence cells at 10 km have ten times the physical area, and may have ten times as many scatterers, as those at 1 km. To understand the effect of cell size on pdf, recall that in statistical estimation a sample mean can be defined as:

$$\bar{x} = \frac{x_1 + \ldots + x_n}{n} \tag{17}$$

where $x_i = \{x_1, \ldots x_n\}$ are random variables. $\bar{x}$ itself is then a random variable. It can be shown [27, p. 246] that:

$$E\{\bar{x}\} = \eta \quad \text{and} \quad \sigma_{\bar{x}}^2 = \frac{\sigma}{n}^2 \tag{18}$$

where η and σ are the mean and variance of the random variable x_i. The power received from a large cell can therefore be regarded as equivalent to the summation of power from n individual smaller cells each of 1/n the large

cell's area. σ° for the large cell could be computed by averaging n sub-cell σ°s. Instead of doing this, the model standard deviation is made proportional to $1/\sqrt{R}$ (R in km), and the usual statistical procedure is followed to generate σ° for the large cell. Hence published standard deviation values upon which the model is based are modified at ranges other than 1 km. While 1 km is an arbitrary range, few published clutter measurements indicate the range (or cell size) at which the data was taken. The goal was to replicate the effect increasing cell size has on the nature of the clutter--the software can be easily modified if new clutter data is published that indicates an inaccuracy in the model.

The received power P_r is calculated using a logarithmic form of equation (6):

$$P_r = \frac{P_t G_A^2 \lambda^2 \sin\theta_{baz} (c\tau/2) \sigma^o}{(4\pi)^3 R^3} \tag{19}$$

$$P_r\ (dB) = P_t\ (dB) + 2G_A\ (dB) + 20\log\lambda + 10\log(\sin\theta_{baz} c\tau/2) + \sigma^o\ (dB) - 10\log(4\pi)^3 - 30\log R \tag{20}$$

Because the clutter signals are delivered to power combiners at the preamp outputs rather than to the antenna feeds, P_r must be scaled to produce P_{del}, the appropriate deliverable power. P_{del} is computed taking into account the losses and gains of the various TRS components shown in table 4.

TABLE 4: TRS Component Gains

TRS RECEIVER COMPONENT	GAIN/LOSS (+/- dB)
low noise amplifier	+40.0
hybrid coupler	-3.4
flexible cable	-1.6
PIN attenuator insertion loss	-2.5
PIN attenuator, R≤1000m	-60.0
PIN attenuator, 1000m<R≤30000m	$10\log R^4$-180.0
mixer conversion loss	-7.0
preamp	+30.0

A conversion factor C is defined as:

$$C(dB) = \begin{cases} -4.5 & \text{for } R \leq 1000m \\ 10\log R^4 - 124.5 & \text{for } 1000 < R \leq 30{,}000m \end{cases} \tag{21}$$

Hence:

$$P_{del}(dBm) = P_r(dBm) + C(dB) \tag{22}$$

From P_{del} the required D/A control word W_Σ is calculated using the linearizing attenuator equations.

Search mode resolution cells are three times larger than the track mode cells, due to the larger pulsewidth. It was desired that there be a correlation between search and track mode clutter at a given range and azimuth angle. To achieve this the entire 86° search sector is divided up into track resolution cells, and each one is assigned a $\sigma°$. For a given search cell, $\sigma°$ is computed by averaging the $\sigma°$s from the corresponding three track cells.

Although at least one author [12] indicates a possible advantage to the use of frequency agility when encountering ground clutter, it does not appear to be a popular practice, except as an ECCM. Frequency agile clutter was not simulated in the land case.

To implement a variation in P_{del} with antenna elevation look angle, the terrain or ocean surface is approximated by a flat plane. At range intervals of 1920m depression angle θ_d is computed. (The 1920 figure arises from the use of 16 memory locations to cover the entire available 30 km range.) From [5]:

$$\theta_d = \sin^{-1}(h/R+R/2R_e) \tag{23}$$

where R is range:

$$R = (n+1/2)1920m, \quad 0 \leq n \leq 15 \tag{24}$$

θ_n, the clutter off-axis elevation angle, is calculated as:

$$\theta_n = \theta_{el} + \theta_d \tag{25}$$

where θ_{el} is antenna elevation look angle. θ_{el} is positive in the upwards direction, while θ_d is positive below the horizontal. θ_n is calculated for 128 values of θ_{el} over -5 to +15°. For each θ_n antenna gain is calculated using an equation borrowed from [26]:

$$G(\theta_n) = \begin{cases} \dfrac{\cos \pi u/2}{1-u^2} & \text{for } |u|<2 \text{ and } |u-1| \geq .001 \\ \dfrac{1}{1-u^2} & \text{for } |u| \geq 2 \\ (1.4855-.7u^2) & \text{for } |u-1|<.001 \end{cases} \tag{26}$$

where $u = 2.3779\theta_n/\theta_{bel}$. This function is plotted in Fig. 20. The required attenuation is defined by:

$$AGATTN = -10 \log (G(\theta_n))^2 \tag{27}$$

From AGATTN the antenna gain D/A control word is computed using the equations given in chapter 3. This procedure results in an antenna gain memory containing 16 sets of 128 D/A control words, each set being addressed by a unique θ_d, and addressing within the set being through θ_{el}.

The relationships described in this section for calculation of R_{emax}, C, P_{del} and AGATTN were also used in the remaining models.

4.3 Generic Land Clutter Models

4.3.1 General

Three "generic" land clutter models--those employing log-normal, Weibull, and exponential pdfs--were developed to allow qualitative comparisons between clutter types. The models are generic in that they do not correspond to any particular terrain type, nor do they contain any major terrain features such as shadowed zones that would bear a resemblance to a specific site. Because clutter pdf has a direct effect on constant false alarm rate performance the generic models can also be used in the evaluation of various CFAR algorithms.

To facilitate comparisons between the three generic models, all were given a $\sigma°_{med} = -36$ dB. This value is a compromise between the high and low resolution values of -38 dB and -34 dB, respectively, appearing in [28]. A compromise is necessary as the TRS has a relatively narrow pulsewidth but wide beamwidth.

The radar parameters for these models are the ones used for the detailed land clutter model.

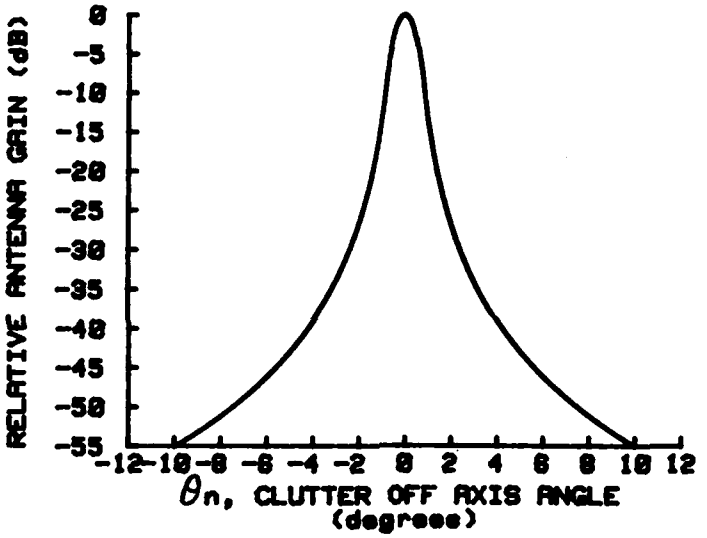

FIGURE 20: PLOT OF ANTENNA GAIN EQUATION

4.3.2 Log-normal Model

This model uses the same procedure to produce σ° values as is described in section 4.1. Unlike the detailed model standard deviation is not a function of range, but has a constant value of 5 dB. While [10] refers to values of 8 and 12 dB as being appropriate for terrain, these caused much of the clutter to exceed the detector's 30 dB dynamic range, which in turn prevented the production of meaningful amplitude histograms.

4.3.3 Weibull Model

The Weibull pdf can be written as:

$$p(v_n) = \alpha\,(\ln 2)\left(\frac{v}{v_{med}}\right)^{\alpha-1}\exp\left[-\ln 2\left(\frac{v}{v_{med}}\right)^{\alpha}\right] \tag{28}$$

where v is the voltage out of the envelope detector, and v_n is v normalized to v_{med}, the median detector voltage. By varying α the shape of the pdf can be made to approach either the log-normal or exponential pdfs. To calculate the Weibull pdf for received power P_w, it is assumed that the detector has a square-law characteristic, so that $v=kP_w$. Letting $k=1$ the equation becomes:

$$p\left(\frac{P_w}{P_{wmed}}\right) = \alpha\,\ln 2\left(\frac{P_w}{P_{wmed}}\right)^{\alpha-1}\exp\left[-\ln 2\left(\frac{P_w}{P_{wmed}}\right)^{\alpha}\right] \tag{29}$$

We can then write:

$$P\left(\frac{P_w}{P_{wmed}} < a\right) = \int_0^a \alpha\,(\ln 2)\left(\frac{P_w}{P_{wmed}}\right)^{\alpha-1}\exp\left[(-\ln 2)\left(\frac{P_w}{P_{wmed}}\right)^{\alpha}\right]d\left(\frac{P_w}{P_{wmed}}\right) \tag{30}$$

Let $P_w/P_{wmed} = P_{wn}$, the normalized received power, and $y = P_{wn}^{\alpha}$ so $dy = \alpha P_{wn}^{\alpha-1}dP_{wn}$. Now:

$$P(P_{wn} < a) = P(y < a^{\alpha}) = \int_0^{a^{\alpha}} (\ln 2)\exp[(-\ln 2)y]dy \tag{31}$$

$$= -\exp\left[(-\ln 2)y\Big|_0^{a^{\alpha}}\right] \tag{32}$$

$$= 1-\exp[(-\ln 2)a^{\alpha}] \tag{33}$$

Therefore:

$$F(P_{wn}) = 1-\exp[(-\ln 2)P_{wn}^{\alpha}]. \tag{34}$$

To generate random numbers with the correct distribution, the inverse method [2] is used. Let $u = F(P_{wn})$, where u is a uniformly distributed random variable between 0 and 1. A solution for P_{wn} is required for a given value of u, ie.:

$$P_{wn} = F^{-1}(u) \tag{35}$$

$$\text{Hence} \quad 1-\exp[(-\ln 2)P_{wn}^{\alpha}] = u \tag{36}$$

$$\exp[(-\ln 2)P_{wn}^{\alpha}] = 1-u \tag{37}$$

$$(-\ln 2)P_{wn}^{\alpha} = \ln(1-u) \tag{38}$$

$$P_{wn} = \left[\frac{\ln(1-u)}{(-\ln 2)}\right]^{\frac{1}{\alpha}} \approx \left[\frac{\ln(u)}{-\ln 2}\right]^{\frac{1}{\alpha}} \tag{39}$$

Equation (39) can be used to generate normalized values of received power P_{wn}. P_{wn} is not by itself sufficient for use in the clutter signal generation process, as it does not have a range or cell area dependence. An expression with these dependencies is required for the median power P_{wmed}. Such an expression can be derived using the radar range equation and the median clutter parameter σ°_{med}. It is convenient to consider the case of $P_{wn} = 1$:

$$P_w = P_{wn}P_{wmed} = P_{wmed} \tag{40}$$

As P_w will be used to represent the radar's received clutter power Pr:

$$P_r = P_{wmed} \tag{41}$$

and from the radar range equation:

$$P_r = \frac{P_t G_A^2 \lambda^2 \sin\theta_{baz} (c\tau/2)\sigma^{\circ}}{(4\pi)^3 R^3} \tag{42}$$

we obtain:

$$P_{wmed} = \frac{K\tau\sigma^{\circ}_{med}}{R^3} \qquad (43)$$

where K is calculated using the radar parameters given in table 3. σ°_{med} is defined here as -36 dB. Equation (43) has the required range and cell area (pulsewidth) dependence, and it is used with equations (39) and (40) to produce the clutter power values.*

An α value of 2.5 was chosen for the Weibull land clutter model based on published values in [29] pertaining to measurements made on cultivated land at X-band with θ_{baz}=1.4 degrees, grazing angles in the 0.7 to 5.0° range, and τ = 0.17 s. α values corresponding to the model's radar parameters were not found in the literature.

4.3.4 Exponential Model

The exponential land clutter model is identical to the Weibull model except that α = 1.0.

4.4 Sea Clutter Model

Unlike land clutter, sea clutter does not contain large shadowed areas. Small shadowed regions caused by prominent wave crests are evenly distributed throughout the sea surface. Because of this, and the uniformity of the reflecting surface, there is no need to describe sea clutter in physical coordinates, as the effect of the distributed shadowed areas can be represented by statistical means [2]. However, in the clutter generation hardware (which is common to all models), the memory addressing is based on physical coordinates of range and azimuth. Hence a modelling procedure similar to that used for the land cases is followed for sea clutter. The sea surface is divided into clutter resolution cells of dimensions determined by the radar azimuth beamwidth and track pulsewidth. Received power for the cells is generated statistically. Unlike the land clutter model, in which different regions contain different σ°s and standard deviations, the entire sea surface is represented with the same pdf parameters. Search resolution cells are based on weighted averages of the corresponding track cells.

---

*For the Σ search memory, an average is taken of the three P_{wn} values applying to sub-cells within the resolution cell. This average is multiplied by P_{wmed} to produce P_r.

The model uses an exponential distribution for received power P_e. The radar being modelled for the sea case has an azimuth beamwidth of 5.36° and transmit pulsewidths of 1 and 2 μs. The Rayleigh voltage/exponential power sea clutter model has been suggested in [5] as appropriate except for pulsewidths less than 0.5 μs. For higher resolution radars the log-normal pdf is often suggested [20], but consensus in the literature seems to be that this exaggerates the tails [3]. The Γ, Weibull, and K distributions, which lie between the exponential and log-normal pdfs, have all been suggested for sea clutter. Note that sometimes differences between the various pdfs is comparable to experimental error [30]. Because of the lack of published pdf parameters appropriate for the sea-states, pulsewidths and beamwidths of interest, the exponential pdf was chosen. The Weibull pdf can be implemented with a one line software modification, and other pdfs can also be implemented if this proves desirable in the future.

The procedure used here for generating P_e is identical to that described in 4.3.2 for Weibull clutter, except that α has been set equal to 1. This produces the density function:

$$p(P_{en}) = 1n2 \exp[-1n2 \frac{P_e}{P_{emed}}] \tag{44}$$

where P_{en} is normalized received power, equal to P_e (received power) divided by P_{emed} (median received power). Mean and variance are 1/1n2 and $(1/1n2)^2$, respectively (from [28] with β=1/1n2). Values of P_{en} are generated using:

$$P_{en} = \frac{1n(1-u)}{-1n2} \approx \frac{1nu}{-1n2} \tag{45}$$

where u is uniformly distributed between 0 and 1. P_e is calculated as:

$$P_e = P_{en}P_{emed} \tag{46}$$

where:

$$P_{emed} = \frac{P_t G_A^2 \lambda^2 \sin\theta_{baz} (c\tau/2) \sigma^o_{med}}{(4\pi)^3 R^3} \tag{47}$$

$$= \frac{K\tau\sigma^o_{med}}{R^3} \tag{48}$$

Values for σ°_{med} are based on published σ° values appearing in [5]. These values have been plotted in Fig. 21. The wide variation of σ° with grazing angle ψ and sea-state has been incorporated into the simulation, through use of the equation:

$$\sigma^\circ_{med}\,(dB) = \begin{cases} \sigma^\circ_{min,ss} + DIFF\sin(\psi-0.1)\,\pi/6 \\ \qquad \text{for } 0.1 \leq \psi \leq 3.0^\circ \\ \sigma^\circ_{min,ss} \quad \text{for } \psi < 0.1^\circ \\ \sigma^\circ_{max,ss} \quad \text{for } \psi > 3.0^\circ \end{cases} \tag{49}$$

where $\sigma^\circ_{min,ss}$ is the minimum published value for a given sea-state and $\sigma^\circ_{max,ss}$ is the maximum value. (See table 5.) DIFF is defined by:

$$DIFF = \sigma^\circ_{max,ss} - \sigma^\circ_{min,ss} \tag{50}$$

Equations for σ°_{med} versus ψ and sea-state are plotted in Fig. 21. Note that a large portion of the clutter falls in the $\psi < 0.1$ degree range, where data were unavailable.

The radar parameters for the sea clutter model are listed in table 6. These have been chosen to represent a generic anti-ship missile seeker and are also computationally convenient.

TABLE 6: Missile Borne Radar Parameters

PARAMETER	VALUE
search pulsewidth	2.0 μs
track pulsewidth	1.0 μs
elevation beamwidth θ_{bel}	5.36°
azimuth beamwidth θ_{baz}	5.36°
antenna height h	13.0 m
antenna gain G_A	30 dB
transmitter peak power P_t	50 kW
transmitter wavelength	.033 m

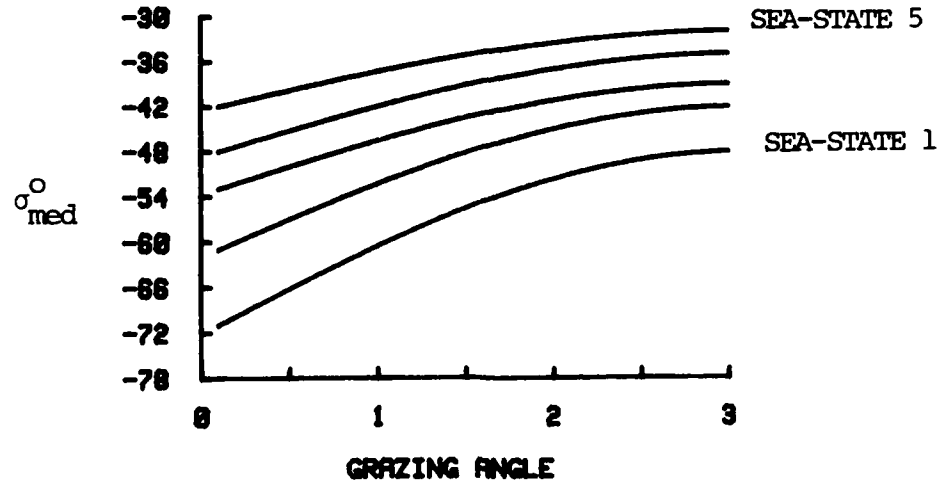

FIGURE 21: EQUATIONS USED TO MODEL σ°_{med} GRAZING ANGLE DEPENDENCE Based on published data from [5].

TABLE 5: Parameter Values Used in σ°_{med} Equations (Values are derived from data in [5] pertaining to horizontally polarized radars.)

Sea-state	σ°_{min}(dB)	σ°_{max}(dB)	DIFF(dB)
1	-71	-48	23
2	-61	-42	19
3	-53	-39	14
4	-48	-35	13
5	-42	-32	10

The sea surface is defined as three arrays of clutter resolution cells, as illustrated in Fig. 22a). The cell dimensions are determined by azimuth beamwidth and radar pulsewidth. Each resolution cell is assigned a P_e value. Because adjacent clutter resolution cells are statistically independent, an intermediate cell scheme was devised to produce gradual decorrelation at intermediate range and azimuth angles. The scheme is illustrated in Fig. 22b), where an intermediate cell (shown as shaded) overlaps four clutter resolution cells. P_e for the intermediate cell is a weighted average of the P_es in the four clutter cells. W_Σ corresponding to the intermediate cell P_e is placed in the memory location indicated. Each of the other memory locations has its own intermediate cell, consisting of sea-surface preceding it in range and centred about it in azimuth angle, as shown in the figure. A further advantage of the scheme is that it allows correlation between search and track mode clutter in the "track sector".

The VCXO control hardware was not operational at time of writing, but equations to be used for doppler offsets have been included in Appendix B. The clutter will be doppler shifted by an amount proportional to windspeed plus platform velocity.

To implement the decorrelating effect of frequency agility, two dedicated memories--the Σfa/track and Σfa/search memories were included in the generator design, as described in Chapter 3. When the TRS is in its frequency agile mode, the appropriate memory is activated, and a different 1 k row of memory is read on successive PRIs. This produces clutter that during a given PRI has the proper correlation in range but from PRI to PRI is decorrelated.

A range dependency of standard deviation was not implemented in the sea clutter model. The cumbersome relationship between the standard deviation and the Weibull parameter α is a disadvantage to using the Weibull pdf that complicates scaling with cell area [30].

5.0 EXPERIMENTAL RESULTS

To verify correct operation of the completed clutter signal generation system, measurements were performed on the TRS "linear sum" signal, which is a summation of the linear detector outputs. Measurements were made using a Data Precision model Data 6000 digital oscilloscope with a model 620 plug-in, and a Hewlett Packard plotter. These measurements appear in Figs. 23 to 28.

To prove that the generator was producing signals with the desired spatial pdfs, measurements were made using the log-normal, Weibull and exponential generic land clutter models. Amplitude histograms were plotted for each of the three waveform types. Histograms produced by the Data 6000 appear in Fig. 23, which also contains computer plots of the actual pdf equations. The histograms approximate the equations in all three cases. Note that in order to obtain meaningful plots, the software for the three generic models was temporarily modified to eliminate the mean power variation with range that would otherwise have distorted their shapes.

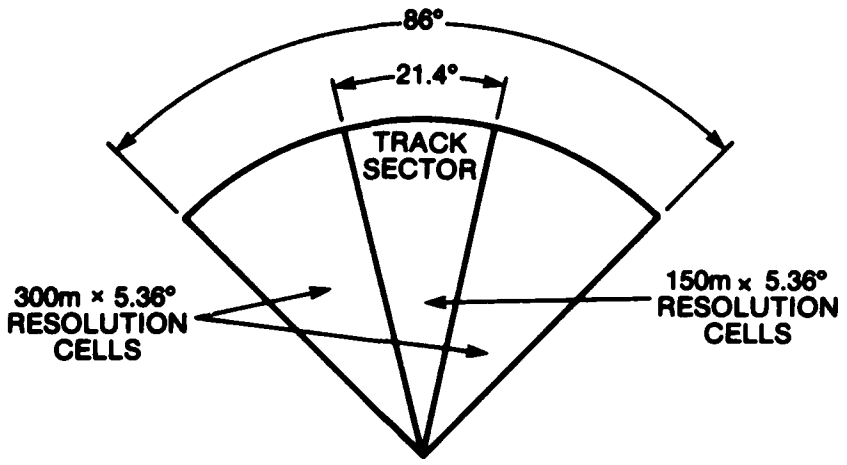

FIGURE 22a): SEA SURFACE ARRAY COVERAGE

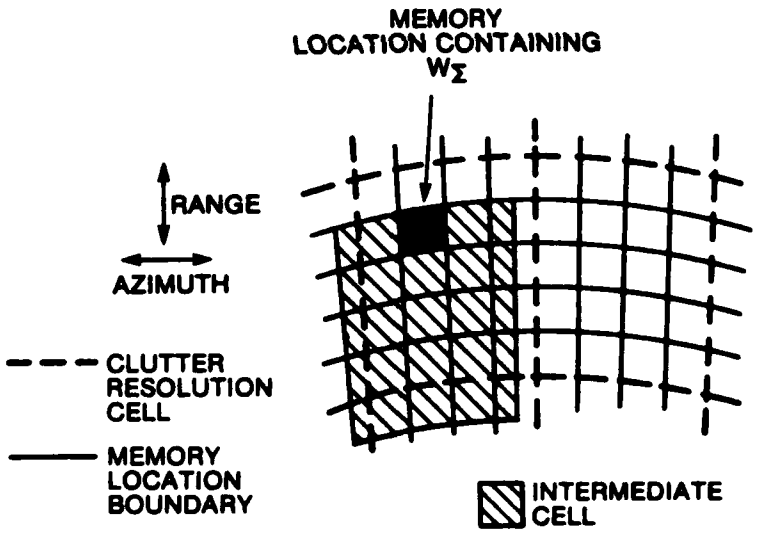

FIGURE 22b): INTERMEDIATE RESOLUTION CELL

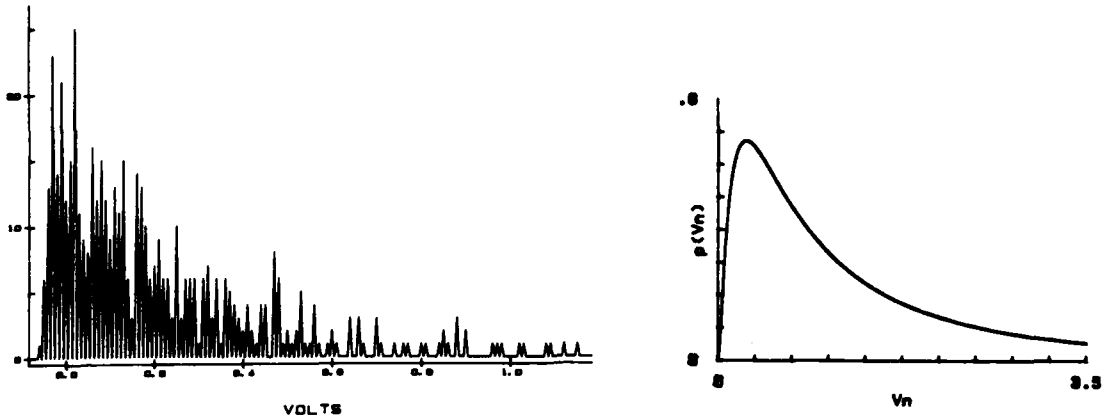

FIGURE 23a): LOG-NORMAL CLUTTER AMPLITUDE HISTOGRAM
Pdf curve is from Fig. 7.

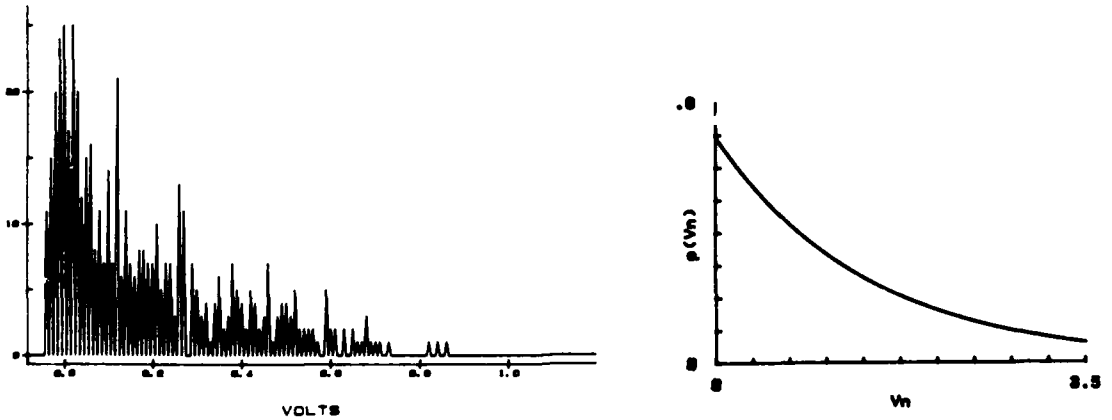

FIGURE 23b): EXPONENTIAL CLUTTER AMPLITUDE HISTOGRAM
Pdf curve is from Fig. 7.

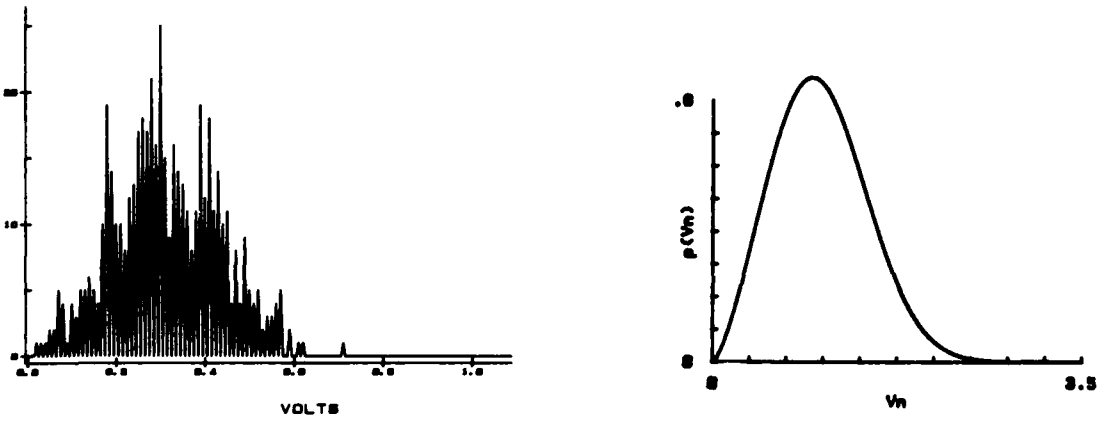

FIGURE 23c): WEIBULL CLUTTER AMPLITUDE HISTOGRAM
Pdf curve is from Fig. 7.

Amplitude versus time plots appear in Figs. 24 through 28. These show the envelope detected clutter waveforms as they would appear to an operator using the TRS A scope display. Fig. 24 shows the generic land clutter waveforms for the log-normal case. The model uses a standard deviation of 5 dB. This clutter is relatively severe, ie. it contains a large number of spikes that could easily be declared as targets, either by automatic thresholding circuitry or by an operator. The Weibull waveforms appear in Fig. 25. As expected, the Weibull clutter is intermediate in severity [3], with the exponential clutter appearing in Fig. 26 being the least severe of the three models. All plots show a mean power increase in proportion to range caused by the TRS sensitivity time control's R^4 variation of receiver gain. A decrease in mean power caused by narrowing of the pulsewidth is also evident, as is the resultant increase in range resolution.

The detailed land clutter waveforms appear in Fig. 27. These waveforms were generated using the log-normal procedure of chapter 4. Parameters describing each terrain region appear in Table 2. The clutter in each region appears to have the required mean and standard deviation. Some clipping at the farther ranges occurs for the 0.6 μs case as the 30 dB dynamic range of the linear detectors is exceeded.

Th ea clutter waveforms appear in Fig. 28. These have exponential pdfs. [illegible] waveforms have less high frequency content than the generic exponential clutter due to the wider pulsewidths used. Changing the sea-state number and rerunning the software produces clutter with a similar envelope but with a different mean power.

Frequency agility clutter was viewed on an analog oscilloscope. As expected, a number of uncorrelated waveforms were superimposed on the scope.

The generation system was interfaced with the TRS, and clutter signals were viewed on the A scope. Signals reached maximum amplitude when the antenna was at an elevation look angle slightly below the horizontal, as was expected. Moving the antenna in azimuth caused different waveforms to be observed as adjacent rows of memory were addressed. These waveforms appeared to be uncorrelated for land clutter, as expected because of the narrow beamwidth. For the sea clutter model, waveforms from adjacent memory rows had a high degree of correlation, due to the wider beamwidth.

Finally, the effect of the clutter on the TRS's angle tracking was investigated. The range gate was observed to lock up on portions of the clutter exceeding the detection threshold. Upon entering the track mode the TRS antenna was driven to and held at a position slightly below the horizontal. To verify that the antenna was actually angle tracking the clutter in the elevation plane, its pointing angle was manually altered. It was found that strong drive torque existed, and after release the antenna quickly resumed its original position.

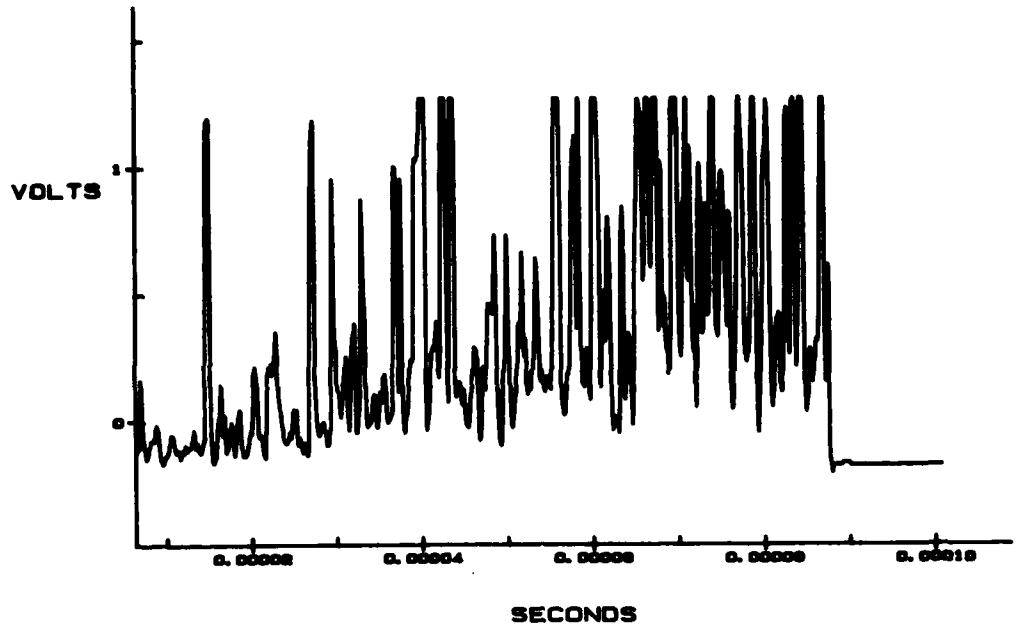

FIGURE 24a): GENERIC LAND CLUTTER-LOG-NORMAL MODEL
For 0.6 μs pulsewidth. Clipping is caused by clutter spikes exceeding the 30 dB dynamic range of the linear detectors.

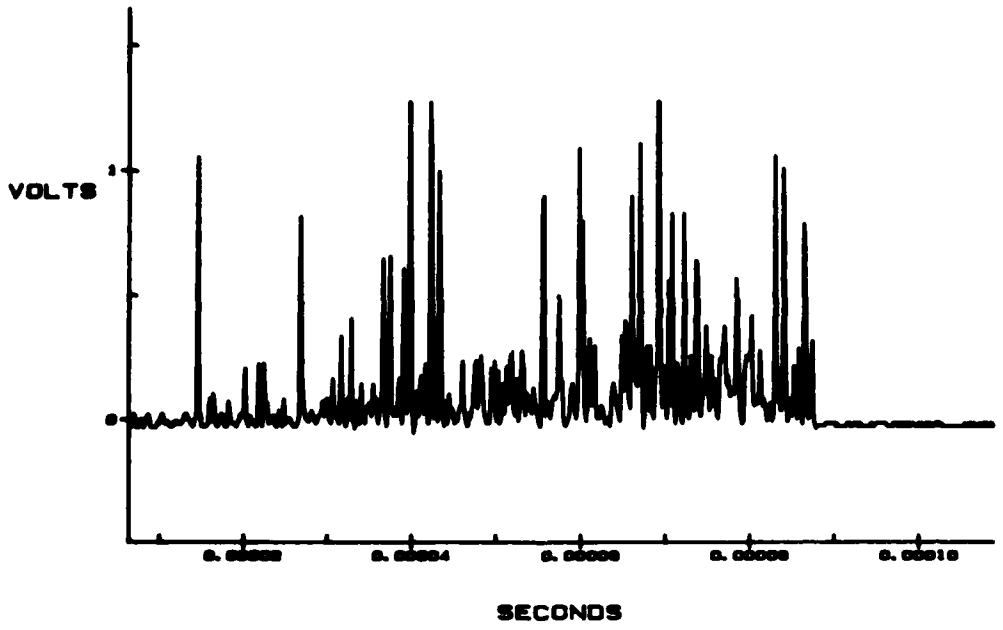

FIGURE 24b): GENERIC LAND CLUTTER--LOG-NORMAL MODEL
For 0.2 μs pulsewidth. Both plots correspond to the same azimuth sector.

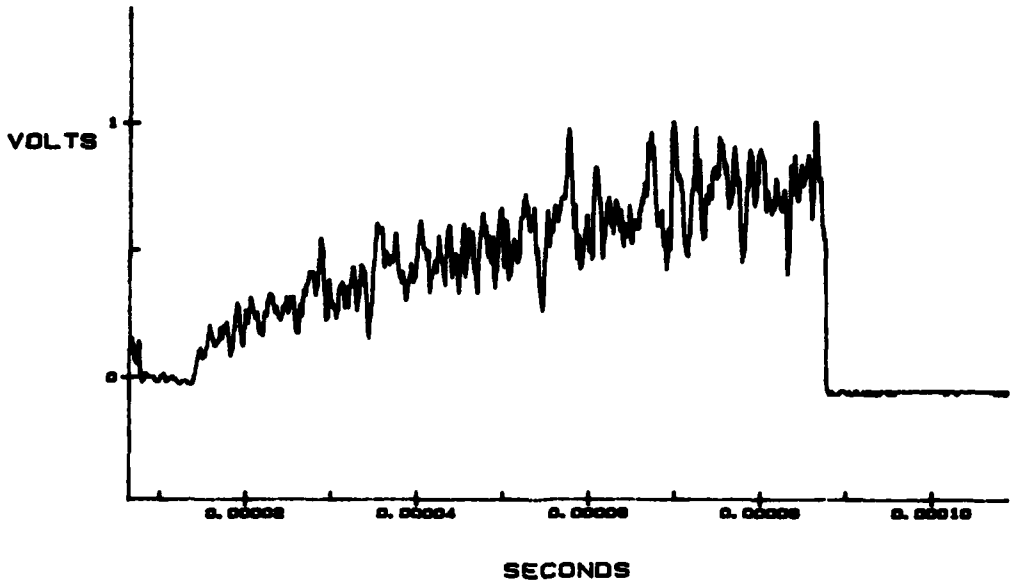

FIGURE 25a): GENERIC LAND CLUTTER--WEIBULL MODEL
For 0.6 μs pulsewidth.

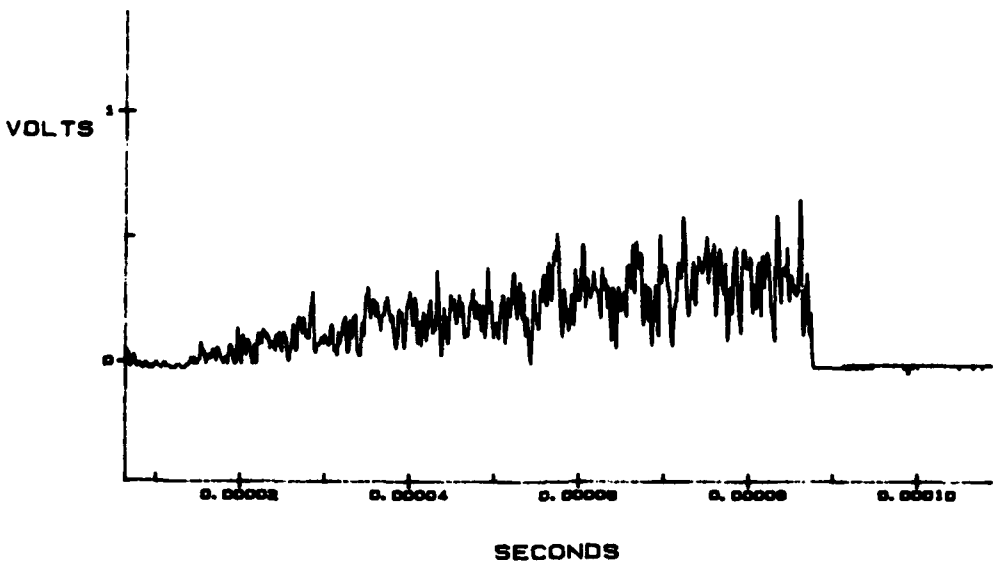

FIGURE 25b): GENERIC LAND CLUTTER--WEIBULL MODEL
For 0.2 μs pulsewidth. Both plots
correspond to the same azimuth sector.

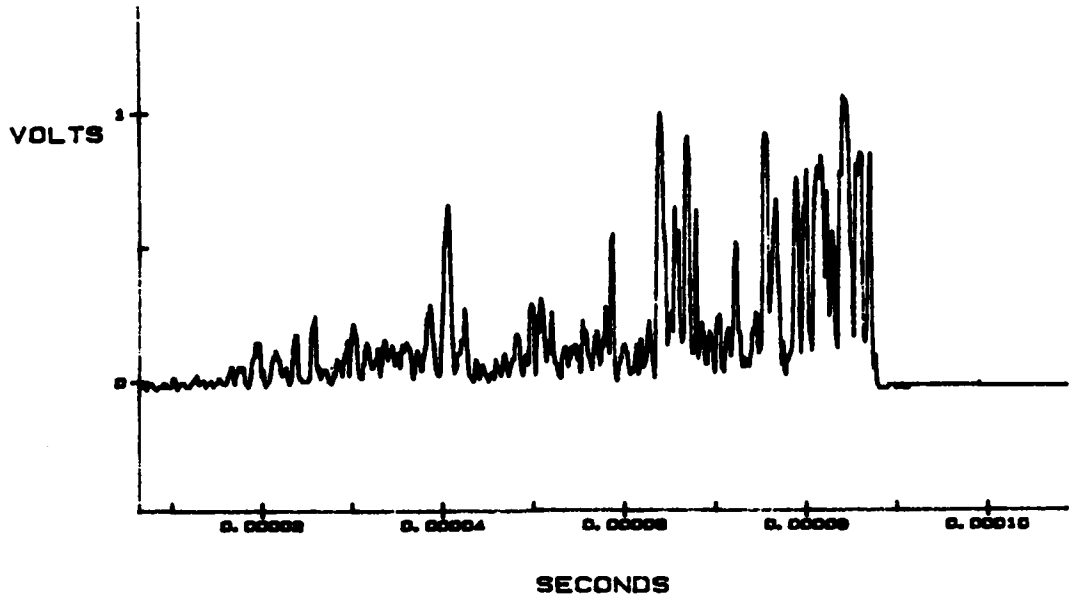

FIGURE 26a): GENERIC LAND CLUTTER--EXPONENTIAL MODEL
For 0.6 μs pulsewidth.

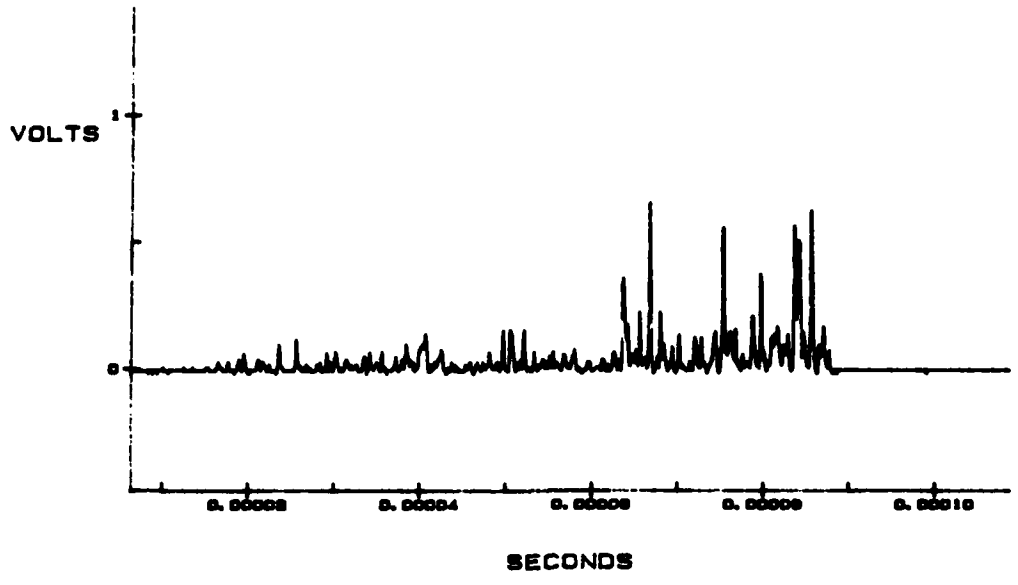

FIGURE 26b): GENERIC LAND CLUTTER--EXPONENTIAL MODEL
For 0.2 μs pulsewidth. Both plots
correspond to the same azimuth sector.

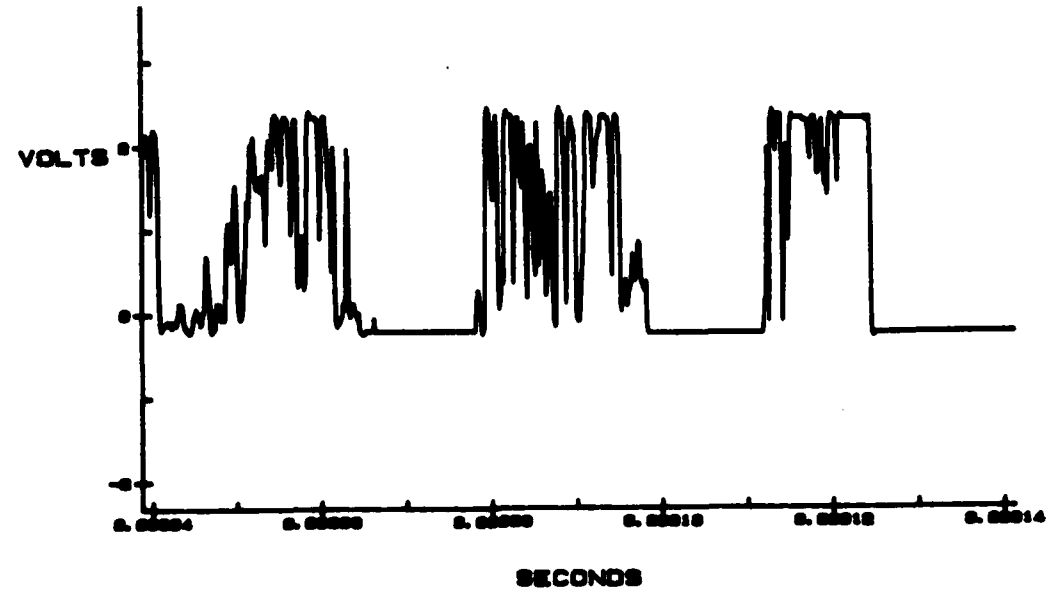

FIGURE 27a): DETAILED LAND CLUTTER
For 0.6 μs pulsewidth.
Note differing terrain regions
and shadowed zones.

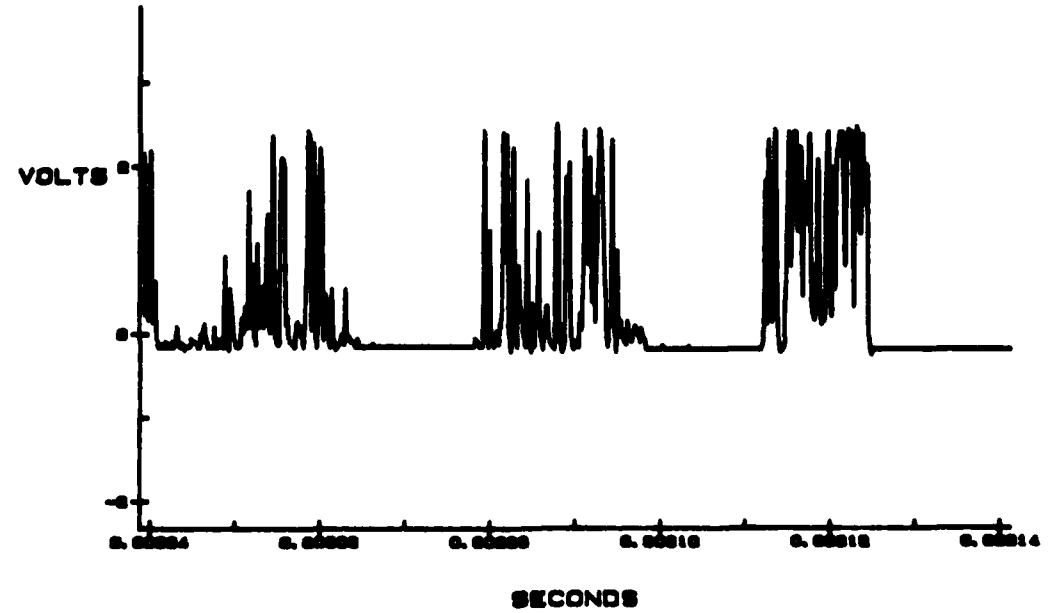

FIGURE 27b): DETAILED LAND CLUTTER
For 0.2 μs pulse width.
Both plots correspond to
the same azimuth sector.

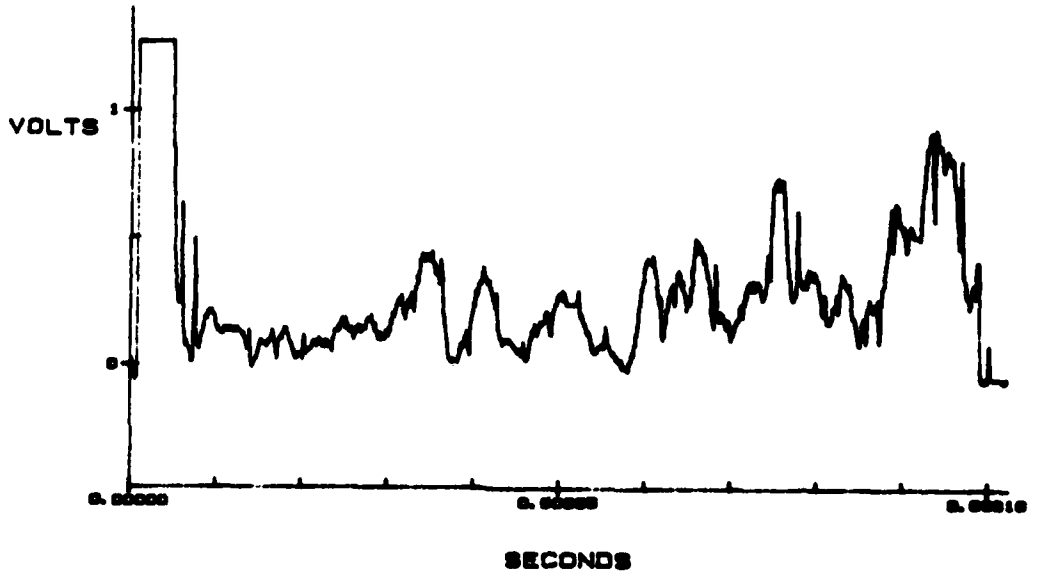

FIGURE 28a): SEA CLUTTER
For 2.0 μs pulsewidth.

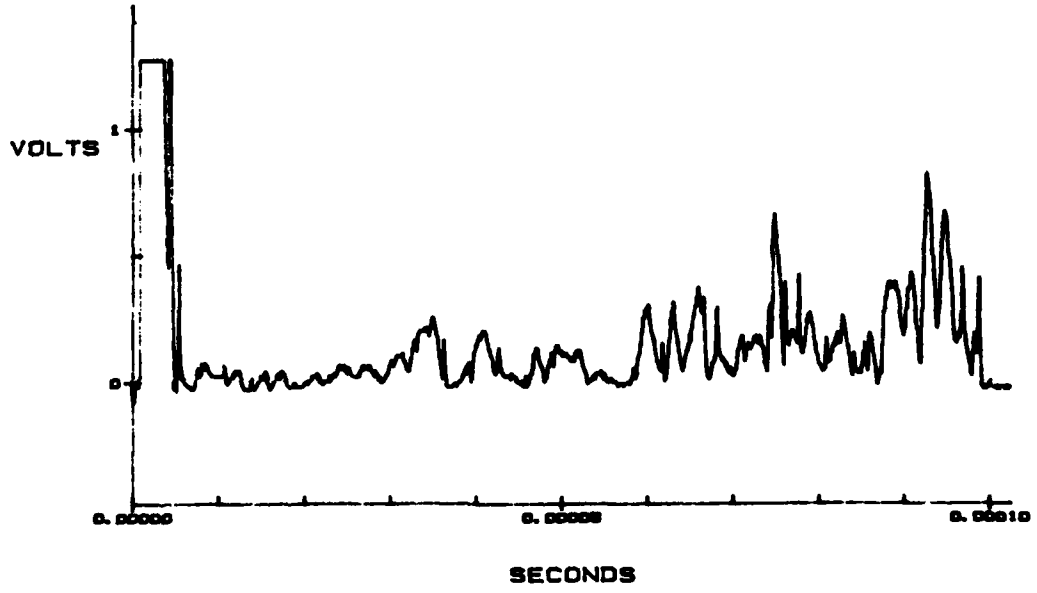

FIGURE 28b): SEA CLUTTER
For 1.0 μs pulsewidth.
Both plots correspond
to the same azimuth sector.

6.0 CONCLUSION

The purpose of this project was to implement a clutter simulation for DREO's Electronic Warfare Engagement Simulation Facility. To this end, the relevant radar theory for distributed targets was developed. Clutter characteristics relevant to noncoherent radars in low grazing angle scenarios were investigated. Hardware was developed to generate signals with those characteristics. Based on published data, relationships were derived relating clutter characteristics to radar and environmental parameters. These relationships, plus algorithms for the generation of random variables with log-normal, Weibull and exponential pdfs were combined in computer programs for control of the generation hardware. Validation of the resultant signals was achieved through the recording of correctly shaped amplitude histograms.

Five clutter models have been implemented: a "detailed" land clutter model using the log-normal pdf, log-normal, Weibull and exponential generic land clutter models, and an exponential sea clutter model. In all models power varies with elevation look angle, and statistically independent signals are produced for adjacent sectors. Search and track mode waveforms are correlated so that surface features become more resolved when the pulsewidth is narrowed. The radar horizon is determined by antenna height, and mean clutter power is determined by the radar range equation parameters. A variation of pdf standard deviation with cell size (hence range) has been implemented in the detailed land model. Decorrelated returns for frequency agile radars have been implemented in the sea clutter model. The hardware is capable of producing clutter that is doppler shifted according to sea-state and platform velocity. All waveforms can be given a controllable fluctuation to replicate the effect of wind-blown scatterers.

One achievement of particular importance is the generator's high resolution capability. Defining signal amplitude at 200 ns intervals allows the fine structure associated with narrow pulsewidth clutter to be replicated. Also of importance is the realism achieved by the inclusion of angle track errors in the clutter simulation. At time of writing, this feature is thought to be novel in an IF clutter generator.

For scenarios involving MTI, it was found that a valid beat note can be produced in a radar receiver if clutter is injected into the receiver at the IF, with the target(s) at RF. The penalty in simulation fidelity is negligible except for extremely high power level cases, where third order mixer intermodulation products will not exist in the simulation.

Future work could be directed at upgrading the models to overcome the more notable deficiencies. Upgrades are facilitated by the generator's programmability. Some upgrades will only become possible once new clutter data becomes available. The models do not include a dependence of σ°med on transmit frequency or polarization, as modelling formulae were based only on

X-band, horizontally polarized data. For the land case, terrain zones could be defined in a more realistic manner, and the effect of moisture content on vegetation reflectivity could be included. For the sea case, a dependence of both $\sigma°$med and doppler shift on the azimuth look angle relative to up/downwind could be included, as could the effect of polarization and sea-state on spatial amplitude distribution. A variation in pdf standard deviation with cell area could be added, as could signal fluctuation due to long term modifications to the sea surface. By modification of the memory addressing scheme, resolution cells could be made to move towards zero range for moving platform scenarios.

Other work might include software upgrades so that radar and model parameters could be entered by the user at run time. A graphics terminal would facilitate easy terrain zone definition as opposed to the present "hard coded" scheme. The present work could also be adapted to higher altitude scenarios. Additional work could centre on the inclusion of angle tracking effects due to multipath. Work could also be done to facilitate the inclusion of actual recorded clutter data in the generator memory.

7.0 REFERENCES

[1] S.M. Sherman, Monopulse Principles and Techniques, Artech House Inc., Dedham, Mass., 1984.

[2] R. L. Mitchell, Radar Signal Simulation, Artech House Inc., Dedham, Mass., 1976.

[3] M. I. Skolnik, Introduction to Radar Systems, McGraw-Hill Book Company, Toronto, 1980.

[4] M. I. Skolnik, Radar Handbook, McGraw-Hill Book Company, Toronto, 1970.

[5] F. E. Nathanson, Radar Design Principles, McGraw-Hill Book Company, New York, 1969.

[6] F. E. Nathanson, J. P. Reilly, "Clutter Statistics Which Affect Radar Performance Analysis", IEEE Transaction on Aerospace and Electronic Systems, Vol. AES-3, No. 6, Nov. 1967.

[7] S. Haykin, Communication Systems, John Wiley & Sons, Toronto, 1978.

[8] D. C.Schleher, MTI Radar, Artech House, Inc., Dedham, Mass., 1978.

[9] G. B. Goldstein, "False-Alarm Regulation in Log-Normal and Weibull Clutter", IEEE Transactions on Aerospace and Electronic Systems, Vol. AES-9, No. 1, Jan. 1973.

[10] J. L. Ekstrom, "The Detection of Steady Targets in Weibull Clutter", IEE, 1973. (Reprinted in Radars Volume 5 by D. K. Barton).

[11] M. Sekine, "Suppression of Weibull-Distributed Clutters Using a Cell-Averaging LOG/CFAR Receiver", IEEE Trans. on Aerospace and Electronic Systems, Vol. AES-14, No. 5, pp. 823-826, Sept. 1978.

[12] T. H. Einstein, "Effect of Frequency-Averaging on Estimation of Clutter Statistics Used in Setting CFAR Detection Thresholds", Project Report TT-60, M. I. T. Lincoln Laboratory, 9 Nov 1982.

[13] F. E. Nathanson, "The Environment", Technology Service Corporation course notes, 1977.

[14] K. D. Ward, S. Watts, "Radar Clutter in Airborne Maritime Reconnaissance Systems", Military Microwaves '84 International Conf. Proc., pp. 222-228, Oct. 1984.

[15] G. Lind, B. Bergkvist, "A Method to Calculate the Density of Sea Clutter Echoes at Low Grazing Angles", IEEE International Radar Conf. Proc., pp. 230-234, 1975.

[16] Tagsea Program Final Report, Volume 1, Clutter Models, prepared by Raytheon Company for General Dynamics, 27 Aug. 1976.

[17] M. W. Long, Radar Reflectivity of Land and Sea, Artech House, Dedham, Mass., 1983.

[18] G. V. Trunk, "Detection of Targets in Non-Rayleigh Sea Clutter", IEEE EASCON'71 Conf. Proc., pp. 239-245.

[19] B. L. Hicks, et al, "The Spectrum of X-Band Radiation Backscattered from the Sea Surface", Journal of Geophysical Research, Vol. 65, No. 3, March 1960.

[20] M. Yuhai, "Frequency Agility Radar", translated by Foreign Technology Division, Wright Patterson AFB, 6 Dec. 1982.

[21] W. K. McRitchie, "Threat Radar Simulator Receiver", DREO Technical Note 85-15, May 1985.

[22] "17 Most Asked Questions About Mixers!", Minicircuits Q & A No. 1, Brooklyn, N.Y., 1981.

[23] M. A. Copeland, "Signal Processing Electronics", Carleton University course notes, Sept.-Dec. 1983.

[24] I. Miller, J. E. Freund, Probability and Statistics for Engineers, Prentice-Hall, Inc., Englewood Cliffs, N.J., 1977.

[25] D. K. Barton., "Land Clutter Models for Radar Design and Analysis", Proc. of IEEE, Vol. 73, No. 2, pp. 198-204, Feb. 1985.

[26] S. P. Zehner, M. T. Tuley, "Development and Validation of Multipath and Clutter Models for Tac Zinger in Low Altitude Scenarios", Georgia Institute of Technology under contract to USAF, Atlanta, Georgia, March 1979.

[27] A. Papoulis, Probability, Random Variables, and Stochastic Processes, McGraw-Hill Book Company, Toronto, 1965.

[28] J. W. Henn et al, "Land Clutter Study: Low Grazing Angles (Backscattering)", IEE Radar-82 Int. Conf. Proc., pp. 380-384, Oct. 1982.

[29] H. E. King et al, "Terrain Backscatter Measurements at 40 to 90 GHz", IEEE Trans. on Antennas and Propagation, Vol. AP-18, No. 6, Nov. 1970.

[30] E. Jakeman, P. N. Pusey, "Statistics of Non-Rayleigh Microwave Sea Echo", IEEE Radar-77 Int. Conf. Proc., pp. 105-109, Oct. 1977.

[31] ADC-0800 8-Bit A/D Converter Specification Sheets, National Semiconductor.

APPENDIX A

CLUTTER CONTROLLER MEMORY RELATED CIRCUITRY

The purpose of this appendix is to describe the memory related circuitry that comprises the majority of the clutter controller. While schematics have been included, the intent is to illustrate system architecture and key features rather than provide detailed documentation.

The controller has two operating modes: LOAD and RUN. During LOAD, addresses and data arrive at the controller from the host PDP 11/44 computer via a DR11c parallel interface. This interface drives all memory device address and data lines. During RUN, address lines are driven by counters and A/D converters and the data bus is partitioned into three separate buses, one for each D/A. The input/output data bus scheme is illustrated in Fig. 29.

Communication via the DR11c is strictly one-way, ie. no handshaking exists. This speeds the LOAD operation and simplifies the hardware required. To verify proper memory loading the resultant clutter signals can be checked manually using an oscilloscope to ensure they have the right characteristics. Also, test programs have been developed to test individual memory subsections with their respective D/As and attenuators. For example, a square wave bit pattern can be written into the Σ memory and the presence of a 60 MHz "clutter" signal with a 2.5 MHz square wave modulation will confirm correct operation.

Some of the key memory control circuitry appears in Fig. 30. Buffered DR11c lines supply both addresses and data. The LOAD procedure is to place a memory address on the lower 12 bits, which are latched as commanded by CRS1. Then the 8 bit data word corresponding to the address is placed on the lower bits, and a chip selection code plus two control signals are placed on 6 of the upper bits. These signals are not latched but are applied simultaneously to the memory chips and control circuitry along with the latched address. The tri-state buffers in Fig. 30 allow all three I/O buses to be driven from the DR11c in LOAD and to be separated in RUN. The input latches are tri-stated in RUN to prevent the DR11c from driving address lines in that mode.

The various memory subsections are activated in RUN mode through the decoding of control signals using an arrangement of gates. The antenna gain memory is always active (except in ROM), the Δ_{el} subsection operates during alternate track mode PRIs, and the various subsections are activated according to the frequency agility and search/track TTL lines. Logic for control of the memories appears in Fig. 31.

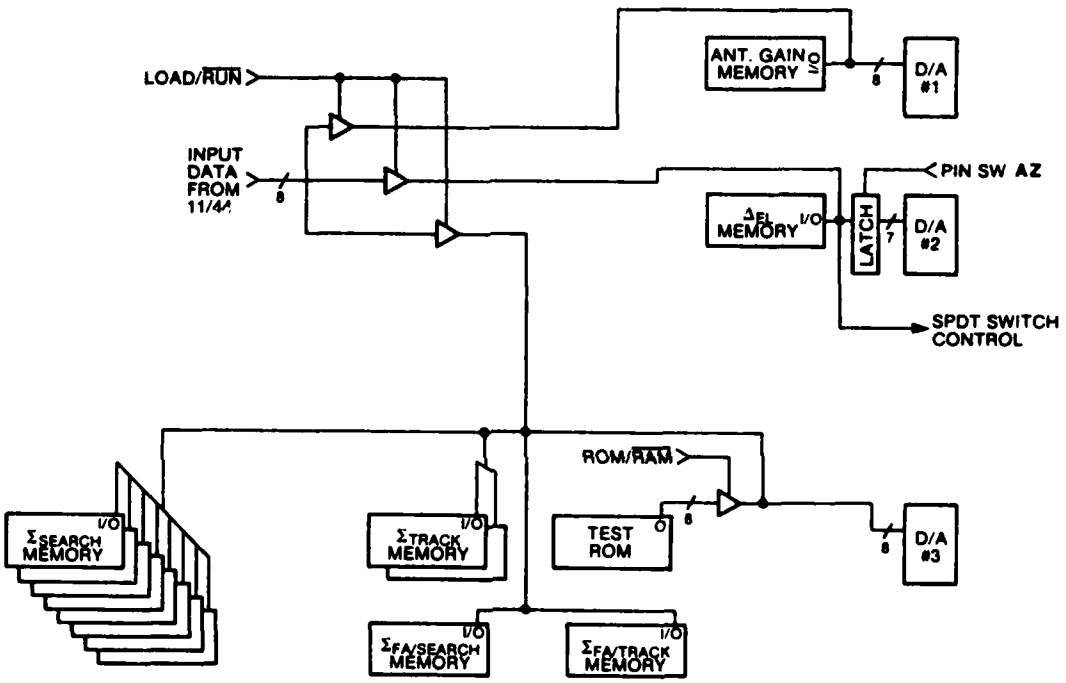

FIGURE 29: CONTROLLER INPUT AND OUTPUT DATA PATHS

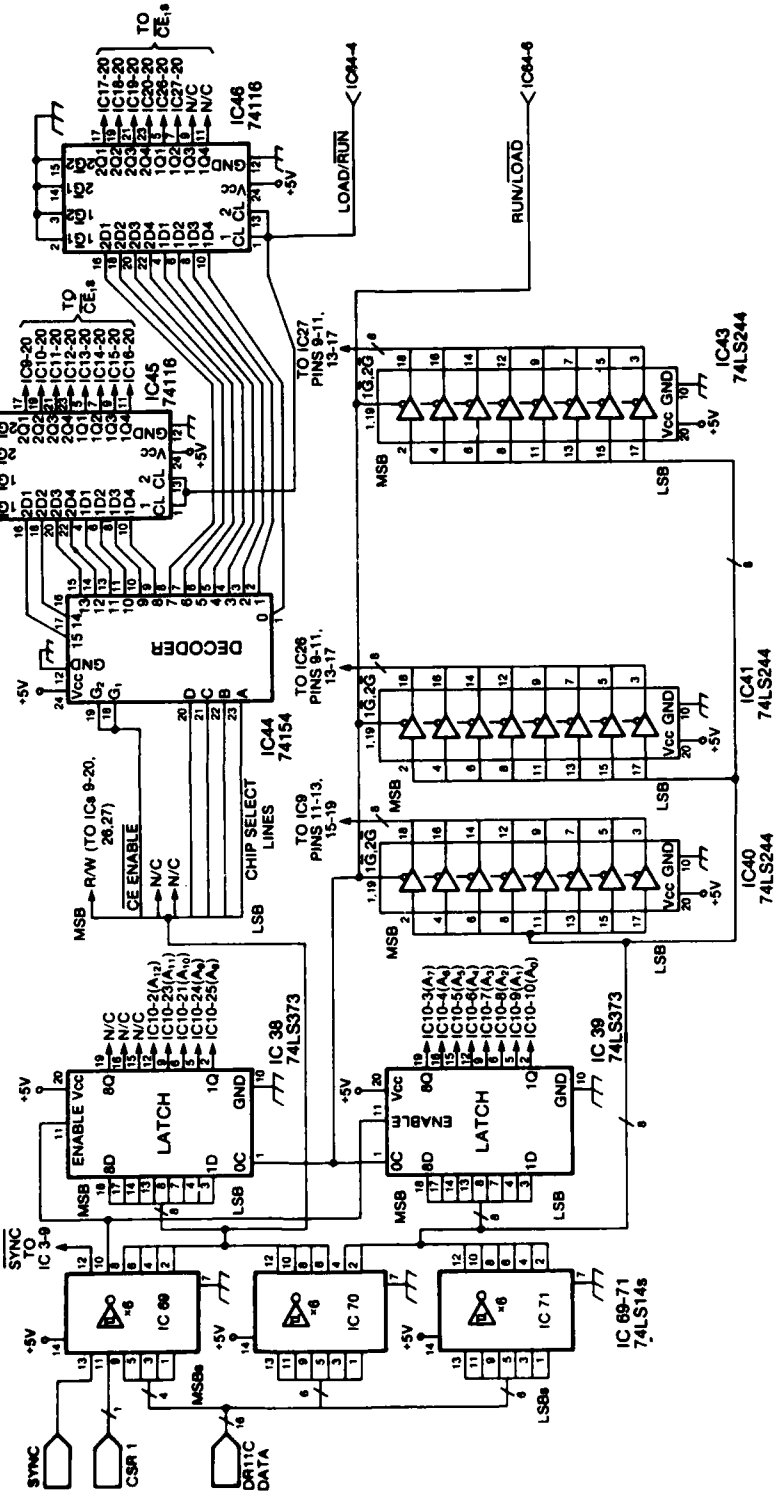

FIGURE 30: CLUTTER CONTROLLER INPUT LATCHING ARRANGEMENT

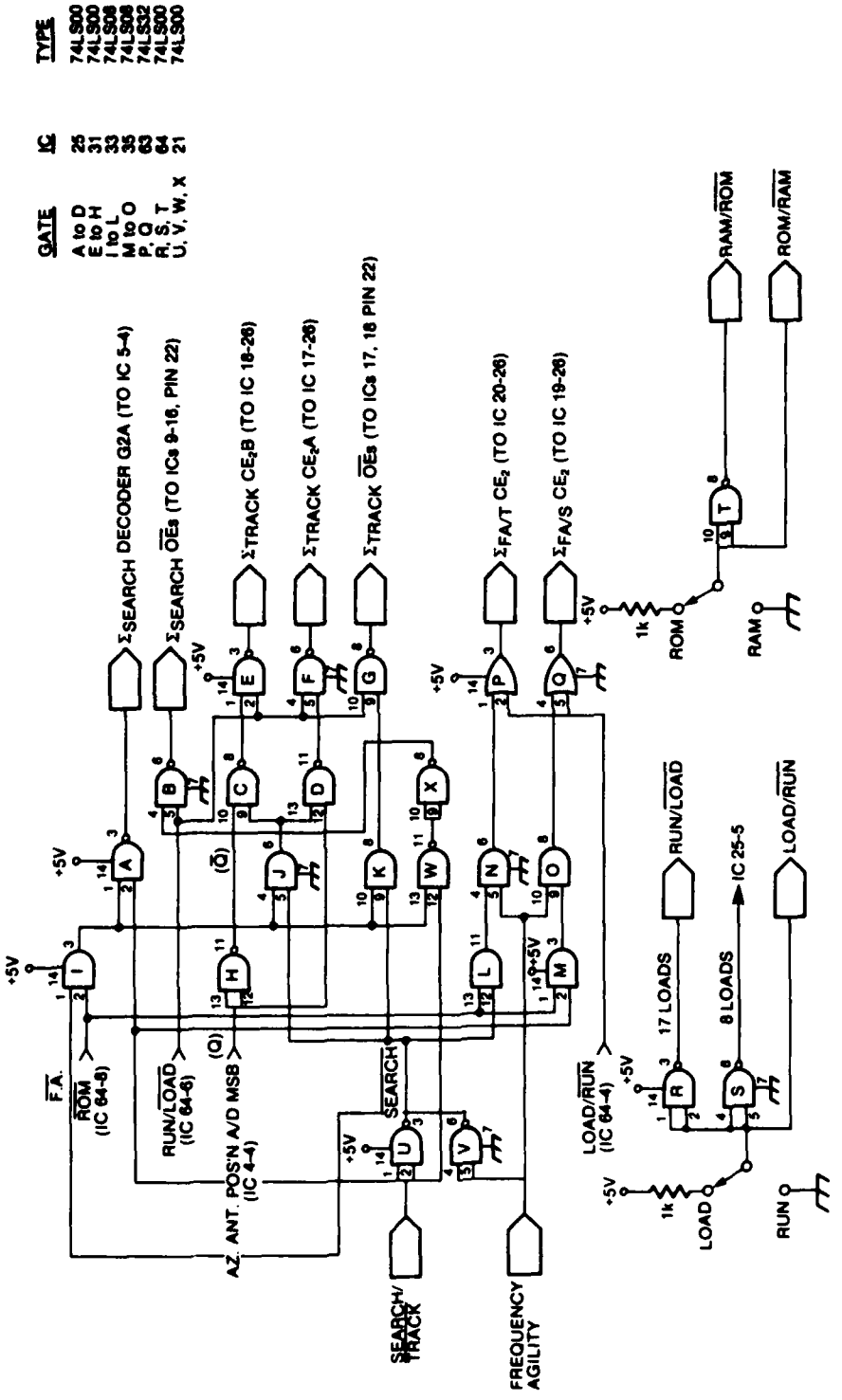

FIGURE 31: CLUTTER CONTROLLER MODE CONTROL LOGIC

The range counter appears in Fig. 32. Three down counters are loaded with the number 1111111111 at the start of each PRI.

Counting takes 200 μs, allowing clutter to be generated for radar horizons up to 30 km. This can be doubled using the front panel RADAR HORIZON extension switch, which causes the 1 k of memory addresses to be sequenced through twice. Note that use of the switch results in clutter in the 30-60 km range that is identical to that in the 0-30 km range. While being somewhat rudimentary it does allow a basic capability for airborne radar clutter simulation, should this be required in the future.

Because the ROM chip has a slower access time than the RAM chips, the range counter is clocked at one-half its usual speed when ROM based clutter is selected. Clock signals are derived from an external 10 MHz clock via a counter. Besides a one-shot for triggering the A/Ds, Fig. 32 contains a decoder for the most significant azimuth antenna A/D position bits. These bits select individual RAM chips by activating their CE_2 lines. NAND gates drive these lines high in LOAD so that CE_1s can be used for control.

The range counter output bits do not drive the address lines of the memory chips directly. Instead, the output bits are applied to the D-type latches appearing in Fig. 33. The range counter outputs are latched when they are certain to be valid. Latching prevents transitional range counter outputs --such as those that occur during a most significant bit transition--from causing incorrect memory addressing. Also, tri-stating the latches during LOAD prevents the range counter from driving the memory address lines in that mode.

Because the Σmemory is read each 200 ns, careful timing of all circuitry is required, as is illustrated in Fig. 34. The $\overline{\text{RC CLK}}$ signal is used to clock the Σ D/A. After the range counter's outputs become stable, the $\overline{\text{RC CLK}}$ signal goes high. This causes the latches to pass the outputs through to the memory address lines. When $\overline{\text{RC CLK}}$ goes low the address is latched. The TC556 Memory device sees the address for 200 ns. After 120 ns it produces valid output data. Some time later the rising edge of $\overline{\text{RC CLK}}$ is used to trigger the TDC1016 high speed Σ D/A. When ROM based clutter is selected the one-shot clocks the TDC1016.

The TC5518 memory devices used in the antenna gain and Δel subsections have as their range address the four most significant bits from the latch. The D/As driven by the TC5518s convert continuously rather than being clocked as is the TDC1016. While transitional memory outputs are converted they have no effect on the clutter signals as the ZMAS-3 devices cannot respond quickly enough to them.

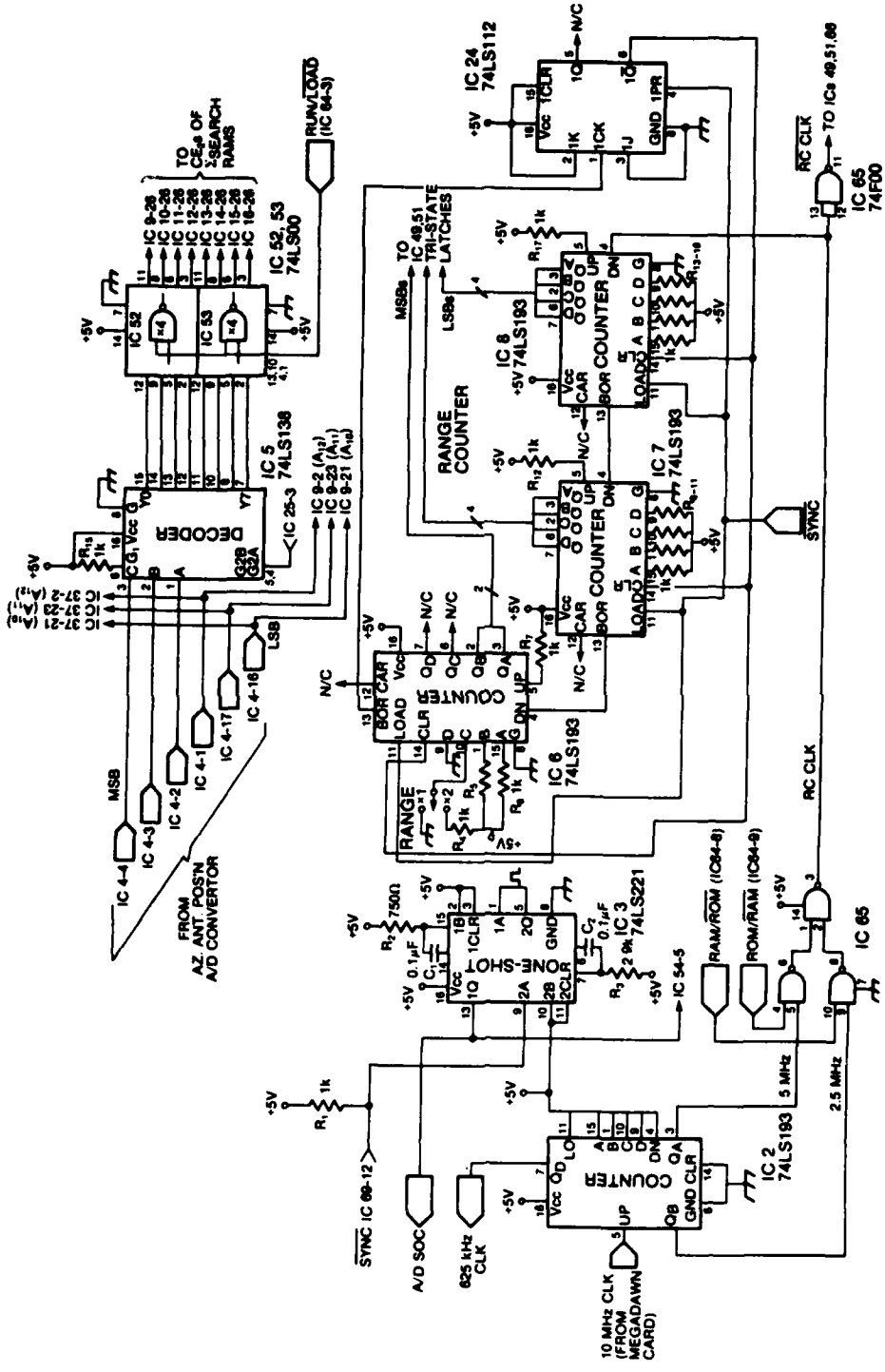

FIGURE 32: CLUTTER CONTROLLER RANGE COUNTER CIRCUITRY

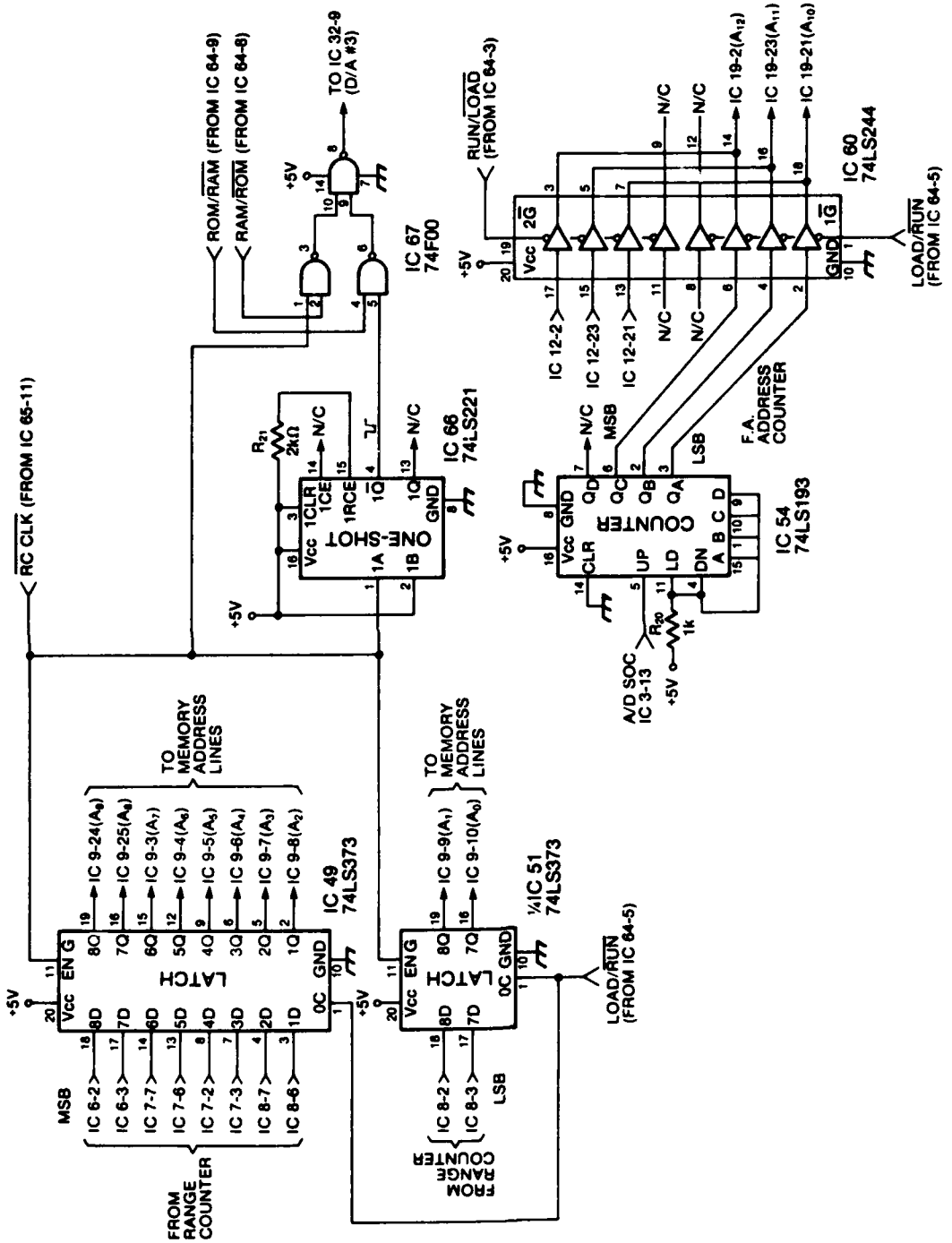

FIGURE 33: CLUTTER CONTROLLER ADDRESS LINE LATCHES AND BUFFERS

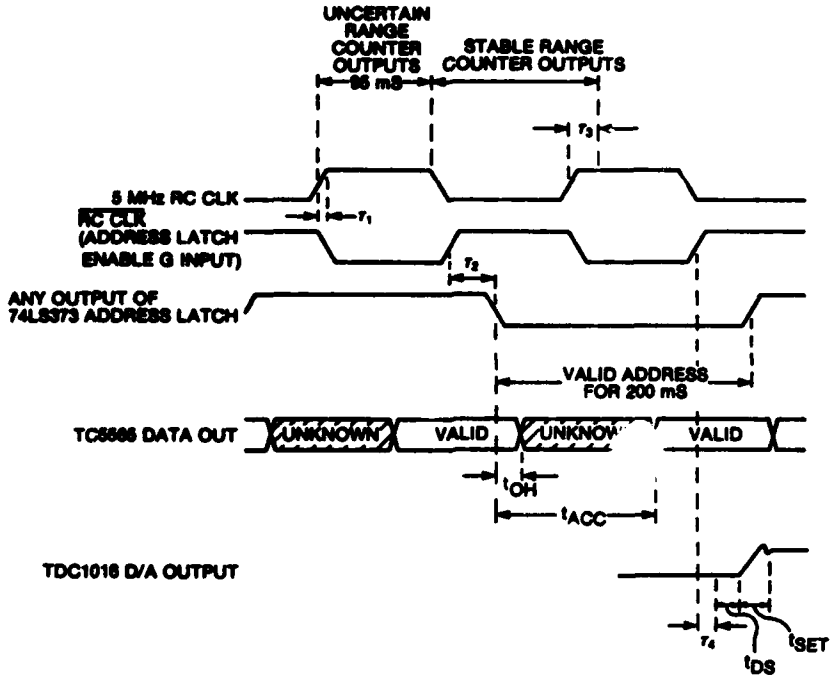

FIGURE 34: CLUTTER CONTROLLER -- RUN MODE TIMING DIAGRAM

TABLE 7: Run Mode Timing Data

PARAMETER	VALUE
$\tau 1$	6 ns max. for 74F00
$\tau 2$	36 ns max. from enable to any Q for 4LS373
$\tau 3$	25 ns typically for 74LS193
$\tau 4$	11.3 ns max. for low to high plus high to low transitions with 74F00
t_{OH}	20 ns min. output data hold time
t_{ACC}	120 ns max. address access time
t_{DS}	20 ns max. data turn-on delay
t_{SET}	30 ns max. settling time

Fig. 33 also contains the frequency agility address counter. This is clocked by the A/D SOC (start of conversion) line to increment the A_{10} to A_{12} address lines of the Σfa/search and Σfa/track memories before the beginning of each PRI. This causes a different row of 1 k memory locations to be read out each PRI, in order to generate uncorrelated clutter returns. The tri-state buffers in the figure connect A_{10}-A_{12} to the frequency agility counter in RUN and the DR11C input latches in LOAD.

As described earlier, digitized versions of the TRS antenna elevation and azimuth position voltages are used in memory addressing. Azimuth and elevation A/Ds appear in Fig. 35. Each A/D employs an op amp at the input to perform scaling and offset of the position voltages. Accurate $\pm$ 5V reference voltages for the A/D resistor networks are provided by the arrangement comprised of a zener diode, resistors, and two op amps [31]. Conversion is triggered by the A/D SOC signal generated by a dual one-shot (IC 3 Fig. 32). This signal is timed so that the A/Ds change outputs during the dead time between the radar horizon and the start of the next PRI. This prevents address lines from changing during memory reading. Note that the A/Ds are tri-stated in LOAD to allow the DR11c input latches to drive the memory address lines.

The actual memory devices appear in Figs. 36 to 38. The Σ memory is entirely made up of 8k x 8 Toshiba TC5565PL-12s, which have a 120 ns access time. The Δ_{el} and antenna gain memories are 2kx8 Toshiba TC5518BPLs with a 200 ns access time. All RAMs are the static type so no refresh circuitry is required.

In Fig. 38 the tri-state buffers allow the TC5518 address bits A_0 to A_6 to be driven by the elevation antenna position A/D in RUN and the DR11c input latches in LOAD. NAND gates on the antenna gain memory output provide a means of setting the antenna gain attenuator to minimum attenuation when the ROM is activated. Similarly, the 74116 latch with clear on the Δ_{el} memory outputs provides a way of setting the Δ_{el} attenuator to maximum attenuation during alternate PRIs and when the ROM is activated.

The three D/As appear in Fig. 39. D/As 1 and 2 are low cost DAC-08HQ devices featuring an 85 ns output current settling time and continuous conversion. They are used to produce digitally controlled currents for driving the antenna gain and el attenuators. D/A 3 is a video speed converter capable of 20 Mega samples per second. While ten input bits exist, the chip version used here is specified as linear over only 8 bits, as required for this application. The TDC1016 produces an voltage output. As a current output with a 0 to 6 mA range was required, a voltage-to-current circuit was constructed using a high slew rate op amp and transistor.

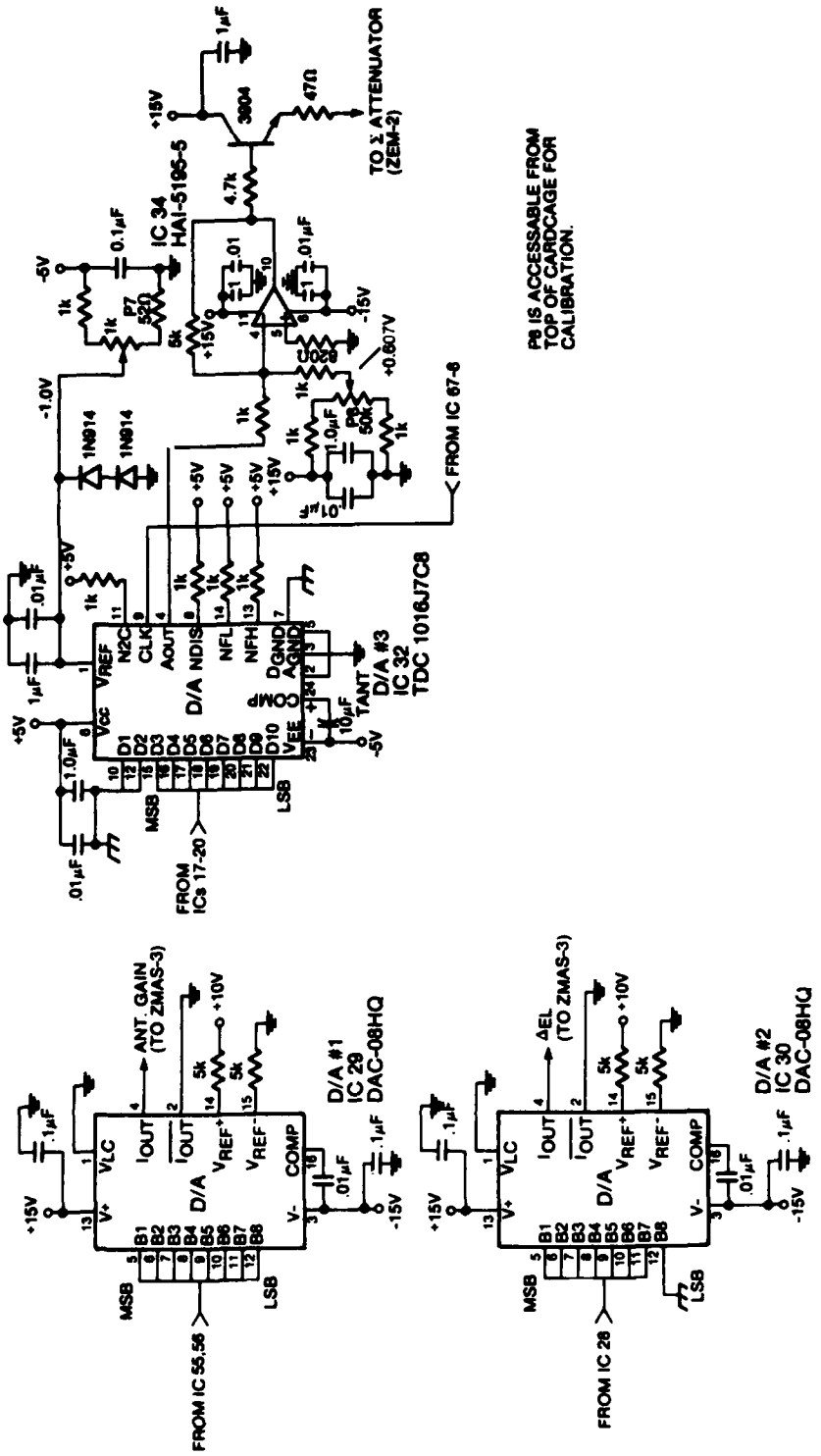

FIGURE 35: CLUTTER CONTROLLER A/Ds USED FOR MEMORY ADDRESSING

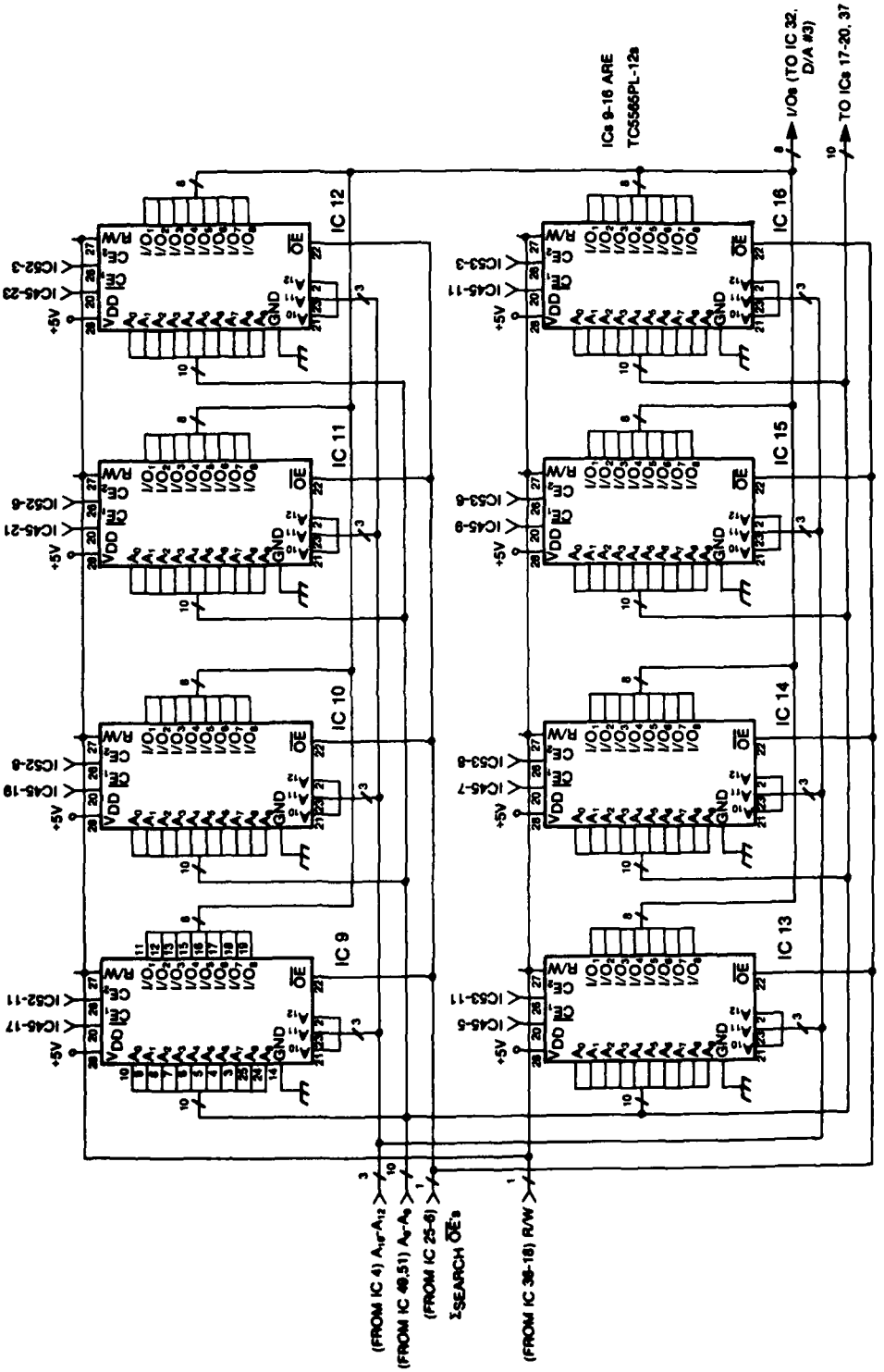

FIGURE 36: CLUTTER CONTROLLER ΣSEARCH MEMORY

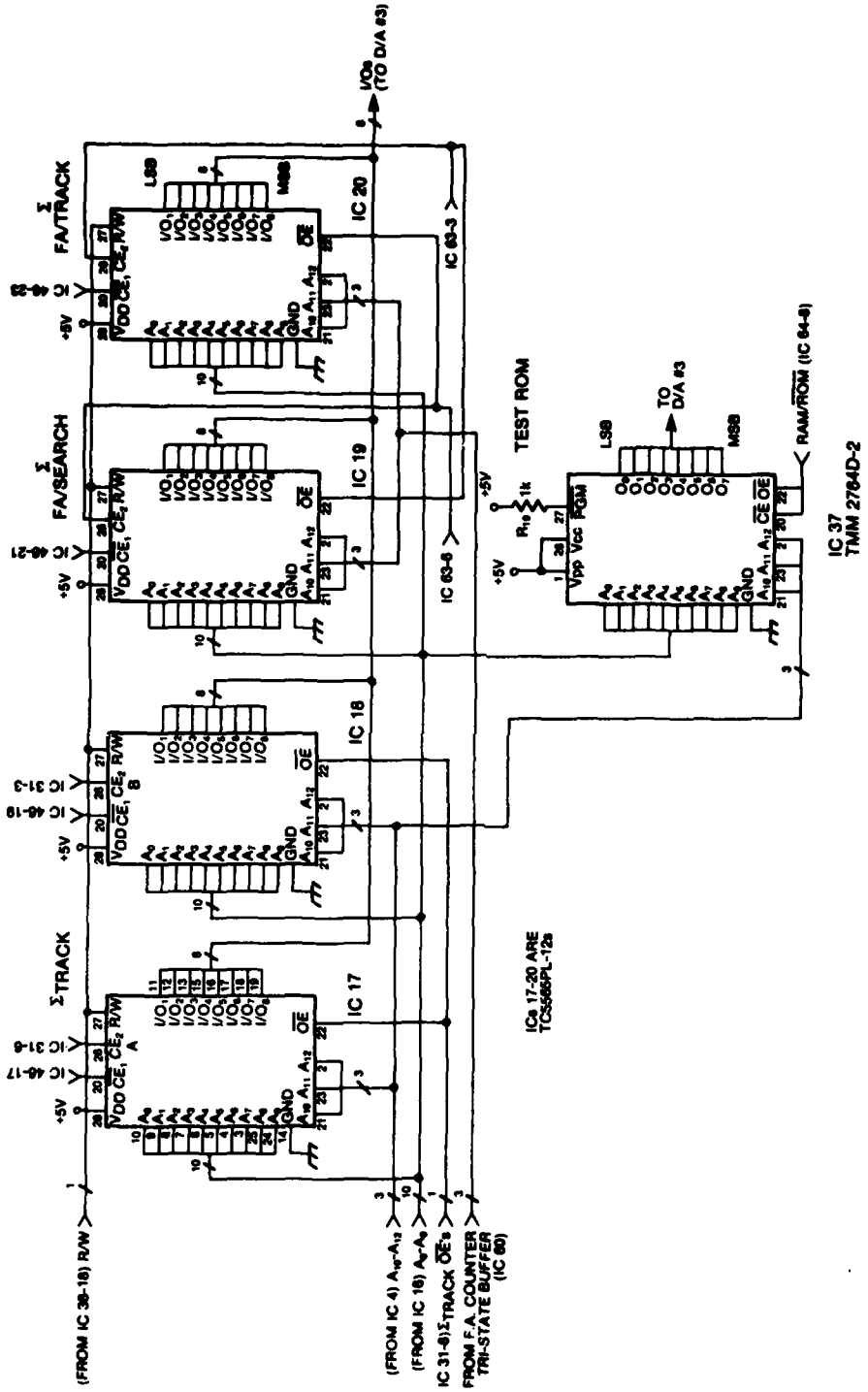

FIGURE 37: CLUTTER CONTROLLER Σtrack, Σfa/search, Σfa/track AND ROM MEMORIES

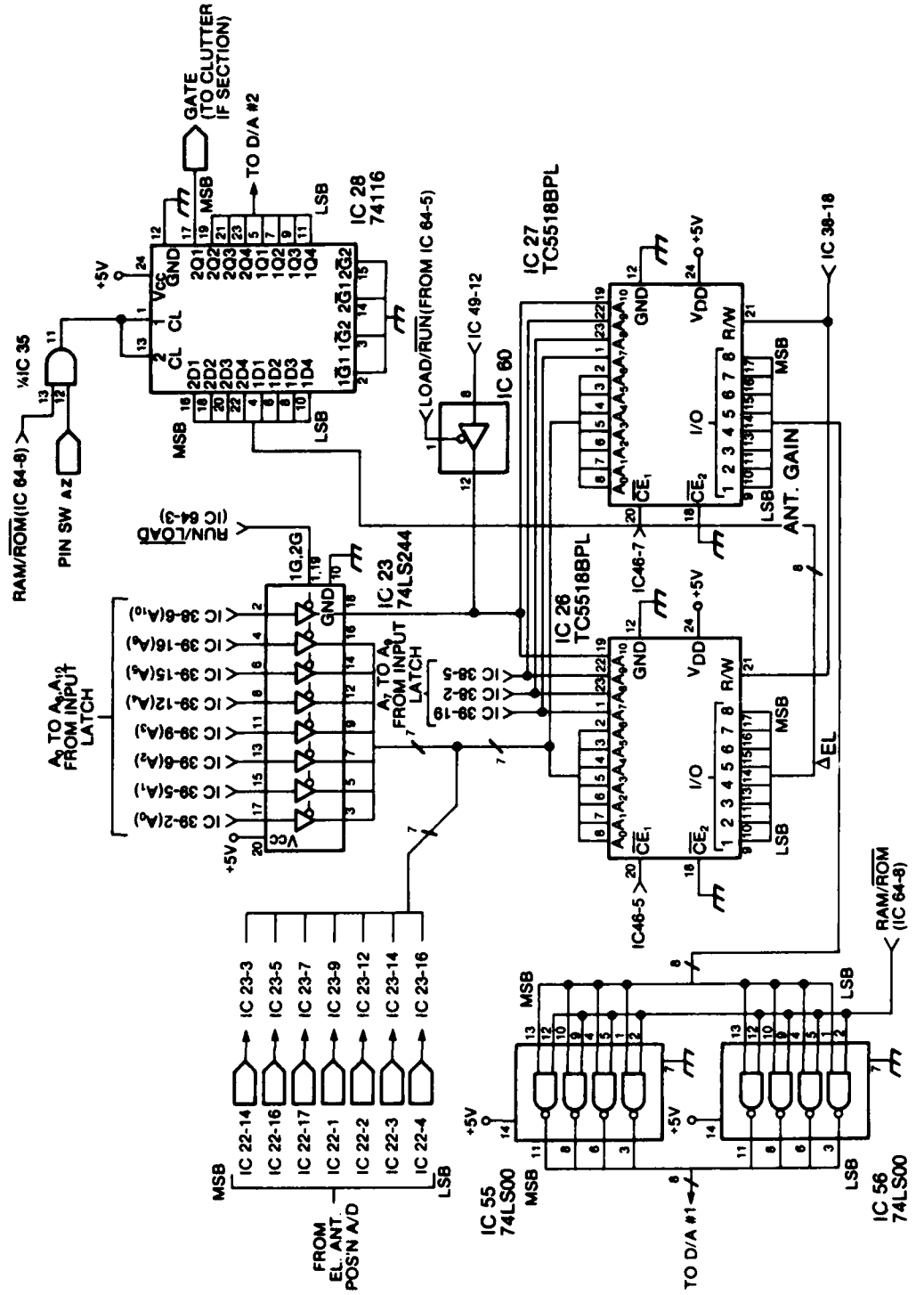

FIGURE 38: CLUTTER CONTROLLER Δ_{EL} AND ANTENNA GAIN MEMORIES

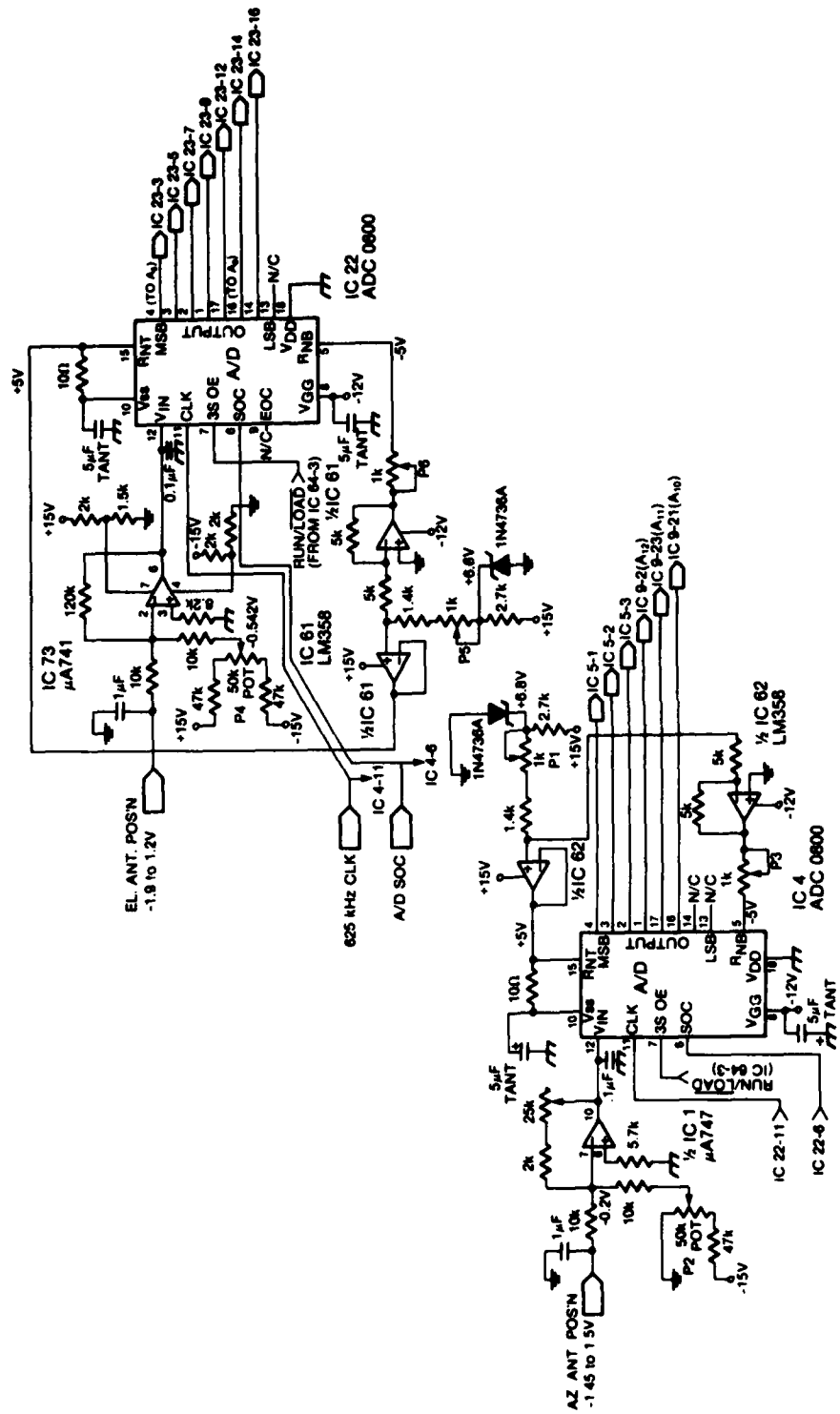

FIGURE 39: CLUTTER CONTROLLER OUTPUT D/As

APPENDIX B

DOPPLER OFFSET RELATIONSHIPS

The motion of waves produces a non-zero mean of the clutter doppler spectrum. This offset is greatest looking up or downwind [5], and increases with windspeed. While the variation with azimuth look angle is not included here, the clutter is given a doppler offset, defined as f_{dss}, that is a function of sea-state and hence windspeed. Table 8 shows simulation doppler shift f_{dss} for sea-states 1 to 5. Doppler values were assigned based on graphically presented data in [5] but fidelity was limited by the 30 Hz resolution of the VCXO control hardware.

TABLE 8: Sea Clutter Doppler Offsets for Sea-States 1 to 5

SEA-STATE	MEAN DOPPLER SHIFT FOR H. POL'N From [5] (Hz)	SIMULATION DOPPLER f_{dss}(Hz)
1	0-106	60
2	106-121	120
3	121-141	120
4	141-152	150
5	152-164	150

Clutter doppler shift is also proportional to platform velocity. Because of the low altitude of the radar (h=12m) platform velocity and slant range rate are assumed equal. Slant range is the distance from the radar antenna to the clutter reflecting surface. The doppler shift f_{dpv} due to platform velocity V is calculated using the standard relationship:

$$f_{dpv} = 2V/\lambda \tag{51}$$

where platform velocity is input by the user. The total clutter doppler shift f_d is given by:

$$f_d = f_{dpv} + f_{dss} \tag{52}$$

UNCLASSIFIED

Security Classification

DOCUMENT CONTROL DATA - R & D

(Security classification of title, body of abstract and indexing annotation must be entered when the overall document is classified)

1 ORIGINATING ACTIVITY
Defence Research Establishment Ottawa
Shirley Bay, Ottawa, Ontario K1A 0Z4 CANADA

2a DOCUMENT SECURITY CLASSIFICATION
UNCLASSIFIED

2b GROUP

3 DOCUMENT TITLE
AN IF CLUTTER SIGNAL GENERATOR FOR THE DREO EW ENGAGEMENT SIMULATION FACILITY

4 DESCRIPTIVE NOTES (Type of report and inclusive dates)
DREO Report

5 AUTHOR(S) (Last name, first name, middle initial)
WARDLE, Geoffrey A.

6 DOCUMENT DATE
December 1986

7a TOTAL NO OF PAGES
81

7b NO OF REFS
31

8a PROJECT OR GRANT NO
041LD12

8b CONTRACT NO

9a ORIGINATOR'S DOCUMENT NUMBER(S)
DREO Report 956

9b OTHER DOCUMENT NO(S) (Any other numbers that may be assigned this document)

10 DISTRIBUTION STATEMENT
Unlimited

11 SUPPLEMENTARY NOTES

12 SPONSORING ACTIVITY
DREO

13 ABSTRACT

This report describes the implementation of an intermediate frequency (IF) radar clutter generator. The generator provides signals for the monopulse tracking radar which forms part of the Electronic Warfare Engagement Simulation Facility at the Defence Research Establishment Ottawa. Land clutter signals with log-normal, Weibull and exponential spatial amplitude distributions are produced, as well as exponential sea clutter signals. Fluctuating clutter from wind blown scatterers is modelled using narrowband amplitude modulation. Clutter induced angle tracking errors are also represented. The report describes the major clutter mechanisms relevant to noncoherent radars in low grazing angle scenarios. The hardware and equations used in modelling are described, and the report presents envelope detected waveform plots and histograms. This work has applications in accurate modelling of radar performance in low-altitude engagements.

DSIS

AD-A101 529 AN IF (INTERMEDIATE FREQUENCY) CLUTTER SIGNAL GENERATOR 2/2
FOR THE DREO EW (..(U) DEFENCE RESEARCH ESTABLISHMENT
OTTAWA (ONTARIO) G A WARDLE DEC 86 DREO-956

UNCLASSIFIED F/G 17/4.3 NL

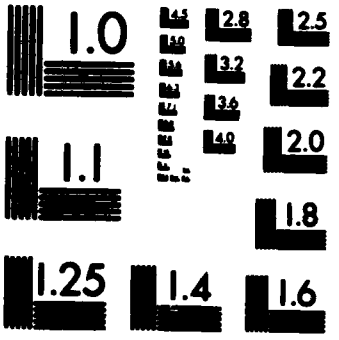

UNCLASSIFIED

Security Classification

KEYWORDS:

CFAR
cross section
distribution
EW
exponential
grazing angle
intermediate frequency
jamming
land clutter
log-normal
missile seeker
model
monopulse
MTI
polarization
radar
random process
reflectivity
scatterers
sea clutter
sea state
simulation
spatial
spectrum
temporal
threat
tracking
Weibull

INSTRUCTIONS

1. ORIGINATING ACTIVITY Enter the name and address of the organization issuing the document.

2a. DOCUMENT SECURITY CLASSIFICATION Enter the overall security classification of the document including special warning terms whenever applicable.

2b. GROUP Enter security reclassification group number. The three groups are defined in Appendix 'M' of the DRB Security Regulations.

3. DOCUMENT TITLE Enter the complete document title in all capital letters. Titles in all cases should be unclassified. If a sufficiently descriptive title cannot be selected without classification, show title classification with the usual one capital-letter abbreviation in parentheses immediately following the title.

4. DESCRIPTIVE NOTES Enter the category of document, e.g. technical report, technical note or technical letter. If appropriate, enter the type of document, e.g. interim, progress, summary, annual or final. Give the inclusive dates when a specific reporting period is covered.

5. AUTHOR(S) Enter the name(s) of author(s) as shown on or in the document. Enter last name, first name, middle initial. If military, show rank. The name of the principal author is an absolute minimum requirement.

6. DOCUMENT DATE Enter the date (month, year) of Establishment approval for publication of the document.

7a. TOTAL NUMBER OF PAGES The total page count should follow normal pagination procedures, i.e., enter the number of pages containing information.

7b. NUMBER OF REFERENCES Enter the total number of references cited in the document.

8a. PROJECT OR GRANT NUMBER If appropriate, enter the applicable research and development project or grant number under which the document was written.

8b. CONTRACT NUMBER If appropriate, enter the applicable number under which the document was written.

9a. ORIGINATOR'S DOCUMENT NUMBER(S) Enter the official document number by which the document will be identified and controlled by the originating activity. This number must be unique to this document.

9b. OTHER DOCUMENT NUMBER(S) If the document has been assigned any other document numbers (either by the originator or by the sponsor), also enter this number(s).

10. DISTRIBUTION STATEMENT Enter any limitations on further dissemination of the document, other than those imposed by security classification, using standard statements such as:

(1) "Qualified requesters may obtain copies of this document from their defence documentation center."

(2) "Announcement and dissemination of this document is not authorized without prior approval from originating activity."

11. SUPPLEMENTARY NOTES Use for additional explanatory notes.

12. SPONSORING ACTIVITY Enter the name of the departmental project office or laboratory sponsoring the research and development. Include address.

13. ABSTRACT Enter an abstract giving a brief and factual summary of the document, even though it may also appear elsewhere in the body of the document itself. It is highly desirable that the abstract of classified documents be unclassified. Each paragraph of the abstract shall end with an indication of the security classification of the information in the paragraph (unless the document itself is unclassified) represented as (TS), (S), (C), (R), or (U).

The length of the abstract should be limited to 20 single-spaced standard typewritten lines; 7½ inches long.

14. KEY WORDS Key words are technically meaningful terms or short phrases that characterize a document and could be helpful in cataloguing the document. Key words should be selected so that no security classification is required. Identifiers, such as equipment model designation, trade name, military project code name, geographic location, may be used as key words but will be followed by an indication of technical context.

END

7-87

DTIC